ornl

ORNL/CON-172

OAK RIDGE
NATIONAL
LABORATORY

MARTIN MARIETTA

Linear Harmonic Analysis of Free-Piston Stirling Engines

N. C. J. Chen
F. P. Griffin

OPERATED BY
MARTIN MARIETTA ENERGY SYSTEMS, INC.
FOR THE UNITED STATES
DEPARTMENT OF ENERGY

Printed in the United States of America. Available from
National Technical Information Service
U.S. Department of Commerce
5285 Port Royal Road, Springfield, Virginia 22161
NTIS price codes—Printed Copy: A06 Microfiche A01

This report was prepared as an account of work sponsored by an agency of the United States Government. Neither the United States Government nor any agency thereof, nor any of their employees, makes any warranty, express or implied, or assumes any legal liability or responsibility for the accuracy, completeness, or usefulness of any information, apparatus, product, or process disclosed, or represents that its use would not infringe privately owned rights. Reference herein to any specific commercial product, process, or service by trade name, trademark, manufacturer, or otherwise, does not necessarily constitute or imply its endorsement, recommendation, or favoring by the United States Government or any agency thereof. The views and opinions of authors expressed herein do not necessarily state or reflect those of the United States Government or any agency thereof.

ORNL/CON-172

Engineering Technology Division*

LINEAR HARMONIC ANALYSIS OF FREE-PISTON STIRLING ENGINES

N. C. J. Chen F. P. Griffin

*Work Performed for the
Building Equipment Research Program
Energy Division

JUN 1986

Prepared by the
OAK RIDGE NATIONAL LABORATORY
Oak Ridge, Tennessee 37831
operated by
MARTIN MARIETTA ENERGY SYSTEMS, INC.
for the
U.S. DEPARTMENT OF ENERGY
Under Contract No. DE-AC05-84OR21400

CONTENTS

	Page
EXECUTIVE SUMMARY	v
ABSTRACT	1
1. INTRODUCTION	1
2. THEORETICAL FORMULATION	5
2.1 Governing Equations	6
2.2 Engine Performance Parameters	10
3. LHA SOLUTION METHOD	12
3.1 Equivalent Load Representation	12
3.2 Nondimensional Equations	13
3.3 Harmonic Oscillations	17
3.4 Integrated Energy Equations	18
3.5 Homogeneous Algebraic Equations	20
3.6 Nonhomogeneous Algebraic Equations	24
3.7 Successive Approximations	26
3.8 FPSE/Load Matching	28
3.9 Summary of LHA Procedures	30
4. LHA RESULTS AND DISCUSSION	33
4.1 Base Case Predictions	33
4.2 Comparison with Nonlinear Solution	39
4.3 Adiabatic Cylinder Effects	46
4.4 Sensitivity to Pressure Drop and Seal Leakage Losses	49
5. SUMMARY AND CONCLUSIONS	55
REFERENCES	57
APPENDIX A. IMPERFECT HEAT EXCHANGER ANALYSIS	59
APPENDIX B. NONLINEAR DASHPOT EQUATIONS	69
APPENDIX C. NOMENCLATURE	73
APPENDIX D. COMPUTER PROGRAM: LHA VERSION 1	79

EXECUTIVE SUMMARY

An almost closed-form solution method called the linear harmonic analysis (LHA) has been developed for the coupled thermodynamic/dynamic problem that is associated with a free-piston Stirling engine (FPSE). The governing equations are differential because most of the parameters describing an FPSE (pressure, temperature, piston position, etc.) are time-dependent. The LHA method is based on three primary assumptions: (1) linearization of the ideal gas law, (2) representation of all time-dependent variables with harmonic functions, and (3) replacement of terms in the governing equations that contain products of harmonic functions with truncated Fourier series. The assumptions reduce the nonlinear differential equations to a system of almost linear algebraic equations that are solved using standard matrix algebra, with iterations as required. The motivation for developing this simplified analytical method was not that it saves computer time (although it does do that), but that it reveals causes and effects much more effectively than a column of numerical output.

In the LHA solution, the load is initially represented by a linear function of power piston position and velocity so that the nonlinear differential equations can be solved in almost closed form. This procedure allows the engine analysis to be performed independently from the load analysis. The FPSE calculations are completed first; the characteristics of a particular load, including nonlinearities, are accounted for later in the LHA solution during an FPSE/load matching analysis.

A computer program called LHA Version 1 (LHA1) was written for the Sunpower RE-1000 FPSE configuration. A listing of the program is included in Appendix D. The RE-1000 engine contains a single power piston and a displacer sprung to the engine housing. The working space of the engine is divided into only three control volumes, and motion of the engine housing is neglected. However, the LHA method is not limited to such a simple representation, and more control volumes or dynamic equations could be added if they were desired. Cylinder heat transfer, pressure drop, and seal leakage losses are all included in the present version of the LHA program. These losses are not calculated separately and then added to the analysis. They are included as a simultaneous part of the thermodynamic/dynamic calculations so that all of the interactions between the losses, thermal performance, and dynamic behavior are accounted for.

The time required for execution of the LHA1 program is about 100 times less than the execution time required for an equivalent numerical integration method. Even with its speed, the LHA method has sufficient mathematical accuracy for most practical Stirling engine applications. The mathematical accuracy of the LHA assumptions was verified by independently solving the same nonlinear differential equations using a numerical integration method and comparing the results with those from the LHA1 program. The differences between the LHA and numerical predictions were <5% for all important parameters, which is about equal to or less than the uncertainty associated with typical Stirling engine experimental measurements. This combination of computational speed and mathematical accuracy makes the LHA method ideal for FPSE optimization programs.

In addition to speed, the LHA method has other advantages over numerical integration methods. Numerical techniques usually require some artistic guesswork to select step sizes and initial conditions so that the solution is numerically stable, mathematically accurate, and converges quickly to a periodic steady state. The closed-form analytical approach of the LHA method avoids these problems. The LHA method does require iterations, but the assumption of isothermal cylinders provides a good starting point for the calculations, and LHA convergence usually occurs in <20 iterations.

The LHA method also has advantages over other linear closed-form solution methods that have been developed for FPSE dynamic problems. All previously published closed-form solutions treat the thermodynamic losses separately. In the LHA method, the thermodynamic losses, as well as their interactions, are included intrinsically in the FPSE dynamic solution. Sample calculations using the LHA1 program have shown that substantial errors in predicting dynamic behavior can occur if an isothermal calculation is used to represent an adiabatic FPSE. LHA predictions have also indicated that unrealistic assumptions about the pressure drop losses can lead to additional errors.

LINEAR HARMONIC ANALYSIS OF FREE-PISTON STIRLING ENGINES

N. C. J. Chen F. P. Griffin

ABSTRACT

The equations that govern the behavior of free-piston Stirling engines are nonlinear differential equations. Traditional solution methods have been time-stepping integrations that can be plagued by numerical instabilities and can use large amounts of computer time. Closed-form analytical solutions are possible if the working gas behaves isothermally or if the nonlinear terms in the governing equations are replaced with accurate approximations. An almost closed-form solution method, called the linear harmonic analysis (LHA), has been developed for free-piston Stirling engine applications by representing all of the periodic variables with harmonic functions. The solution method accounts for the important thermodynamic losses that are coupled together in free-piston engines, yet it is efficient enough for optimization studies. The LHA method was compared with a standard numerical integration method to verify its mathematical accuracy. The LHA and numerical predictions for a sample free-piston Stirling engine configuration differed by <5% for all important parameters. Sensitivity studies using the LHA method have also shown that the thermodynamic loss assumptions used in an analysis can have a significant impact on the predicted dynamic behavior of a free-piston Stirling engine.

---

1. INTRODUCTION

As a prerequisite to dealing with interactions between thermodynamics and dynamics that occur in a free-piston Stirling engine (FPSE), a simplified thermodynamic analysis with applications in kinematic engines has been performed.[1,2] The analysis is based on an almost closed-form solution called the linear harmonic analysis (LHA). In the analysis, variables are represented in terms of harmonic oscillations, and nonharmonic terms in the conservation equations are replaced with truncated Fourier series so that the equations can be solved in almost closed form, leading to a better understanding of Stirling engine behavior. The theory further includes a Second Law analysis, where the efficiency and power losses resulting from effects of adiabatic cylinders, cylinder heat

transfer, pressure drop, and seal leakage can be allocated unambiguously, and the degree of coupling between different losses can be assessed.

Because of inherently strong thermodynamic and dynamic interactions, a simultaneous coupled solution is required to predict free-piston Stirling engine performance. For kinematic machine performance predictions, a decoupled solution is sufficient because the thermodynamics can be solved separately once volume variations are specified. However, for free-piston engines, the volume variations are no longer specified; in fact, there exists a significant coupling between thermodynamics and dynamics. The pressure waves (thermodynamics) in the respective spaces determine the power piston and displacer motions (dynamics); the piston motions, in turn, produce the pressure waves that act on the pistons. This complicated problem is further compounded by load interactions. The load must be represented properly and considered as an integrated part of the system analysis before complete FPSE performance predictions can be made. Generally, the energy absorbed by the load depends on the piston motions (displacement and velocity) on the one hand; the load modifies the motions on the other hand.

The objectives of this report are twofold: to extend the existing LHA methodology from kinematic to free-piston Stirling engine applications and to discuss the advantages of the LHA solution method. The basic methodology that applies to kinematic engines remains valid, but additions are needed because of coupled thermodynamics and dynamics. The FPSE additions include the piston and displacer dynamic formulation with proper load representation and the displacer gas spring thermodynamic formulation. LHA advantages include fast execution times with good mathematical accuracy and realistic representation of the thermodynamic losses and their interactions with each other and with the dynamic behavior.

The formulation in this report focuses on the Sunpower RE-1000 FPSE, although the analysis can be extended to other configurations if desired. Sample calculations are presented for an RE-1000 base case as well as for sensitivity studies around the base case. Correlations for heat transfer, pressure drop, and seal leakage have not been added to the analysis yet, so the loss coefficients must be specified in the input data. The

loss coefficients for the RE-1000 base case were selected so that the LHA predictions were in general agreement with experimentally measured performance.

The formulation in the main text is based on the assumption of perfect heat transfer in the heater, cooler, and regenerator. However, a simplified thermal analysis that accounts for imperfect heat exchangers is described in Appendix A. In the formulation, heat transfer is assumed to occur during two steady flow processes: the hot and cold blows. When incorporated into the engine analysis, the simplified heat transfer analysis shows that the effects of imperfect heat exchangers are significant with regard to thermodynamic performance, but are less significant in dynamic performance.

A brief literature survey of existing free-piston Stirling engine analyses revealed that the analyses may be conveniently categorized into two approaches: isothermal and nonisothermal cylinders. Many previous approaches to the analysis of coupled FPSE dynamics/thermodynamics begin with the assumption that the gas in the cylinders is isothermal with respect to time; representative works include those of Cooke-Yarborough,[3] Marusak and Chiu,[4] Berchowitz and Wyatt-Mair,[5] Goldberg,[6] West,[7] and Chap. 3 in Urieli and Berchowitz.[8] When the analysis is extended to nonisothermal cylinders, as it must be for a physically realistic formulation, most work has depended entirely on numerical solutions to the equations, such as analyses by Vincent et al.,[9] Gedeon,[10] Giansante,[11] Tew,[12] General Electric Co.,[13] and Martini.[14] The works of Rauch[15–17] are among the few that attempt to treat by nonnumerical methods the coupled dynamics and thermodynamics of free-piston machines with nonisothermal cylinders; however, few details have been released because of proprietary restrictions. Rauch's approach uses a linearized approximation in which the variables are represented by harmonic functions.

This literature review leads to the belief that there is a need for further development of linearized analyses because closed-form analytical solutions provide a much clearer understanding of the physical processes occurring in Stirling machines than do numerical treatments. However, a closed-form, or almost closed-form solution should not oversimplify the physics of the problem; major losses and their interactions must be

included to provide a realistic representation of free-piston engine behavior. Therefore, a form of the LHA method that takes into account interactions between major losses has been chosen for studying free-piston Stirling engine performance.

2. THEORETICAL FORMULATION

The coupled thermodynamic and dynamic analysis described in this report is derived for an engine configuration similar to the RE-1000 FPSE manufactured by Sunpower, Inc. The engine, shown schematically in Fig. 2.1, contains a displacer sprung to the engine housing and a power piston connected to a dashpot load that is controlled by a variable orifice.

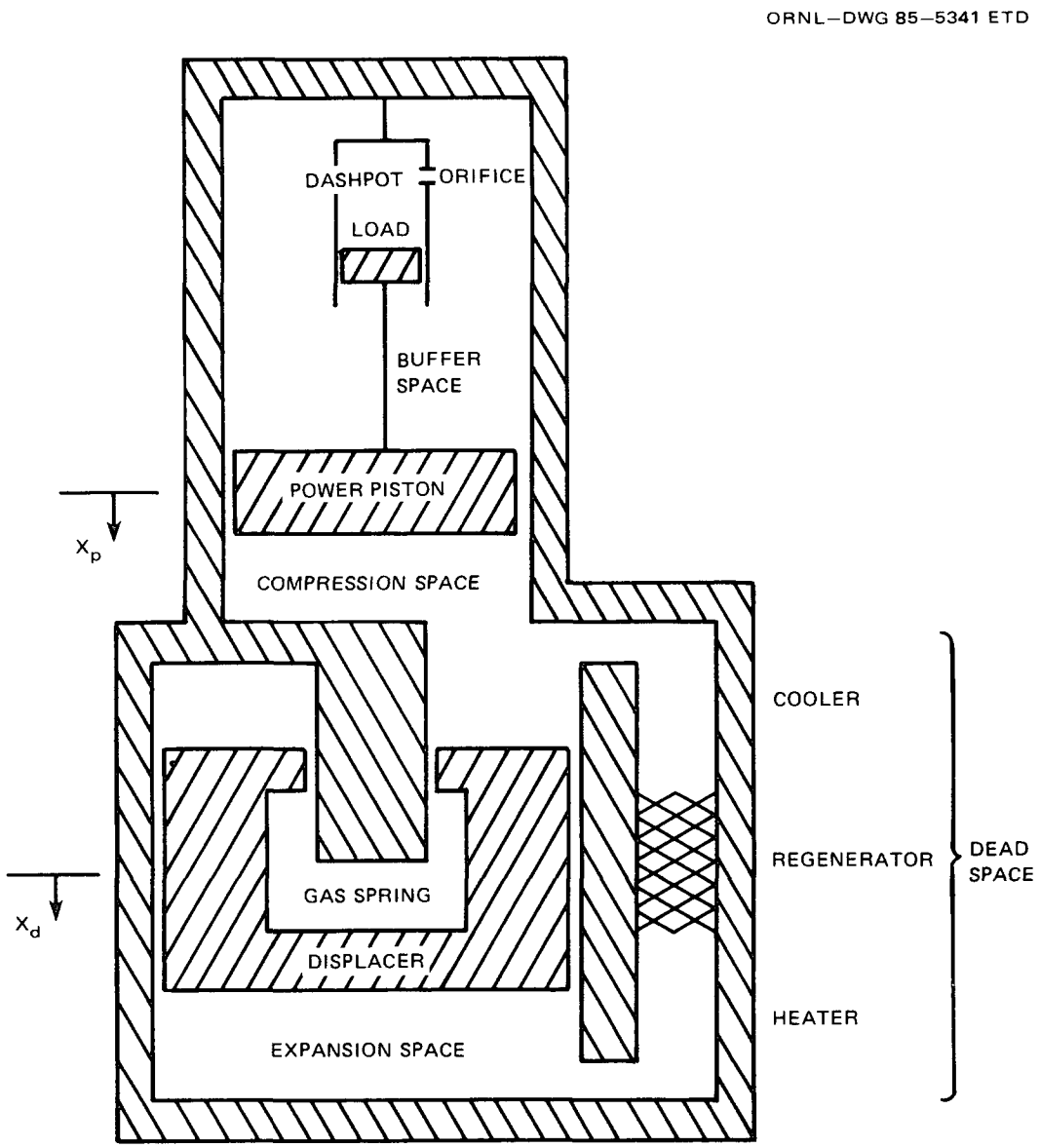

Fig. 2.1. Simplified schematic of RE-1000 free-piston Stirling engine.

The thermodynamic formulations for the engine working space (consisting of the expansion space, heater, regenerator, cooler, and compression space) and displacer gas spring are identical to those described in ORNL/CON-155 (Ref. 1). Dynamic equations are added to the analysis to relate the gas pressure and load forces to the power piston and displacer motions.

2.1 Governing Equations

The working gas in the engine is represented by five control volumes: expansion, dead (sum of heater, regenerator, and cooler), compression, gas spring, and buffer spaces. The primary assumptions for the analysis are (1) pressure and temperature of gas in the buffer space are constant and equal to, respectively, the average working space pressure $\overline{P}_w$ and the cooler temperature T_K; (2) finite heat transfer between the gas and walls in the expansion, compression, and gas spring spaces; (3) isothermal gas behavior in the dead space; (4) pressure drop between the expansion and dead spaces and the dead and compression spaces; (5) power piston seal leakage between the compression and buffer spaces; (6) displacer gas spring seal leakage between the gas spring and buffer spaces; and (7) ideal working gas with constant properties. Constant buffer space pressure is assumed because the power piston volume stroke in the RE-1000 engine is very small relative to the total volume in the buffer space. Also, the gas spring seal leakage assumption is based on the fact that the primary leakage path in the RE-1000 engine is from the gas spring through the displacer rod clearance seal to the centering port in the displacer rod, which communicates with the gas in the buffer space.

Most of the variables describing an FPSE are time-dependent, and the governing equations are therefore differential. The masses and temperatures of the gas in the control volumes and the positions of the pistons were selected as the independent variables in the current FPSE analysis. Nine independent variables are needed to describe the engine shown in Fig. 2.1: the masses and temperatures of the gas in the expansion, compression, and gas spring spaces; the mass of gas in the dead space; and the positions of the power piston and displacer. Variable volumes and

pressures are treated as dependent variables. Volumes are a geometric function of the power piston and displacer positions. Gas pressure in a control volume is related by the ideal gas law to the mass, temperature, and volume of the gas.

The conservation equations that govern the behavior of the free-piston Stirling engine shown in Fig. 2.1 are derived as follows. The mass conservation laws for the expansion space, expansion and dead spaces combined, and working space can be stated, respectively, as

$$\frac{dm_e}{dt} = \frac{1}{k_{pe}} (P_d - P_e) \ , \tag{2.1}$$

$$\frac{dm_e}{dt} + \frac{dm_d}{dt} = \frac{1}{k_{pc}} (P_c - P_d) \ , \tag{2.2}$$

$$\frac{dm_e}{dt} + \frac{dm_d}{dt} + \frac{dm_c}{dt} = k_{mc}(\overline{P}_w - P_c) \ , \tag{2.3}$$

where all variables are defined in the list of nomenclature in Appendix C.

By the First Law of Thermodynamics, the instantaneous energy balances in the expansion and compression spaces are, respectively,

$$c_p \frac{dm_e}{dt} T_{e\ flux} + h_e \overline{A}_{se} (\overline{T}_{we} - T_e) = P_e \frac{dV_e}{dt} + c_v \frac{d(m_e T_e)}{dt} \ , \tag{2.4}$$

$$c_p \frac{dm_c}{dt} T_{c\ flux} + h_c \overline{A}_{sc} (\overline{T}_{wc} - T_c) = P_c \frac{dV_c}{dt} + c_v \frac{d(m_c T_c)}{dt} \ , \tag{2.5}$$

where the enthalpy flux temperatures are defined by

$$T_{e\ flux} = \begin{cases} T_H, & \text{if } \frac{dm_e}{dt} > 0 \\ T_e, & \text{if } \frac{dm_e}{dt} < 0 \end{cases} \tag{2.6}$$

for the expansion space and

$$T_{c\ flux} = \begin{cases} T_K, & \text{if } \frac{dm_c}{dt} > 0 \\ T_c, & \text{if } \frac{dm_c}{dt} < 0 \end{cases} \tag{2.7}$$

for the compression space.

Equations (2.1)–(2.7) are identical to those derived in ORNL/CON-155 (Ref. 1). Thus, there is no need to define variables and explain physical meanings for each term again. Readers who require more detailed information should refer to the previous report.

The dynamic equations are derived from Newton's Second Law of Motion, which states that the sum of the external forces acting on a mass are equal to the rate of change of momentum of the mass. Engine housing motion is neglected because the housing of the RE-1000 FPSE is much more massive than the power piston or displacer. The dynamic system therefore contains only two degrees of freedom: displacer motion and power piston motion.

There are three pressure forces acting on the displacer of the RE-1000 FPSE shown in Fig. 2.1. The gas spring force P_sA_r and the compression space force $P_c(A_d - A_r)$ act in a downward (positive) direction, where all variables are defined in the list of nomenclature in Appendix C. The expansion space force P_eA_d acts in an upward (negative) direction. The dynamic equation for the displacer is, therefore,

$$P_s\ A_r + P_c\ (A_d - A_r) - P_e\ A_d = m_{dp}\ \frac{d^2X_d}{dt^2}\ . \tag{2.8}$$

Referring again to Fig. 2.1, two pressure forces and the load force act on the power piston. The buffer space force $\overline{P}_wA_p$ acts in a positive direction, and the compression space force P_cA_p acts in a negative direction. The force the load produces on the power piston depends on the type of load; dashpots, linear alternators, compressors, and hydraulic pumps will all have different characteristics. For now, the load force will be

represented arbitrarily by F_1, and the power piston dynamic equation is written as

$$\overline{P}_w A_p - P_c A_p + F_1 = m_{pp} \frac{d^2 X_p}{dt^2} . \tag{2.9}$$

To complete the formulation, mass and energy conservation equations for the gas spring are needed. The rate of change of mass inside the gas spring is assumed to be linearly proportional to the pressure difference between the buffer and gas spring spaces. A gas spring leakage coefficient k_{ms} lumps the combined effects of leakage caused by the displacer rod clearance seal and the centering port. The gas spring mass conservation equation is

$$\frac{dm_s}{dt} = k_{ms} (\overline{P}_w - P_s) . \tag{2.10}$$

The instantaneous energy equation for the gas spring, similar in form to the ones for the expansion and compression spaces, is

$$c_p \frac{dm_s}{dt} T_{s\ flux} + h_s \overline{A}_{ss} (\overline{T}_{ws} - T_s) = P_s \frac{dV_s}{dt} + c_v \frac{d(m_s T_s)}{dt} , \tag{2.11}$$

where the enthalpy flux temperature is

$$T_{s\ flux} = \begin{cases} T_K, & \text{if } \frac{dm_s}{dt} > 0 \\ T_s, & \text{if } \frac{dm_s}{dt} < 0 \end{cases} . \tag{2.12}$$

Equations (2.10)—(2.12) were derived in ORNL/CON-155 (Ref. 1) and, thus, a detailed description will not be repeated here. The enthalpy flux associated with the gas spring arises from the mass leakage between the gas spring and buffer spaces, whereas the enthalpy fluxes in the expansion and compression spaces arise from the motion of the displacer, which

shuttles gas between the hot and cold ends of the machine. The gas spring enthalpy flux temperature is based on the assumption that the buffer space gas temperature is constant and equal to the cooler temperature.

This completes the formulation of the coupled thermodynamic and dynamic equations for the RE-1000 free-piston Stirling engine configuration. There are nine differential equations to solve for nine independent variables (m_e, m_d, m_c, m_s, T_e, T_c, T_s, X_p, X_d). The ideal gas law is used to express the pressure variables (P_e, P_d, P_c, P_s) in terms of the independent variables. The volume variables are geometric functions of the piston positions (see Fig. 2.1)

$$V_e = \overline{V}_e - A_d X_d \ , \tag{2.13}$$

$$V_c = \overline{V}_c + (A_d - A_r)\ X_d - A_p X_p \ , \tag{2.14}$$

$$V_s = \overline{V}_s + A_r X_d \ . \tag{2.15}$$

2.2 Engine Performance Parameters

When the thermodynamic analysis for kinematic Stirling engines described in ORNL/CON-155 (Ref. 1) was extended to include free-piston dynamics, thermodynamic calculations were added for the displacer gas spring. The presence of the gas spring changes the overall energy balance in the FPSE analysis. Leakage and heat transfer losses in the gas spring reduce the indicated power output from the engine, and the resultant thermal energy either increases the heat rejection or reduces the heat input. The assumption in this analysis is that all thermal energy from the gas spring losses ends up in the engine cooler. The physical implications of this assumption are that heat transferred to the gas spring walls and heat lost to the buffer space by leakage must be conducted or convected to the cooler.

After an engine has reached a periodic steady state, the heat input, heat output, and indicated power are calculated as

$$\overline{\dot{Q}}_{in} = \overline{\dot{W}}_e \ , \tag{2.16}$$

$$\overline{\dot{Q}}_{out} = -\overline{\dot{W}}_c - \overline{\dot{W}}_s \ , \tag{2.17}$$

$$\overline{\dot{W}}_{out} = \overline{\dot{W}}_e + \overline{\dot{W}}_c + \overline{\dot{W}}_s \ , \tag{2.18}$$

where

$$\overline{\dot{W}}_e = f \oint P_e \, dV_e \ , \tag{2.19}$$

$$\overline{\dot{W}}_c = f \oint P_c \, dV_c \ , \tag{2.20}$$

$$\overline{\dot{W}}_s = f \oint P_s \, dV_s \tag{2.21}$$

are the cyclic integrals of pressure and volume in the expansion, compression, and gas spring spaces. In general, the value of $\overline{\dot{W}}_e$ will be positive, and $\overline{\dot{W}}_c$ and $\overline{\dot{W}}_s$ will be negative. Note that the heat input is indeed equal to the sum of heat output and indicated power. Indicated thermal efficiency is calculated from Eqs. (2.16) and (2.18) as

$$\eta_{it} = \frac{\overline{\dot{W}}_{out}}{\overline{\dot{Q}}_{in}} \times 100\% \ . \tag{2.22}$$

3. LHA SOLUTION METHOD

All of the LHA solution procedures for kinematic engines described in ORNL/CON-155 (Ref. 1) apply equally well to free-piston machines. However, some additions are needed for FPSE applications because the operating frequency is not known at the beginning of the solution, and power piston amplitude cannot be solved for directly. The LHA methodology as it applies to FPSE dynamic problems is described in this chapter. To conserve space, some equations that are identical to ones already presented in ORNL/CON-155 (Ref. 1) will be referenced rather than repeated.

3.1 Equivalent Load Representation

Free-piston Stirling engines have driven a number of different loads, including dashpots, linear alternators, compressors, and hydraulic pumps. None of these loads display purely linear behavior; that is, the force they produce on the power piston is not a linear function of piston position and velocity. The linearity of a load has a significant impact on the stability of an FPSE, where stability is defined as the tendency of an engine to maintain constant piston strokes with no beating oscillations. Nonlinear loads are actually desirable in FPSE applications because they improve engine stability. For example, a load that produces a force proportional to velocity squared will result in greater stability than a load with a force directly proportional to velocity.

An FPSE analysis cannot completely ignore load nonlinearities because of their impact on engine stability. In the LHA solution, the load is initially assumed to be linear so that the differential equations can be solved in almost closed form. Later in the LHA solution, load nonlinearities are included during an FPSE/load matching analysis. All loads are initially represented by an equivalent linear spring and dashpot. The load force in Eq. (2.9) is assumed to have the form

$$F_l = -c_{ls} X_p - c_{ld} \frac{d X_p}{dt} , \tag{3.1}$$

where c_{1s} and c_{1d} are the equivalent spring and damping coefficients. The equivalent load spring accounts for the reactive forces that the load produces on the power piston. Negative values of c_{1s} can be used if the load acts like additional inertia in the system. The equivalent load dashpot accounts for the power absorbed by the load.

3.2 Nondimensional Equations

To simplify subsequent analysis, it is convenient to deal with the governing equations in dimensionless form. Many of the dimensionless variables and parameters were defined in ORNL/CON-155 (Ref. 1) [Eqs. (3.10)–(3.18)]. Additional dimensionless parameters are defined below.

Rate constants:

$$h^*_s = \frac{h_s \, \bar{A}_{ss}}{\omega \, \bar{m}_s \, c_v} , \qquad k^*_{ms} = \frac{k_{ms} \, \bar{P}_w}{\omega \, \bar{m}_s} . \tag{3.2}$$

Independent variables:

$$m^*_s = \frac{m_s}{\bar{m}_s} , \qquad T^*_s = \frac{T_s}{\bar{T}_s} . \tag{3.3}$$

Dependent variables:

$$P^*_s = \frac{P_s}{\bar{P}_w} , \qquad V^*_s = \frac{V_s}{\bar{V}_s} . \tag{3.4}$$

Temperature constants:

$$\bar{T}^*_{ws} = \frac{\bar{T}_{ws}}{\bar{T}_s} . \tag{3.5}$$

Enthalpy flux temperature variables:

$$T^*_{s\ flux} = \frac{T_{s\ flux}}{\overline{T}_s} . \tag{3.6}$$

Volume constants:

$$a_4 = \frac{A_r X_{pm}}{\overline{V}_s} . \tag{3.7}$$

Average performance parameters:

$$\overline{\dot{H}}^*_s = \frac{\overline{\dot{H}}_s}{c_v \overline{m}_s \overline{T}_s \omega} , \quad \overline{\dot{Q}}^*_{ws} = \frac{\overline{\dot{Q}}_{ws}}{c_v \overline{m}_s \overline{T}_s \omega} , \quad \overline{\dot{W}}^*_s = \frac{(\gamma - 1)\overline{\dot{W}}_s}{\overline{P}_w \overline{V}_s \omega} . \tag{3.8}$$

Area constants:

$$a_{11} = \frac{A_d}{A_p} , \quad a_{12} = \frac{A_r}{A_p} , \quad a_{13} = \frac{A_d - A_r}{A_p} . \tag{3.9}$$

Dynamic mass constants:

$$m^*_{pp} = \frac{m_{pp}\ \omega^2\ X_{pm}}{\overline{P}_w\ A_p} , \quad m^*_{dp} = \frac{m_{dp}\ \omega^2\ X_{pm}}{\overline{P}_w\ A_p} . \tag{3.10}$$

Load coefficients:

$$c^*_{1s} = \frac{c_{1s}\ X_{pm}}{\overline{P}_w\ A_p} , \quad c^*_{1d} = \frac{c_{1d}\ (60\ \pi)\ X_{pm}}{\overline{P}_w\ A_p} . \tag{3.11}$$

Using the dimensionless parameters defined previously and the linearized ideal gas laws

$$
\begin{aligned}
P_e^* &= m_e^* + T_e^* - V_e^* , \\
P_d^* &= m_d^* , \\
P_c^* &= m_c^* + T_c^* - V_c^* , \\
P_s^* &= m_s^* + T_s^* - V_s^* ,
\end{aligned}
\tag{3.12}
$$

the governing equations [Eqs. (2.1)–(2.12)] transform into a system of dimensionless differential equations

$$\frac{\bar{m}_e}{\bar{m}_w} k_{pe}^* \frac{dm_e^*}{dt^*} = m_d^* - m_e^* - T_e^* + V_e^* , \tag{3.13}$$

$$\frac{\bar{m}_e}{\bar{m}_w} k_{pc}^* \frac{dm_e^*}{dt^*} + \frac{\bar{m}_d}{\bar{m}_w} k_{pc}^* \frac{dm_d^*}{dt^*} = m_c^* + T_c^* - V_c^* - m_d^* , \tag{3.14}$$

$$\frac{\bar{m}_e}{\bar{m}_w} \frac{dm_e^*}{dt^*} + \frac{\bar{m}_d}{\bar{m}_w} \frac{dm_d^*}{dt^*} + \frac{\bar{m}_c}{\bar{m}_w} \frac{dm_c^*}{dt^*} = k_{mc}^* (1 - m_c^* - T_c^* + V_c^*) , \tag{3.15}$$

$$\frac{d(m_e^* T_e^*)}{dt^*} + (\gamma - 1)(m_e^* + T_e^* - V_e^*) \frac{dV_e^*}{dt^*} = \gamma T_e^* \text{ flux } \frac{dm_e^*}{dt^*} + h_e^* (\bar{T}_{we}^* - T_e^*) , \tag{3.16}$$

$$\frac{d(m_c^* T_c^*)}{dt^*} + (\gamma - 1) (m_c^* + T_c^* - V_c^*) \frac{dV_c^*}{dt^*} = \gamma T_c^* \text{ flux } \frac{dm_c^*}{dt^*} + h_c^* (\bar{T}_{wc}^* - T_c^*) , \tag{3.17}$$

$$m^*_{dp} \frac{d^2X^*_d}{dt^{*2}} = a_{13}\,(m^*_c + T^*_c - V^*_c) + a_{12}\,(m^*_s + T^*_s - V^*_s)$$

$$- a_{11}\,(m^*_e + T^*_e - V^*_e)\ , \qquad (3.18)$$

$$m^*_{pp} \frac{d^2X^*_p}{dt^{*2}} = (1 - m^*_c - T^*_c + V^*_c) - c^*_{1s}\,X^*_p - c^*_{1d}\,\frac{\omega}{60\pi}\,\frac{dX^*_p}{dt^*}\ , \qquad (3.19)$$

$$\frac{dm^*_s}{dt^*} = k^*_{ms}\,(1 - m^*_s - T^*_s + V^*_s)\ , \qquad (3.20)$$

$$\frac{d(m^*_s T^*_s)}{dt^*} + (\gamma - 1)(m^*_s + T^*_s - V^*_s)\,\frac{dV^*_s}{dt^*} = \gamma\,T^*_{s\ \mathrm{flux}}\,\frac{dm^*_s}{dt^*}$$

$$+ h^*_s\,(\overline{T}^*_{ws} - T^*_S)\ , \qquad (3.21)$$

where the dimensionless enthalpy flux temperatures are

$$T^*_{e\ \mathrm{flux}} = \begin{cases} T^*_H\ , & dm^*_e > 0 \\ T^*_e\ , & dm^*_e < 0 \end{cases}\ , \qquad (3.22)$$

$$T^*_{c\ \mathrm{flux}} = \begin{cases} T^*_K\ , & dm^*_c > 0 \\ T^*_c\ , & dm^*_c < 0 \end{cases}\ , \qquad (3.23)$$

$$T^*_{s\ \mathrm{flux}} = \begin{cases} T_K/\overline{T}_s\ , & dm^*_s > 0 \\ T^*_s\ , & dm^*_s < 0 \end{cases}\ . \qquad (3.24)$$

3.3 Harmonic Oscillations

The nine governing equations [Eqs. (3.13)–(3.24)] will contain only constants and the nine independent variables, after the volume variables are replaced with dimensionless forms of Eqs. (2.13)–(2.15)

$$V_e^* = 1 - a_1 X_d^* ,$$

$$V_c^* = 1 + a_2 X_d^* - a_3 X_p^* , \tag{3.25}$$

$$V_s^* = 1 + a_4 X_d^* .$$

Because steady state solutions are the only ones of interest, the nine independent variables are assumed to undergo simple harmonic oscillations. This assumption is very reasonable because the piston motions in most free-piston engines have waveforms that can be closely approximated by harmonic functions. The harmonic assumptions are as follows:

$$m_e^* = 1 + y_1 \sin t^* + y_2 \cos t^* ;$$

$$m_d^* = 1 + y_3 \sin t^* + y_4 \cos t^* ;$$

$$m_c^* = 1 + y_5 \sin t^* + y_6 \cos t^* ;$$

$$T_e^* = 1 + y_7 \sin t^* + y_8 \cos t^* ;$$

$$T_c^* = 1 + y_9 \sin t^* + y_{10} \cos t^* ; \tag{3.26}$$

$$X_d^* = y_{11} \sin t^* + y_{12} \cos t^* ;$$

$$X_p^* = y_{14} \sin t^*, \quad c_{1d}^* = y_{13}/y_{14} ;$$

$$m_s^* = 1 + y_{15} \sin t^* + y_{16} \cos t^* ;$$

$$T_s^* = 1 + y_{17} \sin t^* + y_{18} \cos t^* ;$$

where y_1 through y_{18} are all unknowns to be solved for simultaneously by the method of undetermined coefficients.

The dimensionless power piston position is arbitrarily defined to have only a sin t* component, with an unknown amplitude represented by y_{14}. All other variables contain both sin t* and cos t* components, with relative amplitudes that depend on the phase angle between the variables and power piston position. The equivalent load damping coefficient is treated as one of the unknowns, y_{13}. This mathematical procedure is necessary because of the linearized representation of the load and is very important to the success of the LHA solution. The physical explanation is that the magnitude of the equivalent load damping force is calculated so that it balances the power piston dynamic equation. Nonlinear load behavior is accounted for later in the LHA solution during an FPSE/load matching analysis.

When the assumed harmonic solutions [Eq. (3.26)] are substituted into the governing equations [Eqs. (3.13)–(3.24)], the resulting instantaneous equations will be in harmonic form except for the instantaneous power, internal energy, and enthalpy flux terms in the energy equations, which will contain products of sin t* and cos t*. These nonharmonic terms are replaced by truncated Fourier series. The procedure for truncated Fourier series expansion of each nonharmonic term was described in detail in ORNL/CON-155 (Ref. 1) and will not be repeated here.

3.4 Integrated Energy Equations

After the nonharmonic terms are replaced by truncated Fourier series, the instantaneous energy equations [Eqs. (3.16), (3.17), (3.21)] are separated into two systems — integrated and fluctuating equations. The system of integrated energy equations comes from the constant terms (zero-order coefficients) in the Fourier expansions, and each equation represents the steady state average energy balance for a control volume.

The integrated energy equations in nondimensional form are

$$\overline{\dot{H}^*_e} + \overline{\dot{Q}^*_{we}} = \overline{\dot{W}^*_e} \ ,$$

$$\overline{\dot{H}^*_c} + \overline{\dot{Q}^*_{wc}} = \overline{\dot{W}^*_c} \ , \tag{3.27}$$

$$\overline{\dot{H}^*_s} + \overline{\dot{Q}^*_{ws}} = \overline{\dot{W}^*_s} \ ,$$

where the average energy flow rates in the expansion and compression spaces were defined in ORNL/CON-155 (Ref. 1) [Eqs. (3.44), (3.56), (3.59), and (3.78)—(3.80)]. The average energy flow rates in the gas spring are

$$\overline{\dot{H}}_s = (c_v \overline{m}_s \overline{T}_s \omega)\ \overline{\dot{H}^*_s} = Z1(5)\ (T_K - \overline{T}_s) + Z1(6) \ ,$$

$$\overline{\dot{Q}}_{ws} = (c_v \overline{m}_s \overline{T}_s \omega)\ \overline{\dot{Q}^*_{ws}} = h_s\ \overline{A}_{ss}\ (\overline{T}_{ws} - \overline{T}_s) \ ,$$

$$\overline{\dot{W}}_s = \left(\frac{\overline{P}_w\ \overline{V}_s\ \omega}{\gamma - 1}\right)\ \overline{\dot{W}^*_s} = \frac{\omega}{2}\ \overline{P}_w \overline{V}_s\ a_4\ [y_{11}(y_{16} + y_{18}) - y_{12}\ (y_{15} + y_{17})] \ , \tag{3.28}$$

where

$$Z1(5) = \frac{\omega}{\pi}\ c_p\ \overline{m}_s \sqrt{y_{15}^2 + y_{16}^2} \ ,$$

$$Z1(6) = \frac{\gamma}{4(\gamma - 1)}\ \omega\ \overline{P}_w\ \overline{V}_s\ (y_{15}\ y_{18} - y_{16}\ y_{17}) \ . \tag{3.29}$$

After the unknowns (y_1 to y_{18}) have been determined, the integrated energy equations are rearranged to calculate the mean gas temperatures

$$\overline{T}_e = \frac{Z1(1)T_H + Z1(2) + h_e \overline{A}_{se} \overline{T}_{we} - \overline{\dot{W}}_e}{Z1(1) + h_e \overline{A}_{se}} ,$$

$$\overline{T}_c = \frac{Z1(3)T_K + Z1(4) + h_c \overline{A}_{sc} \overline{T}_{wc} - \overline{\dot{W}}_c}{Z1(3) + h_c \overline{A}_{sc}} , \qquad (3.30)$$

$$\overline{T}_s = \frac{Z1(5)T_K + Z1(6) + h_s \overline{A}_{ss} \overline{T}_{ws} - \overline{\dot{W}}_s}{Z1(5) + h_s \overline{A}_{ss}} ,$$

where Z1(1) to Z1(4) were defined in ORNL/CON-155 (Ref. 1) [Eqs. (3.83)–(3.86)]. The solution for the unknowns is discussed in Sect. 3.5.

3.5 Homogeneous Algebraic Equations

Taking the difference between the instantaneous and integrated equations results in the system of fluctuating equations. The general form of each fluctuating equation is

$$\Sigma \sin(\omega t) \text{ terms} + \Sigma \cos(\omega t) \text{ terms} = 0 . \qquad (3.31)$$

Because sine and cosine are orthogonal functions, a solution exists at all times only if

$$\Sigma \sin(\omega t) \text{ terms} = 0 ,$$

$$\Sigma \cos(\omega t) \text{ terms} = 0 . \qquad (3.32)$$

This leads to a set of homogeneous algebraic equations with y_1 to y_{18} as unknowns, which may be represented by an 18 × 18 matrix:

$$
\begin{bmatrix}
1 & -\frac{\bar{m}_e}{\bar{m}_w}k^*_{pe} & -1 & 0 & 0 & 0 & 1 & 0 & 0 & 0 & a_1 & 0 & 0 & 0 & 0 & 0 & 0 & 0 \\
\frac{\bar{m}_e}{\bar{m}_w}k^*_{pe} & 1 & 0 & -1 & 0 & 0 & 0 & 1 & 0 & 0 & 0 & a_1 & 0 & 0 & 0 & 0 & 0 & 0 \\
0 & -\frac{\bar{m}_e}{\bar{m}_w}k^*_{pc} & 1 & -\frac{\bar{m}_d}{\bar{m}_w}k^*_{pc} & -1 & 0 & 0 & 0 & -1 & 0 & a_2 & 0 & 0 & -a_3 & 0 & 0 & 0 & 0 \\
\frac{\bar{m}_e}{\bar{m}_w}k^*_{pc} & 0 & \frac{\bar{m}_d}{\bar{m}_w}k^*_{pc} & 1 & 0 & -1 & 0 & 0 & 0 & -1 & 0 & a_2 & 0 & 0 & 0 & 0 & 0 & 0 \\
0 & -\frac{\bar{m}_e}{\bar{m}_w} & 0 & -\frac{\bar{m}_d}{\bar{m}_w} & k^*_{mc} & -\frac{\bar{m}_c}{\bar{m}_w} & 0 & 0 & k^*_{mc} & 0 & -a_2k^*_{mc} & 0 & 0 & a_3k^*_{mc} & 0 & 0 & 0 & 0 \\
\frac{\bar{m}_e}{\bar{m}_w} & 0 & \frac{\bar{m}_d}{\bar{m}_w} & 0 & \frac{\bar{m}_c}{\bar{m}_w} & k^*_{mc} & 0 & 0 & 0 & k^*_{mc} & 0 & -a_2k^*_{mc} & 0 & 0 & 0 & 0 & 0 & 0 \\
D(7,1) & D(7,2) & 0 & 0 & 0 & 0 & h^*_e & -1 & 0 & 0 & 0 & (\gamma-1)a_1 & 0 & 0 & 0 & 0 & 0 & 0 \\
D(8,1) & D(8,2) & 0 & 0 & 0 & 0 & 1 & h^*_e & 0 & 0 & -(\gamma-1)a_1 & 0 & 0 & 0 & 0 & 0 & 0 & 0 \\
0 & 0 & 0 & 0 & D(9,5) & D(9,6) & 0 & 0 & h^*_c & -1 & 0 & -(\gamma-1)a_2 & 0 & 0 & 0 & 0 & 0 & 0 \\
0 & 0 & 0 & 0 & D(10,5) & D(10,6) & 0 & 0 & 1 & h^*_c & (\gamma-1)a_2 & 0 & 0 & -(\gamma-1)a_3 & 0 & 0 & 0 & 0 \\
a_{11} & 0 & 0 & 0 & -a_{13} & 0 & a_{11} & 0 & -a_{13} & 0 & D(11,11) & 0 & 0 & -a_3a_{13} & -a_{12} & 0 & -a_{12} & 0 \\
0 & a_{11} & 0 & 0 & 0 & -a_{13} & 0 & a_{11} & 0 & -a_{13} & 0 & D(12,12) & 0 & 0 & 0 & -a_{12} & 0 & -a_{12} \\
0 & 0 & 0 & 0 & 1 & 0 & 0 & 0 & 1 & 0 & -a_2 & 0 & 0 & D(13,14) & 0 & 0 & 0 & 0 \\
0 & 0 & 0 & 0 & 0 & 1 & 0 & 0 & 0 & 1 & 0 & -a_2 & \frac{\omega}{60\pi} & 0 & 0 & 0 & 0 & 0 \\
0 & 0 & 0 & 0 & 0 & 0 & 0 & 0 & 0 & 0 & -a_4k^*_{ms} & 0 & 0 & 0 & k^*_{ms} & -1 & k^*_{ms} & 0 \\
0 & 0 & 0 & 0 & 0 & 0 & 0 & 0 & 0 & 0 & 0 & -a_4k^*_{ms} & 0 & 0 & 1 & k^*_{ms} & 0 & k^*_{ms} \\
0 & 0 & 0 & 0 & 0 & 0 & 0 & 0 & 0 & 0 & 0 & -(\gamma-1)a_4 & 0 & 0 & D(17,15) & D(17,16) & h^*_s & -1 \\
0 & 0 & 0 & 0 & 0 & 0 & 0 & 0 & 0 & 0 & (\gamma-1)a_4 & 0 & 0 & 0 & D(18,15) & D(18,16) & 1 & h^*_s
\end{bmatrix}
\begin{bmatrix}
y_1 \\ y_2 \\ y_3 \\ y_4 \\ y_5 \\ y_6 \\ y_7 \\ y_8 \\ y_9 \\ y_{10} \\ y_{11} \\ y_{12} \\ y_{13} \\ y_{14} \\ y_{15} \\ y_{16} \\ y_{17} \\ y_{18}
\end{bmatrix}
= 0, \quad (3.33)
$$

where

$$
\begin{aligned}
D(7,1) &= FF(1), \\
D(7,2) &= -1 + \gamma\ \tau_e + FF(2), \\
D(8,1) &= 1 - \gamma\ \tau_e + FF(3), \\
D(8,2) &= -FF(1), \\
D(9,5) &= FF(4), \\
D(9,6) &= -1 + \gamma\ \tau_c + FF(5), \\
D(10,5) &= 1 - \gamma\ \tau_c + FF(6), \\
D(10,6) &= -FF(4), \\
D(11,11) &= -m^*_{dp} + a_2 a_{13} + a_4 a_{12} + a_1 a_{11}\ , \\
D(12,12) &= D(11,11), \\
D(13,14) &= -m^*_{pp} + a_3 + c^*_{1s}\ , \\
D(17,15) &= FF(7), \\
D(17,16) &= -1 + \gamma\ \tau_s + FF(8), \\
D(18,15) &= 1 - \gamma\ \tau_s + FF(9), \\
D(18,16) &= -FF(7),
\end{aligned}
\tag{3.34}
$$

and the Fourier correction factors FF(1) to FF(6) were defined in ORNL/CON-155 (Ref. 1) [Eqs. (3.51), (3.52), (3.54), and (3.71)–(3.73)]. The three remaining Fourier correction factors for the gas spring are

$$
\begin{aligned}
FF(7) &= -\frac{2\gamma}{3\pi}\left(y_{18}\cos^3\theta_s - y_{17}\sin^3\theta_s\right)\ , \\
FF(8) &= \frac{2\gamma}{3\pi}\left[y_{17}\cos\theta_s\left(\sin^2\theta_s + 2\right) - y_{18}\sin^3\theta_s\right]\ , \\
FF(9) &= -\frac{2\gamma}{3\pi}\left[y_{17}\cos^3\theta_s - y_{18}\sin\theta_s\left(\cos^2\theta_s + 2\right)\right]\ ,
\end{aligned}
\tag{3.35}
$$

$$
\sin\theta_s = \frac{y_{15}}{\sqrt{y_{15}^2 + y_{16}^2}}\ ,
$$

$$
\cos\theta_s = \frac{y_{16}}{\sqrt{y_{15}^2 + y_{16}^2}}\ .
$$

The algebraic equations are written as a linear system even though some nonlinearities exist. Most of the elements of the coefficient matrix are zeros or constants. However, careful observation reveals that some of the coefficients in the matrix depend on the unknowns (y_1 to y_{18}); examples are elements that include the Fourier correction factors [FF(1) to FF(9)] or the mean gas temperatures ($\overline{T}_e$, $\overline{T}_c$, $\overline{T}_s$). Note that Eq. (3.33) does not contain the mean gas temperatures explicitly, but parameters such as the average masses of gas in the control volumes are calculated from the mean gas temperatures. The problem of algebraic nonlinearities is resolved by an iterative process where Eq. (3.33) is treated as a linear system during each iteration. The iterative calculations are described in Sect. 3.7.

The homogeneous system in Eq. (3.33) has a nontrivial solution only if the determinant of the coefficient matrix is zero. This condition is used to calculate engine angular frequency ω. Frequency appears explicitly in one element of the coefficient matrix and implicitly in elements that contain dimensionless parameters with * superscripts. The determinant, in theory, could be evaluated using a pencil and large quantities of paper, resulting in a complicated algebraic equation that could be solved for the characteristic frequency (or frequencies). However, standard matrix algebra subroutines are used to calculate determinants, and a numerical root-finding routine is used to find the characteristic frequencies where the determinant is zero.

A secant-bisection root-finding method is used in the LHA solution. The bisection logic ensures stable convergence while the secant method minimizes convergence time. The root-finding routine is initialized by specifying two frequencies (ω_{low},ω_{high}) that bound a point where the determinant is zero. Then the secant method is used to find the characteristic frequency where the determinant is zero. If the secant method becomes numerically unstable, the routine automatically shifts to the bisection method, but only until the secant method becomes stable again. If multiple characteristic frequencies exist, then the root-finding routine must be executed once for each zero crossing.

3.6 Nonhomogeneous Algebraic Equations

When the determinant of the coefficient matrix in Eq. (3.33) is zero, the number of independent equations is one less than the number of unknowns. Therefore, one of the 18 rows can be eliminated without loss of generality, after a characteristic frequency has been determined (using the procedure described in Sect. 3.5) and substituted into Eq. (3.33). It makes no difference from the theoretical viewpoint which row is eliminated, though there may be some practical limitations because of round off errors in the matrix algebra computations. In the LHA solution, row 14 is added to row 13 (which is allowable because the equations are linear), and then row 14 is deleted. This reduces the algebraic system from an (18 × 18) to a (17 × 18) matrix.

A unique solution for the 18 unknowns is not possible because there are only 17 independent equations; any solution for y_1 to y_{18} that satisfies the linear equations will also be a solution if all the unknowns are halved, doubled, or multiplied by any factor. The number of unknowns in the LHA solution is reduced to 17 by specifying a value for the power piston amplitude X_{pa} or in dimensionless form

$$y_{14} = \frac{X_{pa}}{X_{pm}} . \tag{3.36}$$

Column 14 in the matrix in Eq. (3.33) can then be multiplied by y_{14} and moved to the right-hand side. The result, after adding row 14 to row 13, deleting row 14, and moving column 14 is a (17 × 17) nonhomogeneous algebraic system:

$$
\begin{bmatrix}
1 & -\frac{\bar{m}_e}{\bar{m}_w}k^*_{pe} & -1 & 0 & 0 & 0 & 1 & 0 & 0 & 0 & a_1 & 0 & 0 & 0 & 0 & 0 & 0 \\
\frac{\bar{m}_e}{\bar{m}_w}k^*_{pe} & 1 & 0 & -1 & 0 & 0 & 0 & 1 & 0 & 0 & 0 & a_1 & 0 & 0 & 0 & 0 & 0 \\
0 & -\frac{\bar{m}_e}{\bar{m}_w}k^*_{pc} & 1 & -\frac{\bar{m}_d}{\bar{m}_w}k^*_{pc} & -1 & 0 & 0 & 0 & -1 & 0 & a_2 & 0 & 0 & 0 & 0 & 0 & 0 \\
\frac{\bar{m}_e}{\bar{m}_w}k^*_{pc} & 0 & \frac{\bar{m}_d}{\bar{m}_w}k^*_{pc} & 1 & 0 & -1 & 0 & 0 & 0 & -1 & 0 & a_2 & 0 & 0 & 0 & 0 & 0 \\
0 & -\frac{\bar{m}_e}{\bar{m}_w} & 0 & -\frac{\bar{m}_d}{\bar{m}_w} & k^*_{mc} & -\frac{\bar{m}_c}{\bar{m}_w} & 0 & 0 & k^*_{mc} & 0 & -a_2k^*_{mc} & 0 & 0 & 0 & 0 & 0 & 0 \\
\frac{\bar{m}_e}{\bar{m}_w} & 0 & \frac{\bar{m}_d}{\bar{m}_w} & 0 & \frac{\bar{m}_c}{\bar{m}_w} & k^*_{mc} & 0 & 0 & 0 & k^*_{mc} & 0 & -a_2k^*_{mc} & 0 & 0 & 0 & 0 & 0 \\
D(7,1) & D(7,2) & 0 & 0 & 0 & 0 & h^*_e & -1 & 0 & 0 & 0 & (\gamma-1)a_1 & 0 & 0 & 0 & 0 & 0 \\
D(8,1) & D(8,2) & 0 & 0 & 0 & 0 & 1 & h^*_e & 0 & 0 & -(\gamma-1)a_1 & 0 & 0 & 0 & 0 & 0 & 0 \\
0 & 0 & 0 & 0 & D(9,5) & D(9,6) & 0 & 0 & h^*_c & -1 & 0 & -(\gamma-1)a_2 & 0 & 0 & 0 & 0 & 0 \\
0 & 0 & 0 & 0 & D(10,5) & D(10,6) & 0 & 0 & 1 & h^*_c & (\gamma-1)a_2 & 0 & 0 & 0 & 0 & 0 & 0 \\
a_{11} & 0 & 0 & 0 & -a_{13} & 0 & a_{11} & 0 & -a_{13} & 0 & D(11,11) & 0 & 0 & -a_{12} & 0 & -a_{12} & 0 \\
0 & a_{11} & 0 & 0 & 0 & -a_{13} & 0 & a_{11} & 0 & -a_{13} & 0 & D(12,12) & 0 & 0 & -a_{12} & 0 & -a_{12} \\
0 & 0 & 0 & 0 & 1 & 1 & 0 & 0 & 1 & 1 & -a_2 & -a_2 & \omega/60\pi & 0 & 0 & 0 & 0 \\
0 & 0 & 0 & 0 & 0 & 0 & 0 & 0 & 0 & 0 & -a_4k^*_{ms} & 0 & 0 & k^*_{ms} & -1 & k^*_{ms} & 0 \\
0 & 0 & 0 & 0 & 0 & 0 & 0 & 0 & 0 & 0 & 0 & -a_4k^*_{ms} & 0 & 1 & k^*_{ms} & 0 & k^*_{ms} \\
0 & 0 & 0 & 0 & 0 & 0 & 0 & 0 & 0 & 0 & 0 & -(\gamma-1)a_4 & 0 & D(17,15) & D(17,16) & h^*_s & -1 \\
0 & 0 & 0 & 0 & 0 & 0 & 0 & 0 & 0 & 0 & (\gamma-1)a_4 & 0 & 0 & D(18,15) & D(18,16) & 1 & h^*_s
\end{bmatrix}
\begin{bmatrix} y_1 \\ y_2 \\ y_3 \\ y_4 \\ y_5 \\ y_6 \\ y_7 \\ y_8 \\ y_9 \\ y_{10} \\ y_{11} \\ y_{12} \\ y_{13} \\ y_{15} \\ y_{16} \\ y_{17} \\ y_{18} \end{bmatrix}
=
\begin{bmatrix} 0 \\ 0 \\ a_3y_{14} \\ 0 \\ -a_3k^*_{mc}y_{14} \\ 0 \\ 0 \\ 0 \\ 0 \\ (\gamma-1)a_3y_{14} \\ a_3a_{13}y_{14} \\ 0 \\ -D(13,14)y_{14} \\ 0 \\ 0 \\ 0 \\ 0 \end{bmatrix}
\qquad (3.37)
$$

Standard matrix algebra subroutines are used to solve Eq. (3.37) for the other unknowns, y_1 to y_{13} and y_{15} to y_{18}. Displacer amplitude and phase angle (relative to the power piston motion) can then be calculated from equations that are easily derived from the original harmonic assumptions in Eq. (3.26),

$$X_{da} = X_{pm} \sqrt{y_{11}^2 + y_{12}^2} \,, \qquad \beta_d = \cos^{-1}\left(\frac{y_{11}}{\sqrt{y_{11}^2 + y_{12}^2}}\right). \tag{3.38}$$

All dynamic parameters have now been determined except for power piston amplitude. A unique solution for the power piston amplitude cannot be found until the engine analysis is matched to a specific load. This will be discussed in Sect. 3.8.

3.7 Successive Approximations

The (18 × 18) algebraic system in Eq. (3.33) is not completely linear because some elements in the coefficient matrix depend on the mean gas temperatures defined in Eq. (3.30) and the Fourier correction factors defined in Eq. (3.35) and in ORNL/CON-155 (Ref. 1) [Eqs. (3.51), (3.52), (3.54), and (3.71)–(3.73)]. An iterative solution process is needed for any case other than the isothermal one. A computer program was written in FORTRAN to perform the iterative calculations more efficiently and to check automatically for convergence. Two subroutines, called DECOMP and SOLVE, were called from a standard FORTRAN library to perform the matrix algebra, which simplified the programming effort. A listing of the computer program is given in Appendix D.

The procedure for the iterative calculations is shown in Fig. 3.1. The solution is initiated by assuming that the expansion, compression, and gas spring spaces are isothermal. The initial isothermal values for $\overline{T}_e$, $\overline{T}_c$, $\overline{T}_s$, and FF(1) to FF(9) are shown in Fig. 3.1. Frequency must also be assigned an initial value to provide a starting point for the root-finding routine.

ORNL–DWG 85–5342 ETD

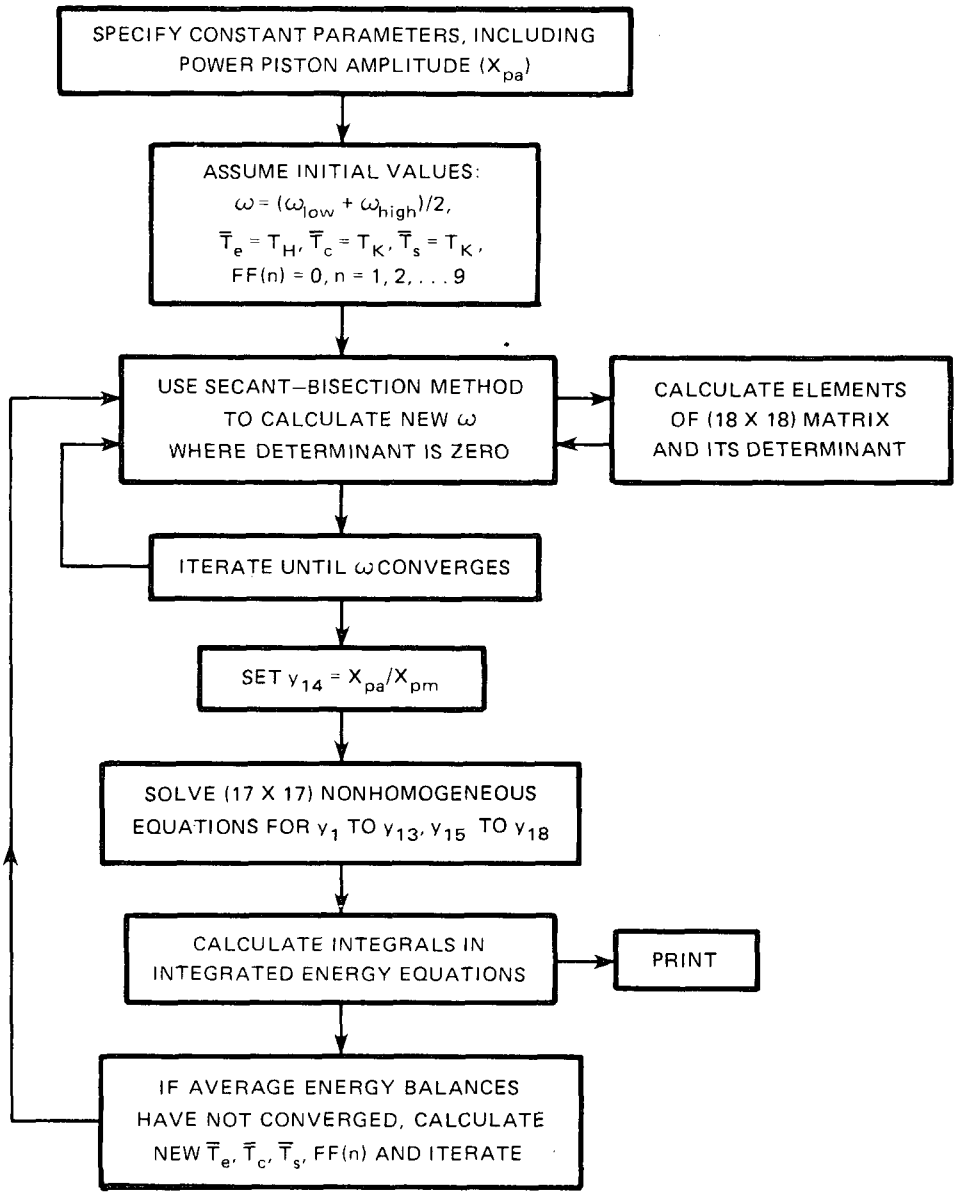

Fig. 3.1. Flow chart for successive approximations.

The computer program contains one large loop plus a smaller loop for frequency root finding. At the beginning of the large loop, the current values of $\bar{T}_e$, $\bar{T}_c$, $\bar{T}_s$, and FF(1) to FF(9) are used to calculate the matrix elements. Then the algebraic equations are solved to determine y_1 to y_{13} and y_{15} to y_{18}. At the end of the large loop, the integrals in the integrated energy equations are evaluated. If the average energy flow rates balance in the expansion and compression spaces, then the solution is

terminated. If the average energy balances have not converged, then new approximations for $\overline{T}_e$, $\overline{T}_c$, $\overline{T}_s$, and FF(1) to FF(9) are calculated from the new values of y_1 to y_{18}, and the calculations return to the top of the large loop for another iteration.

3.8. FPSE/Load Matching

Up to this point in the LHA solution, the force that the load produces on the power piston of the FPSE has been assumed to have the linear form shown in Eq. (3.1). This assumption was made temporarily so that the differential equations could be solved in almost closed form. To complete the solution, load nonlinearities must now be included in the analysis so that a unique value for power piston amplitude can be determined. The general procedure for calculating power piston amplitude is described in this section.

An FPSE will operate at a point where the power produced by the engine just matches the power absorbed by its load, as illustrated in Fig. 3.2. Power piston velocity amplitude ωX_{pa} is used as the abscissa in Fig. 3.2 because power is generally a function of both frequency and piston amplitude. In fact, the power absorbed by the generalized nonlinear dashpot load discussed in Appendix B is proportional to ωX_{pa} raised to a power, which will appear as a straight line when plotted in logarithmic coordinates. Many other loads and engines will also form nearly straight lines on logarithmic plots similar to those in Fig. 3.2.

The match point shown in Fig. 3.2 is stable because the FPSE has a natural tendency to operate at a constant power piston velocity amplitude. If the velocity amplitude is less than the match point, then the engine produces more power than the load absorbs, which tends to drive the velocity amplitude back toward the match point. If the velocity amplitude is greater than the match point, then the engine produces less power than the load absorbs, and this also drives the FPSE back toward the match point. If the engine line is steeper than the load line, then the FPSE will be unstable and will tend to either stall or overstroke.

A unique value for power piston amplitude is determined by matching the power produced by the FPSE to the power absorbed by the load. First,

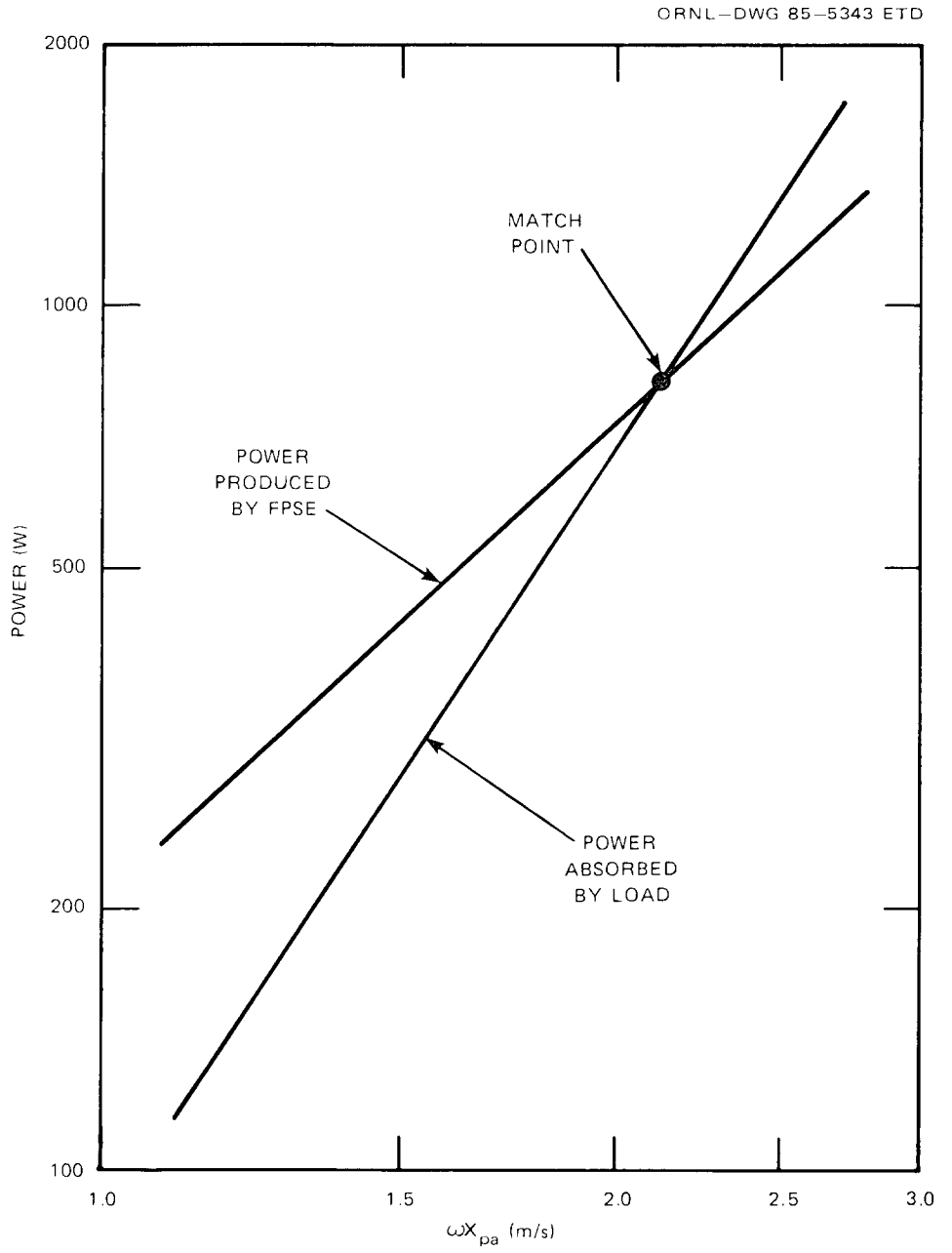

Fig. 3.2. Logarithmic plot showing FPSE/load matching example.

the power output of the engine is calculated for several different power piston amplitudes and is plotted vs power piston velocity amplitude. Then the power absorbed by the load (assuming it is driven sinusoidally) is determined either from actual measurements or from a nonlinear analysis, and it is also plotted vs power piston velocity amplitude. The point where the engine and load curves cross defines the solution for

power piston amplitude. Some specific FPSE/load matching examples are presented in Chap. 4.

The load must also be Fourier analyzed to determine the equivalent load spring coefficient c_{1s} defined in Eq. (3.1). A specific value for the equivalent spring coefficient is needed at the beginning of the LHA calculations. The Fourier analysis can be performed, in some instances, before specific values for frequency and power piston amplitude are known. In general, though, the load cannot be Fourier analyzed until frequency and power piston amplitude are determined at the end of the LHA calculations. The LHA calculations in these circumstances may have to be repeated a few times to ensure that proper values of the equivalent spring coefficient are used in the computations.

3.9 Summary of LHA Procedures

The LHA procedures can be summarized in 15 steps.

1. The working space is divided into control volumes.
2. Conservation equations (mass, momentum, energy) are written for the control volumes, and dynamic equations are written for the moving masses.
3. The force that the load produces on the power piston is represented by an equivalent linear spring and dashpot.
4. P, m, T, and V of gas in each control volume are assumed to have small amplitudes relative to their mean values. A linear form of the ideal gas law is used to express P as a sum of m, T, and V. V is expressed in terms of piston positions X.
5. The LHA method is restricted to steady state solutions. Solutions for the independent variables (m, T, and X) are assumed to have harmonic forms:

$$m = \overline{m} + y_1 \sin(\omega t) + y_2 \cos(\omega t) ,$$

$$T = \overline{T} + y_3 \sin(\omega t) + y_4 \cos(\omega t) , \text{ etc.}$$

The equivalent load damping coefficient is treated as one of the unknowns (y_1, y_2, etc.).

6. The harmonic solutions are substituted into the governing equations, and terms containing products of harmonic functions are replaced by truncated Fourier expansions.
7. The general form of each governing equation becomes

$$\Sigma \text{ constant terms} + \Sigma \sin(\omega t) \text{ terms} + \Sigma \cos(\omega t) \text{ terms} = 0.$$

A solution exists at all times only if

$$\Sigma \text{ constant terms} = 0,$$

$$\Sigma \sin(\omega t) \text{ terms} = 0,$$

$$\Sigma \cos(\omega t) \text{ terms} = 0.$$

8. The Σ sin (ωt) terms = 0 and Σ cos (ωt) terms = 0 equations form a homogeneous system of almost linear algebraic equations in terms of the unknowns (y_1, y_2, etc.). Products of the unknowns are treated in a quasi-linear manner through iteration.
9. The homogeneous algebraic system has a nontrivial solution only if the determinant of the coefficient matrix is zero. Frequency is calculated by finding the value or values that makes the determinant zero.
10. When the determinant is zero, the number of independent equations is one less than the number of unknowns. The homogeneous system is converted to a nonhomogeneous system by assuming a value for power piston amplitude (one of the unknowns). The other unknowns (y_1,y_2, etc.) are calculated with respect to power piston amplitude.
11. After y_1, y_2, etc. are obtained, the Σ constant terms equal 0 equations from the governing equations are solved to compute the values of other unknown parameters such as $\overline{T}_e$, $\overline{T}_c$, $\overline{T}_s$, etc.
12. A few iterations back to step 8 may be needed to include updated values for the quasi-linear approximations $\overline{T}_e$, $\overline{T}_c$, and $\overline{T}_s$.
13. The power produced by the engine is determined by evaluating the appropriate pressure-volume (PV) integral. Engine power is calculated for several different power piston velocity amplitudes.

14. The power absorbed by the load as a function of power piston velocity amplitude is determined either from actual measurements or from nonlinear analysis. The equivalent load spring coefficient is also determined by Fourier analysis.
15. Power piston amplitude is determined by finding the value where engine power just balances the power absorbed by the load. Iterations back to step 8 may be needed to account for coupling between frequency, power piston amplitude, and the equivalent spring coefficient.

4. LHA RESULTS AND DISCUSSION

Sample calculations and results of parametric sensitivity studies are presented to demonstrate the advantages of the LHA method for predicting FPSE dynamic behavior. References are made to other solution methods as part of a general discussion of analytical theory. However, a detailed comparison between the LHA method and other Stirling analysis methods is not intended. The presentation of results emphasizes the important dynamic parameters: frequency, power piston amplitude, displacer amplitude, and displacer phase angle. Thermodynamic performance (power, efficiency, etc.) is discussed to a lesser extent because those results were discussed previously in ORNL/CON-155 (Ref. 1).

Two types of LHA dynamic predictions are presented; to help avoid confusion they are labeled either (1) constrained piston amplitude mode or (2) free-dynamic mode. Constrained piston amplitude mode refers to the engine analysis before it is matched to a specific load. In the constrained piston amplitude mode, power piston amplitude is specified, and the other dynamic parameters are calculated with respect to this specified amplitude. This corresponds to step 12 in the LHA summary in Sect. 3.9. Free-dynamic mode refers to the complete analysis after the characteristics of a particular load have been matched to the behavior of the engine. In the free-dynamic mode, the load force as a function of piston position and velocity is specified rather than piston amplitude.

4.1 Base Case Predictions

All sample calculations in this report are based on the dimensions and typical operating conditions of the RE-1000 FPSE manufactured by Sunpower, Inc. and tested by NASA Lewis Research Center.[18] First sample calculations were performed for a base case and then sensitivity studies were performed around the base case. The engine dimensions and operating conditions selected for the base case are listed in Tables 4.1 and 4.2. The engine dimensions were estimated from a report published by Schreiber.[19] The operating conditions were selected to match a particular data point that has been measured by NASA Lewis but, unfortunately,

Table 4.1. RE-1000 engine dimensions and physical parameters

Maximum stroke, m	
Power piston	0.0420
Displacer	0.0404
Diameter, m	
Power piston	0.05723
Displacer	0.05723
Displacer rod	0.01666
Average volume, m^3	
Expansion space	63.6×10^{-6}
Heater	39.6×10^{-6}
Regenerator	59.4×10^{-6}
Cooler	28.5×10^{-6}
Compression space	103.6×10^{-6}
Displacer gas spring	31.8×10^{-6}
Average heat transfer surface area, m^2	
Expansion space	0.01392
Compression space	0.02292
Displacer gas spring	0.00979
Mass, kg	
Power piston	6.2
Displacer	0.426

Table 4.2. RE-1000 base case operating conditions

Working gas	Helium
Average pressure, Pa	7,085,000
Average wall temperture, K	
Heater	853
Expansion cylinder	853
Cooler	326
Compression cylinder	326
Displacer gas spring cylinder	326
Equivalent load spring coefficient, N/m	0

will not be published in their final report. The wall temperatures were adjusted to yield proper gas temperatures in the expansion and compression spaces.

Correlations for heat transfer, pressure drop, and seal leakage have not been included in the analysis as yet because the initial work was directed towards verifying the LHA mathematical assumptions rather than validating a computer code. The loss coefficients must be specified as part of the input data; the values used for the base case are listed in Table 4.3. The pressure drop and seal leakage coefficients were selected so that the analysis yields reasonable predictions for displacer amplitude, indicated power output, etc. The heat transfer coefficients were estimated from equations that were derived by Lee[20] as part of an analytical study of cylinder heat transfer. Lee's analysis showed that the heat transfer coefficient amplitude in nearly adiabatic cylinders is equal to the square root of two times the gas conductivity divided by the thermal boundary layer thickness for pure conduction. Heat transfer coefficients calculated from this pure conduction model for the RE-1000 base case operating conditions are ~1280 $W/(m^2 \cdot K)$ at the cold end and ~1050 $W/(m^2 \cdot K)$ at the hot end. Thus, the heat transfer coefficient values of 1000 $W/(m^2 \cdot K)$ shown in Table 4.3 appear to be the right order of magnitude.

Some of the RE-1000 base case results predicted by the LHA constrained piston amplitude mode are listed in Table 4.4. A comparison of

Table 4.3. RE-1000 base case loss coefficients

Cylinder heat transfer coefficient, $W/(m^2 \cdot K)$	
Expansion space, h_e	1×10^3
Compression space, h_c	1×10^3
Displacer gas spring, h_s	1×10^3
Pressure drop coefficient, $(Pa \cdot s)/kg$	
Between expansion and dead spaces, k_{pe}	1.5×10^6
Between compression and dead spaces, k_{pc}	1.5×10^6
Seal leakage coefficient, $kg/(Pa \cdot s)$	
Between compression and buffer spaces, k_{mc}	6.8×10^{-9}
Between gas spring and buffer spaces, k_{ms}	2.0×10^{-9}

Table 4.4. LHA constrained piston amplitude mode predictions for RE-1000 base case

Parameter	Base case
	Specified value
Power piston amplitude, X_{pa}, m	0.01300
	Computed values
Frequency, f, Hz	29.44
Displacer amplitude, X_{da}, m	0.01260
Displacer phase angle, β_d, deg	46.68
Compression space pressure amplitude, $\lvert P_c \rvert$, Pa	1,121,500
Compression space pressure phase angle, β_{Pc}, deg	−17.11
Expansion space average gas temperature, $\overline{T}_e$, K	824.8
Compression space average gas temperature, $\overline{T}_c$, K	336.6
Total heat input rate, $\overline{\dot{Q}}_{in}$, W	2852
Total heat output rate, $\overline{\dot{Q}}_{out}$, W	1832
Indicated power output, $\overline{\dot{W}}_{out}$, W	1020
Indicated thermal efficiency, η_{it}, %	35.76

these results and the NASA Lewis experimental data presented by Tew[12] shows that the base case dimensions, operating conditions, and loss coefficients listed in Tables 4.1–4.3 yield realistic LHA predictions for the RE-1000 FPSE. The LHA predictions for frequency, displacer amplitude, compression space pressure phase angle, and indicated power output are all within the range of experimental data presented by Tew. The LHA prediction for displacer phase angle is below the measured values; it is interesting to notice that the NASA Lewis predictions also show a similar trend. The indicated thermal efficiency predicted by LHA is high, but some of this discrepancy is because parasitic losses such as regenerator

reheat, appendix gap losses, and cylinder wall conduction are not included in the results in Table 4.4. Regenerator reheat losses are discussed as part of the imperfect heat exchanger analysis in Appendix A.

An easy way to visualize the dynamic behavior of an FPSE is to plot the dynamic equations in vector diagrams. The force balance for the displacer in Eq. (2.8) and the power piston in Eqs. (2.9) and (3.1) can be rearranged into the following forms:

$$(P_s A_r) + (-P_e A_r) + (P_c - P_e)(A_d - A_r) + \left(-m_{dp} \frac{d^2X_d}{dt^2}\right) = 0 ,$$

$$\begin{pmatrix}\text{gas}\\ \text{spring}\\ \text{force}\end{pmatrix} + \begin{pmatrix}\text{working}\\ \text{space}\\ \text{force}\end{pmatrix} + \begin{pmatrix}\text{pressure}\\ \text{drop force}\end{pmatrix} + \begin{pmatrix}\text{inertial}\\ \text{force}\end{pmatrix} = 0 , \tag{4.1}$$

$$(\overline{P_w} A_p) + (-P_c A_p) + \left(-c_{1s} X_p - c_{1d} \frac{dX_p}{dt}\right) + \left(-m_{pp} \frac{d^2X_p}{dt^2}\right) = 0 ,$$

$$\begin{pmatrix}\text{bounce}\\ \text{space}\\ \text{force}\end{pmatrix} + \begin{pmatrix}\text{working}\\ \text{space}\\ \text{force}\end{pmatrix} + (\text{load force}) + \begin{pmatrix}\text{inertial}\\ \text{force}\end{pmatrix} = 0 . \tag{4.2}$$

When these equations are plotted vectorially they form closed polygons because the sum of the forces is zero. Only the time-dependent portion of the forces are plotted in a vector diagram. Thus, the bounce space force vector will be zero because the bounce space pressure was assumed to be constant. Also the load force for the RE-1000 base case will be a pure damping force because the equivalent load spring coefficient was assumed to be zero.

The LHA predictions for the RE-1000 base case are presented in vector form in Fig. 4.1. The pressure vectors are shown relative to the position vectors in subplot a. The angle between the P_s and $-X_d$ vectors is caused by the heat transfer and seal leakage losses in the displacer gas spring. These two vectors would coincide if the gas spring was perfect. Another interesting observation is that the magnitude of the pressure drop $(P_c - P_e)$ vector is very small compared with the absolute magnitude of the pressure vectors.

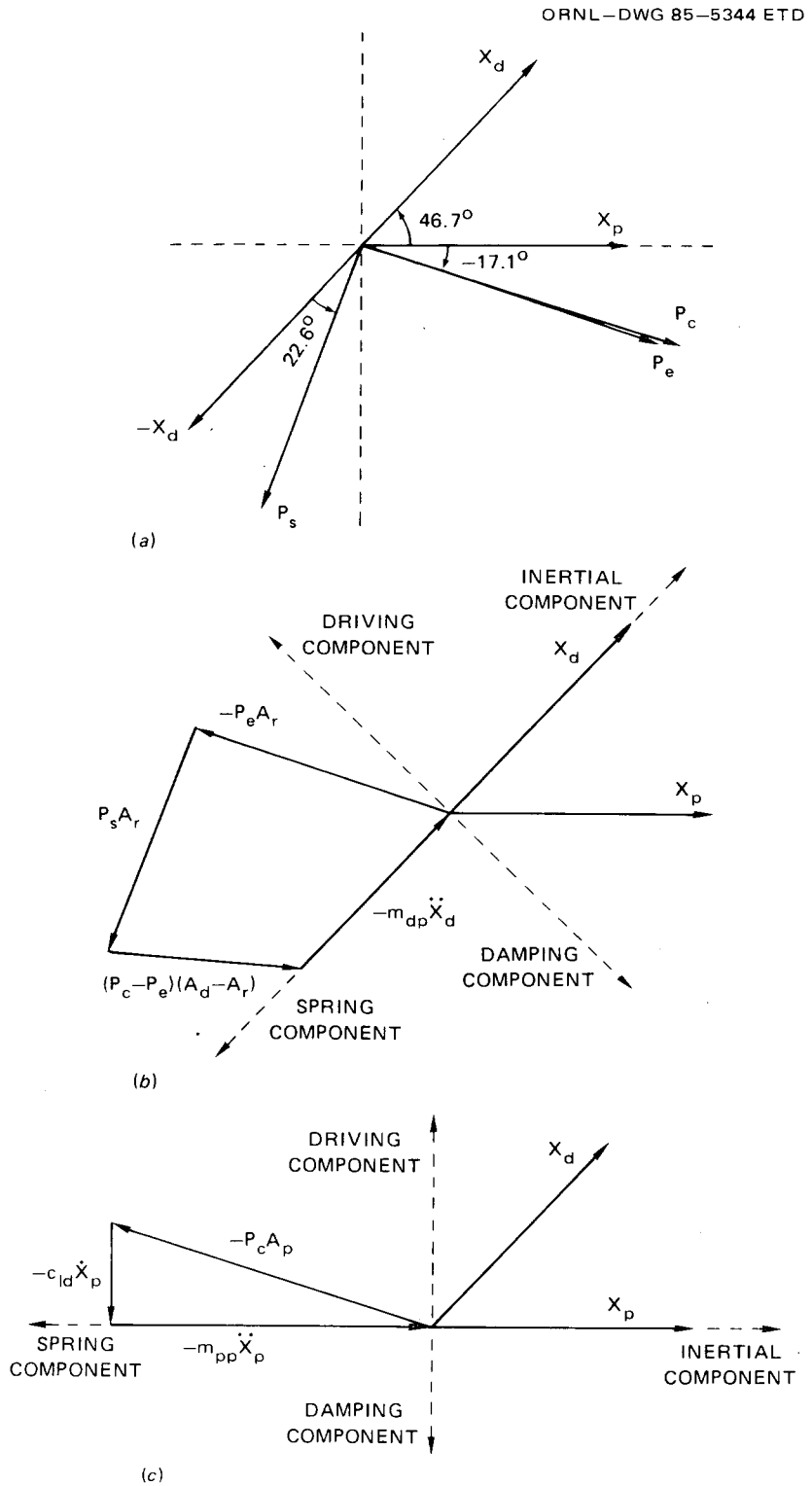

Fig. 4.1. Vector presentation of LHA results for RE-1000 base case; (*a*) position and pressure variables, (*b*) displacer force balance, (*c*) power piston force balance.

The displacer force balance is shown in subplot b along with axes that define the types of forces acting on the displacer. For example, a force vector that points in the $-X_d$ direction represents a pure spring force. The magnitude of the pressure drop force $[(P_c - P_e)(A_d - A_r)]$ vector is about equal to the magnitude of the other displacer force vectors. Even though the pressure drop across the displacer is fairly small, the pressure drop acts on a much larger area than the other pressures, and the resulting forces are about equal.

The power piston force balance is shown in subplot c along with axes that define the types of power piston forces. The dominant forces in the diagram are the spring component of the compression space force and the inertial force. The power piston behaves like a resonant spring-mass system, which is why the RE-1000 FPSE operates over a narrow and well-defined range of frequencies.

4.2 Comparison with Nonlinear Solution

The LHA method depends on a number of mathematical assumptions used to achieve an almost closed-form solution. The assumptions include linearization of the ideal gas law, representation of all variables with harmonic functions, and replacement of terms in the governing equations that contain products of harmonic functions with truncated Fourier expansions. To quantify the errors that are introduced by the LHA assumptions, an independent nonlinear solution of the same governing equations was obtained* and compared with the LHA solution. The results of this comparison for the complete thermodynamic/dynamic problem are presented below. The mathematical accuracy of the simpler thermodynamic version of the LHA solution was discussed in ORNL/CON-155 (Ref. 1).

The nonlinear solution of the governing equations [Eqs. (2.1)–(2.12)] was based on a Runge-Kutta numerical integration method. The Runge-Kutta method, like other explicit numerical methods, is a time-stepping integration where the variables at a new time are computed from previous values.

---

*The work on the nonlinear solution was performed by S. C. Byrd between June and August of 1984 as part of the Oak Ridge Associated Universities Summer Student Program at Oak Ridge National Laboratory.

Calculations proceed forward in small time steps over many cycles of the power piston until a steady state periodic solution is found. Existing IBM software, the Continuous System Modeling Program (CSMP),[21] was used to avoid unnecessary programming efforts in numerical integration. The CSMP software contains the Runge-Kutta integration logic as well as flexible subroutines for data input and data output in both tabular and graphical forms.

The comparison between the nonlinear CSMP and LHA solutions was done for a generalized nonlinear dashpot load. The load force in Eq. (2.9) was assumed to have the form

$$F_1 = -k_1 \dot{X}_p \, (\text{abs } \dot{X}_p)^{n-1} \; . \tag{4.3}$$

Equation (4.3) reduces to the simple linear dashpot formula when the dashpot load exponent n is equal to one. For $n > 1$, the load force is a power function of power piston velocity. The absolute value is needed in the force equation to ensure that negative values of velocity will not be raised to fractional powers. The free-dynamic mode of the LHA solution is needed for the comparison with the nonlinear CSMP solution because a specific load is involved. In the LHA free-dynamic mode, the power absorbed by the load as a function of power piston velocity amplitude is used in the FPSE/load matching analysis. A relationship for the power absorbed by the nonlinear dashpot load in Eq. (4.3) can be derived in closed form; this derivation is given in Appendix B.

The results of the comparison between the nonlinear CSMP and LHA predictions for the RE-1000 base case are presented in Tables 4.5–4.7 for three different dashpot load exponents: $n = 1.5$, 2.0, and 2.5. To make a valid comparison, the CSMP numerical predictions were Fourier analyzed to calculate cyclic averages, amplitudes, and phase angles. The calculation of the Fourier and PV integrals from the CSMP data was complicated by the fact that the operating frequency and, therefore, the number of time steps per engine cycle were not known at the beginning of CSMP computations. Problems also occurred because there was no logic in the CSMP solution to keep the power piston and displacer centered as helium leaked

Table 4.5. Comparison between nonlinear CSMP predictions and LHA free-dynamic mode predictions for $F_1 = -k_1 \dot{X}_p^{1.5}$ loads

Parameter	Example A		Example B		Example C	
			Specified values			
F_1, N	$-252.26\ \dot{X}_p^{1.5}$		$-239.65\ \dot{X}_p^{1.5}$		$-226.4\ \dot{X}_p^{1.5}$	
$\overline{V}_e$, m^3	65.6×10^{-6}		65.5×10^{-6}		64.9×10^{-6}	
$\overline{V}_c$, m^3	105.2×10^{-6}		105.6×10^{-6}		106.2×10^{-6}	
$\overline{V}_s$, m^3	31.6×10^{-6}		31.6×10^{-6}		31.7×10^{-6}	
			Computed values			
	CSMP	LHA	CSMP	LHA	CSMP	LHA
X_{pa}, m	0.01264	0.01263	0.01356	0.01355	0.01463	0.01466
f, Hz	29.39	29.36	29.41	29.38	29.43	29.38
X_{da}, m	0.01220	0.01218	0.01305	0.01304	0.01404	0.01406
β_d, deg	46.95	46.89	47.09	47.06	47.31	47.21
$\lvert P_c \rvert$, Pa	1,083,200	1,084,000	1,162,200	1,163,000	1,254,100	1,256,600
β_{Pc}, deg	−17.54	−17.12	−17.25	−16.87	−16.91	−16.58
$\overline{T}_e$, K	824.8	826.0	822.2	823.5	819.1	820.5
$\overline{T}_c$, K	335.4	336.1	336.3	337.1	337.4	338.3
$\overline{\dot{Q}}_{in}$, W	2710	2664	3110	3058	3605	3561
$\overline{\dot{Q}}_{out}$, W	1746	1708	2015	1973	2352	2313
$\overline{\dot{W}}_{out}$, W	964	956	1095	1085	1253	1248
η_{it}, %	35.57	35.89	35.20	35.50	34.75	35.05

past the gas seals. The CSMP numerical integration required 10 to 20 cycles to achieve a steady state periodic solution. During this time, enough preferential gas leakage occurred to cause the average volumes in the expansion, compression, and displacer gas spring spaces to change away from the RE-1000 base case values listed in Table 4.1. Preferential leakage is accounted for in the comparison by calculating the actual average volumes from the nonlinear CSMP predictions and using these CSMP

Table 4.6. Comparison between nonlinear CSMP predictions and LHA free-dynamic mode predictions for $F_1 = -k_1 \dot{X}_p^{2.0}$ loads

Parameter	Example D		Example E		Example F	
			Specified values			
F_1, N	$-217.0\ \dot{X}_p^{2.0}$		$-173.605\ \dot{X}_p^{2.0}$		$-147.0\ \dot{X}_p^{2.0}$	
$\overline{V}_e$, m^3	65.9×10^{-6}		65.0×10^{-6}		64.1×10^{-6}	
$\overline{V}_c$, m^3	104.6×10^{-6}		105.8×10^{-6}		106.9×10^{-6}	
$\overline{V}_s$, m^3	31.6×10^{-6}		31.7×10^{-6}		31.8×10^{-6}	
			Computed values			
	CSMP	LHA	CSMP	LHA	CSMP	LHA
X_{pa}, m	0.01080	0.01071	0.01299	0.01292	0.01483	0.01479
f, Hz	29.31	29.32	29.35	29.35	29.39	29.37
X_{da}, m	0.01049	0.01039	0.01254	0.01246	0.01425	0.01418
β_d, deg	46.75	46.58	47.16	46.94	47.53	47.26
$\lvert P_c \rvert$, Pa	926,000	920,000	1,117,200	1,107,700	1,275,500	1,266,300
β_{Pc}, deg	−18.21	−17.66	−17.04	−17.07	−16.53	−16.57
$\overline{T}_e$, K	830.1	831.1	823.9	825.2	818.5	820.2
$\overline{T}_c$, K	333.0	334.1	335.1	336.5	336.9	338.5
$\overline{\dot{Q}}_{in}$, W	1980	1930	2831	2782	3662	3617
$\overline{\dot{Q}}_{out}$, W	1246	1222	1811	1786	2375	2350
$\overline{\dot{W}}_{out}$, W	734	708	1020	996	1287	1267
η_{it}, %	37.06	36.70	36.02	35.80	35.15	35.03

values in the corresponding LHA calculations. The average volumes used in the LHA calculations are listed in Tables 4.5–4.7.

The mathematical accuracy of the LHA solution method should be highest for FPSE configurations where the load force is most nearly harmonic. The errors associated with the LHA assumptions should increase for load forces that are far from harmonic. This trend is clearly evident in Tables 4.5–4.7. The nonlinear CSMP and LHA predictions are nearly identical when the dashpot load exponent is n = 1.5. The differences between the two solutions increase, but still remain rather small,

Table 4.7. Comparison between nonlinear CSMP predictions and LHA free-dynamic mode predictions for $F_1 = -k_1 \dot{X}_p^{2.5}$ loads

Parameter	Example G		Example H		Example I	
			Specified values			
F_1, N	$-133.63\ \dot{X}_p^{2.5}$		$-121.48\ \dot{X}_p^{2.5}$		$-109.33\ \dot{X}_p^{2.5}$	
$\overline{V}_e$, m^3	65.4×10^{-6}		65.1×10^{-6}		64.8×10^{-6}	
$\overline{V}_c$, m^3	105.2×10^{-6}		105.6×10^{-6}		106.0×10^{-6}	
$\overline{V}_s$, m^3	31.6×10^{-6}		31.7×10^{-6}		31.7×10^{-6}	
			Computed values			
	CSMP	LHA	CSMP	LHA	CSMP	LHA
X_{pa}, m	0.01227	0.01213	0.01297	0.01283	0.01377	0.01364
f, Hz	29.29	29.35	29.31	29.35	29.33	29.37
X_{da}, m	0.01189	0.01172	0.01253	0.01238	0.01328	0.01312
β_d, deg	47.10	46.84	47.25	46.91	47.41	47.06
$\lvert P_c \rvert$, Pa	1,059,900	1,041,400	1,116,300	1,100,700	1,185,500	1,169,500
β_{Pc}, deg	−16.81	−17.26	−17.10	−17.09	−16.88	−16.87
$\overline{T}_e$, K	826.1	827.3	824.1	825.5	821.8	823.3
$\overline{T}_c$, K	338.8	335.6	334.5	336.4	335.2	337.2
$\overline{\dot{Q}}_{in}$, W	2531	2463	2816	2748	3162	3094
$\overline{\dot{Q}}_{out}$, W	1594	1574	1783	1763	2014	1996
$\overline{\dot{W}}_{out}$, W	937	889	1033	985	1148	1098
η_{it}, %	37.00	36.10	36.69	35.83	36.32	35.49

as the load becomes more nonlinear. Even when n = 2.5, the LHA predictions differ from the CSMP predictions by a maximum of only −1.1% for power piston amplitude, −1.4% for displacer amplitude, −0.35° for displacer phase angle, −5.1% for indicated power output, and −0.90 percentage points for indicated thermal efficiency. These differences are about equal to or less than the uncertainty associated with typical experimental measurements of these parameters.

The comparison between the LHA and CSMP solutions can be seen more clearly in Figs. 4.2 and 4.3. Figure 4.2 shows a plot of indicated power output vs power piston velocity amplitude in a logarithmic format similar to Fig. 3.2. Figure 4.3 shows frequency, displacer amplitude, and displacer phase angle as a function of power piston amplitude. When the LHA predictions from Tables 4.5–4.7 are plotted in the figures, they form unique curves with almost no scatter because the nonlinear dashpot loads are represented in the LHA method by equivalent linear dashpots. The linearity of the load does not affect the LHA results. The scatter of the CSMP data points in the figures indicates that the nonlinear CSMP

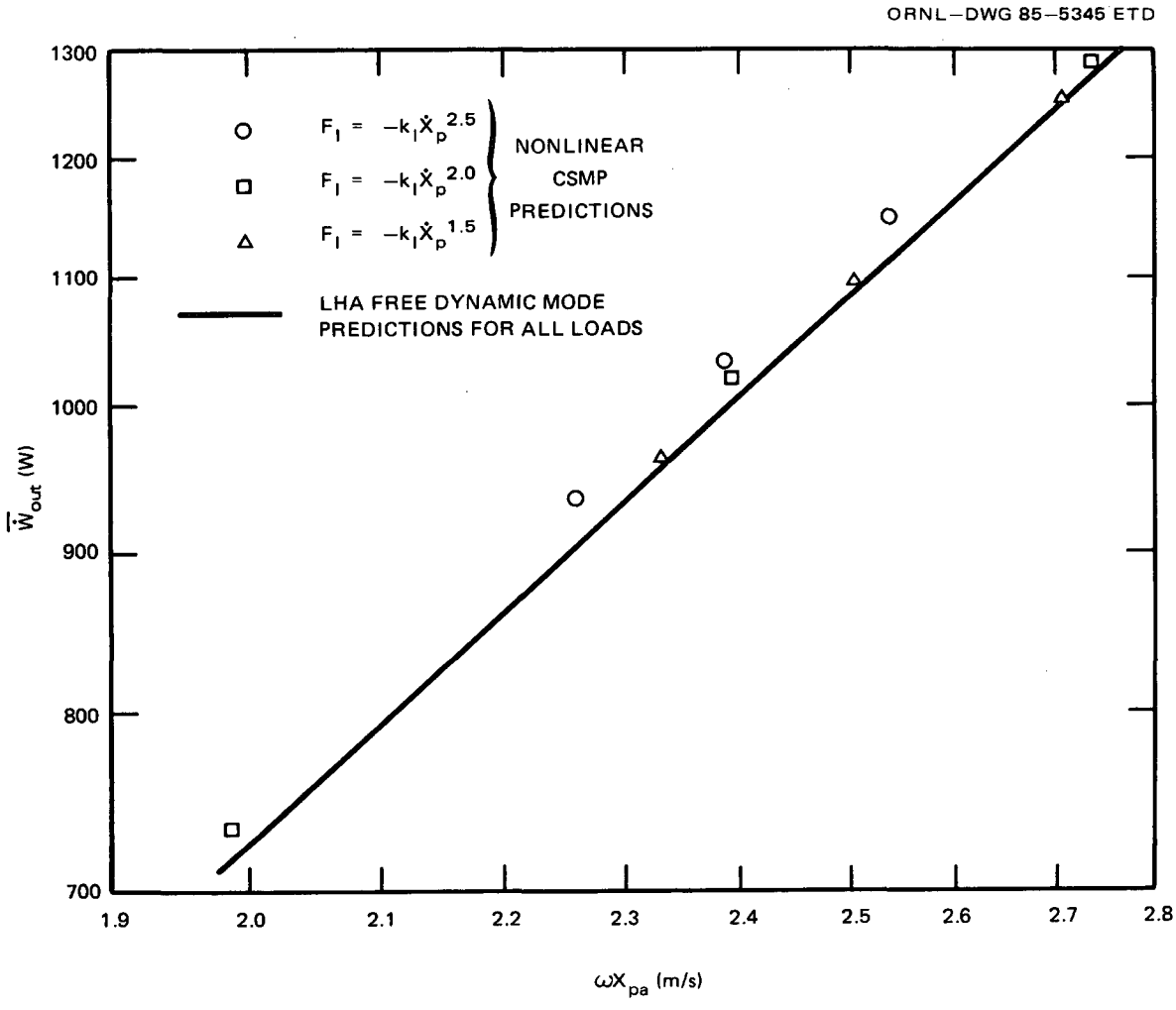

Fig. 4.2. Logarithmic plot of CSMP and LHA predictions for indicated power output vs power piston velocity amplitude.

ORNL–DWG 85–5346 ETD

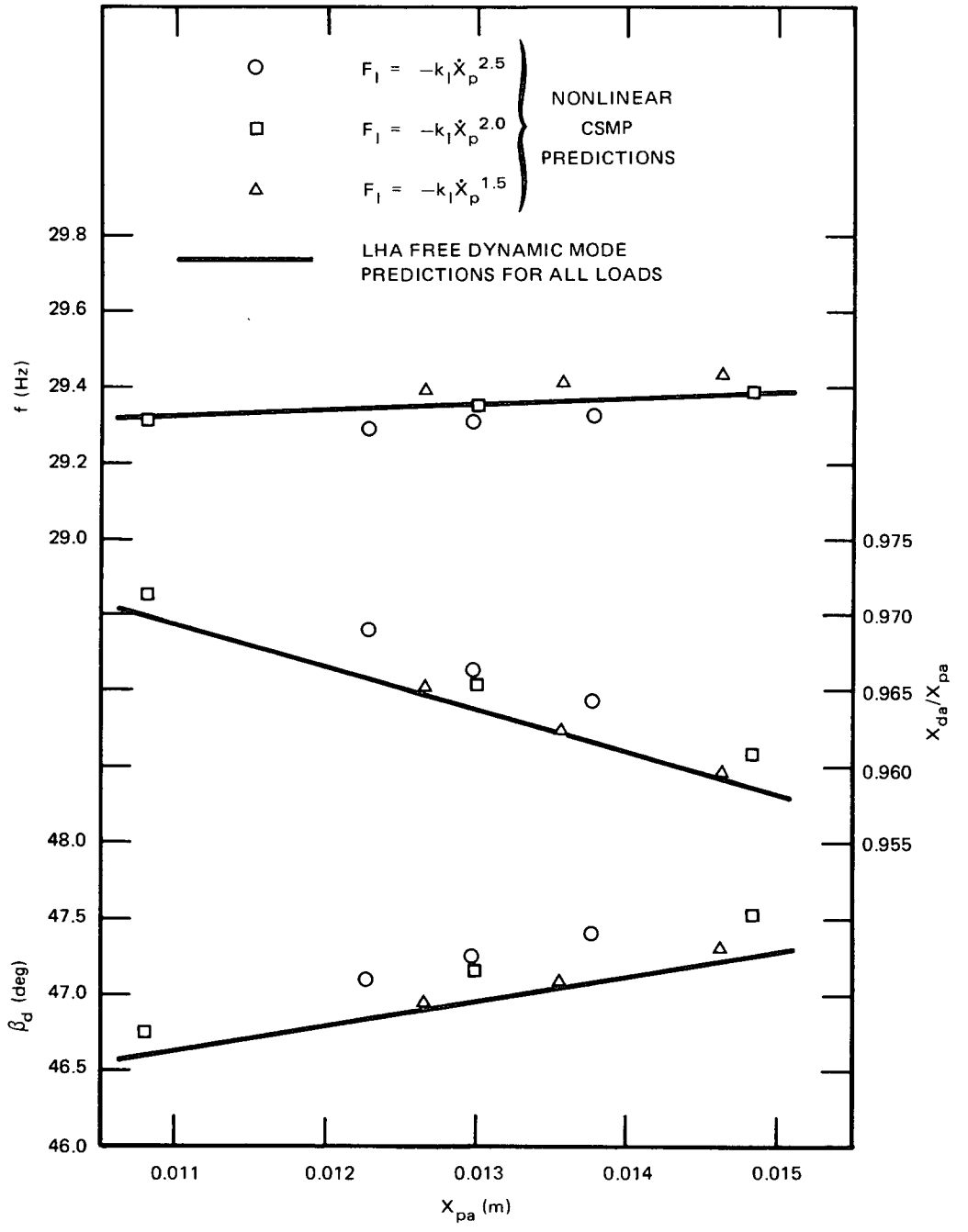

Fig. 4.3. CSMP and LHA predictions for frequency, displacer amplitude, and displacer phase angle vs power piston amplitude.

predictions are affected by the linearity of the load, though the effects are fairly small. The general conclusion is that the LHA solution method should have sufficient mathematical accuracy for most practical applications, even when the load has nonlinearities as strong as a dashpot with an exponent of n = 2.5.

The comparison between the LHA and nonlinear CSMP solutions also demonstrates the advantages that the LHA method has over numerical integrations. Execution times for the CSMP time-stepping integration were about 100 times longer than for the LHA solution. The long CSMP execution times were caused by two factors; short time steps were needed to ensure numerical accuracy and 10 to 20 cycles were required to reach steady state periodic solutions. When the LHA method is used, 100 different cases can be run in the same amount of time that it takes for a single case using the nonlinear CSMP method. This computational efficiency makes the LHA method ideal for optimization programs.

The LHA method also avoids problems with numerical instabilities that can occur in time-stepping integrations. The CSMP solution was found to be rather sensitive to the initial conditions that were selected to start the integration; some sets of initial conditions caused the CSMP integration to explode before a steady state periodic solution was found. The stability of the CSMP numerical method was also dependent on the linearity of the load. When CSMP solutions were attempted for linear dashpot loads (n = 1), more than 50 cycles were needed for convergence to steady state periodic solutions.

4.3 Adiabatic Cylinder Effects

Closed-form solutions to FPSE dynamic problems have been published previously by Urieli and Berchowitz,[8] Goldberg,[6] and others. These analyses were based on the assumption that the expansion and compression spaces in the engine behave isothermally, and gas springs were assumed to be adiabatic. We find that a significant error can occur if an isothermal calculation is used to represent a nearly adiabatic engine such as the RE-1000 FPSE. The compression space pressure produces all of the restoring (spring) force on the power piston in the RE-1000 engine, as is

shown in the power piston force balance in Fig. 4.1. It was shown previously in ORNL/CON-155 (Ref. 1) that an isothermal analysis predicts a smaller compression space pressure amplitude than an adiabatic analysis. An isothermal analysis of the nearly adiabatic RE-1000 FPSE will therefore result in frequency predictions that are too low because the compression space pressure amplitude prediction and associated power piston spring force will be too small.

The errors associated with an isothermal analysis of an adiabatic FPSE were demonstrated by using the LHA method to perform a sensitivity study around the RE-1000 base case. LHA constrained piston amplitude mode results are listed in Table 4.8 for cases where the expansion and compression spaces are either isothermal ($h \rightarrow \infty$) or adiabatic ($h = 0$) and

Table 4.8. LHA constrained piston amplitude mode predictions for RE-1000 base case with isothermal or adiabatic cylinders

Parameter	Isothermal cylinders	Adiabatic cylinders
	Specified values	
X_{pa}, m	0.01300	0.01300
h_s, W/(m^2·K)	0	0
h_e, W/(m^2·K)	1×10^8	0
h_c, W/(m^2·K)	1×10^8	0
	Computed values	
f, Hz	26.58	29.43
X_{da}, m	0.01127	0.01270
β_d, deg	51.44	46.88
$\lvert P_c \rvert$, Pa	921,400	1,123,500
β_{Pc}, deg	−18.44	−17.51
$\bar{\dot{W}}_{out}$, W	814	1045
η_{it}, %	40.98	36.15

the displacer gas spring is adiabatic. The frequency in the isothermal case is indeed −9.7% less than in the adiabatic case. Other predictions for the isothermal case differ from the adiabatic predictions by −11.3% for displacer amplitude, +4.56° for displacer phase angle, and −22.1% for indicated power output. The low power output prediction is a combined effect of the low displacer amplitude and the low frequency.

The linearity of the load has a significant effect on the errors created by an isothermal analysis of an adiabatic FPSE. Table 4.9 lists LHA free-dynamic mode results for two nonlinear dashpot loads with dashpot load exponents of n = 1.5 and 2.5. The dashpot load coefficients were selected so that the power absorbed by the dashpots matched the

Table 4.9. LHA free-dynamic mode predictions for RE-1000 base case with isothermal or adiabatic cylinders

Parameter	n = 1.5; Isothermal cylinders	n = 1.5; Adiabatic cylinders	n = 2.5; Isothermal cylinders	n = 2.5; Adiabatic cylinders
		Specified values		
F_1, N	$-254.84\ \dot{X}_p^{1.5}$	$-254.84\ \dot{X}_p^{1.5}$	$-122.08\ \dot{X}_p^{2.5}$	$-122.08\ \dot{X}_p^{2.5}$
h_s, W/(m²•K)	0	0	0	0
h_e, W/(m²•K)	1×10^8	0	1×10^8	0
h_c, W/(m²•K)	1×10^8	0	1×10^8	0
		Computed values		
X_{pa}, m	0.01312	0.01300	0.01394	0.01300
f, Hz	26.58	29.43	26.58	29.43
X_{da}, m	0.01138	0.01270	0.01208	0.01270
β_d, deg	51.44	46.88	51.42	46.88
$\lvert P_c \rvert$, Pa	930,000	1,123,500	988,200	1,123,500
β_{Pc}, deg	−18.44	−17.51	−18.42	−17.51
$\overline{\dot{W}}_{out}$, W	829	1045	935	1045
η_{it}, %	40.97	36.15	40.96	36.15

power output of the adiabatic engine at a power piston amplitude of 0.013 m. For n = 1.5, the isothermal prediction for power piston amplitude is +0.9% larger than the adiabatic result; the error increases to +7.2% for n = 2.5. This increased error in the power piston amplitude reduces the indicated power output error from −20.7% for n = 1.5 to −10.5% for n = 2.5.

The effects of adiabatic cylinders are seen to be a rather complicated problem in free-piston Stirling engines. Adiabatic cylinders affect both the thermal and dynamic performance of an engine, and the magnitudes of these effects depend on the exact configuration of the FPSE and the linearity of the load. An important advantage of the LHA almost closed-form solution is its ability to account for adiabatic cylinders. The LHA method can also account for all finite cylinder heat transfer conditions between the isothermal and adiabatic extremes.

4.4 Sensitivity to Pressure Drop and Seal Leakage Losses

One of the major losses in a Stirling engine is the pressure drop loss in the regenerator and heat exchangers. Seal leakage losses can also be rather large in free-piston designs that contain clearance seals and gas centering ports. The LHA method can account for both pressure drop and seal leakage losses; and like cylinder heat transfer, these losses are included as a simultaneous part of the dynamic calculations. The losses are not computed separately and then added to the thermodynamic and dynamic calculations as they are in "second-order" analyses. These losses are included in a "third-order" manner, where all of the interactions between the losses and the thermal and dynamic behavior are accounted for. Some sample LHA calculations are presented in this section to show how pressure drop and seal leakage losses affect FPSE dynamic behavior.

The displacer force balance in Fig. 4.1 indicates that most of the damping force on the displacer is produced by the pressure difference between the compression and expansion spaces. If this pressure drop is reduced, then the displacer damping force is reduced and the displacer

amplitude should increase. The effect of reducing pressure drop is shown in Table 4.10, where the middle column is the RE-1000 base case predictions from Table 4.4, and the left and right columns are for higher and lower pressure drops, respectively. Both displacer amplitude and phase angle increase as the pressure drop is reduced. Indicated power and efficiency also increase as expected.

Table 4.10. LHA constrained piston amplitude mode predictions for the RE-1000 base case that show the effect of reducing pressure drop

Parameters	More pressure drop	Base case	Less pressure drop
		Specified values	
X_{pa}, m	0.01300	0.01300	0.01300
k_{pe}, (Pa•s)/kg	2.0×10^6	1.5×10^6	1.0×10^6
k_{pc}, (Pa•s)/kg	2.0×10^6	1.5×10^6	1.0×10^6
		Computed values	
f, Hz	29.77	29.44	28.60
X_{da}, m	0.01091	0.01260	0.01569
β_d, deg	43.47	46.68	49.33
$\lvert P_c \rvert$, Pa	1,120,300	1,121,500	1,125,700
β_{Pc}, deg	−11.80	−17.11	−26.03
$\bar{\dot{W}}_{out}$, W	716	1020	1483
η_{it}, %	31.43	35.76	39.51

These pressure drop trends have some important implications about the validation of FPSE computer codes. Many codes are "calibrated" to experimental data by adjusting the pressure drop correlations so that the indicated power and efficiency predictions agree with the experimental values. This process is fairly straightforward for kinematic Stirling engines. However, the calibration process is more complicated for an

FPSE dynamic code because the displacer amplitude and phase angle predictions must also agree with the experimental data.

Pressure drop in the heater does not have the same effect on FPSE dynamic behavior as pressure drop in the cooler. Even though the present LHA model is rather simple with only three control volumes and two pressure drop coefficients in the working space, the effect of shifting pressure drop from the heater to the cooler was simulated by lowering one pressure drop coefficient (k_{pe}) while raising the other (k_{pc}). The results are listed in Table 4.11, where the middle column is again the RE-1000 base case predictions. Displacer amplitude remains fairly constant, but displacer phase angle and indicated power drop from left to right.

Table 4.11. LHA constrained piston amplitude mode predictions for the RE-1000 base case that show the effect of shifting pressure drop from the heater to the cooler

Parameters	Pressure drop shifted towards heater	Base case	Pressure drop shifted towards cooler
		Specified values	
X_{pa}, m	0.01300	0.01300	0.01300
k_{pe}, (Pa•s)/kg	2.0×10^6	1.5×10^6	1.0×10^6
k_{pc}, (Pa•s)/kg	1.0×10^6	1.5×10^6	2.0×10^6
		Computed values	
f, Hz	29.98	29.44	28.92
X_{da}, m	0.01246	0.01260	0.01281
β_d, deg	50.54	46.68	43.31
$\lvert P_c \rvert$, Pa	1,166,400	1,121,500	1,080,900
β_{Pc}, deg	−17.57	−17.11	−16.81
$\overline{\dot{W}}_{out}$, W	1109	1020	950
η_{it}, %	35.98	35.76	35.68

The results from the left and right columns of Table 4.11 are shown more clearly in Fig. 4.4, where the displacer force balances are plotted in vector diagrams. The magnitude of the pressure drop force remains fairly constant, but the phase of the force with respect to displacer motion changes as pressure drop shifts from the heater to the cooler. Figure 4.4 indicates that the pressure drop force on the displacer has both damping and inertial components. Some second-order dynamic analyses, such as one published by Martini,[14] assume that pressure drop produces a pure damping force on the displacer. This assumption differs significantly from the behavior revealed by the LHA predictions, and it does not account for changes in the phase angle of the pressure drop force as pressure drop shifts from the heater to the cooler. Once again, this demonstrates how errors can occur when the thermodynamic losses are not included as a simultaneous part of the dynamic calculations.

The final LHA example is for power piston seal leakage. The compression space in the RE-1000 FPSE is separated from the bounce space by a clearance seal on the power piston. The effect of reducing helium leakage past the power piston seal is shown in Table 4.12. Displacer phase angle experiences a moderate reduction, while compression space pressure phase angle and indicated power and efficiency increase significantly. Because power piston seal leakage appears to have only a minor effect on the dynamic predictions, adjustment of the leakage correlation might provide a good way to calibrate FPSE computer codes so that indicated power and efficiency predictions agree with experimental values.

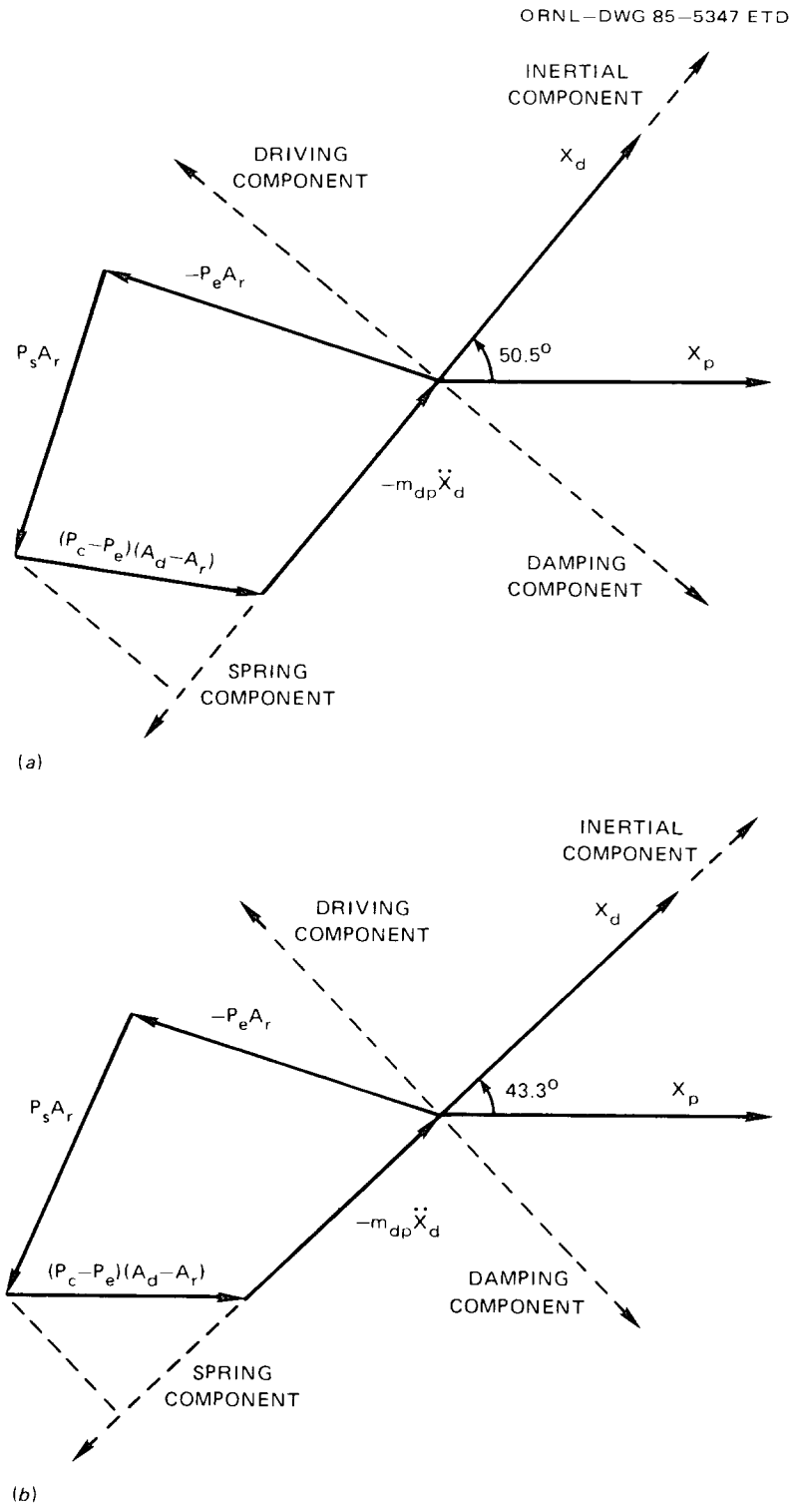

Fig. 4.4. Displacer force balances that show effect of shifting pressure drop from heater to cooler; (*a*) pressure drop shifted toward heater, $k_{pe} > k_{pc}$; (*b*) pressure drop shifted toward cooler, $k_{pc} > k_{pe}$.

Table 4.12. LHA constrained piston amplitude mode predictions for the RE-1000 base case that show the effect of reducing power piston seal leakage

Parameters	More seal leakage	Base case	Less seal leakage
		Specified values	
X_{pa}, m	0.01300	0.01300	0.01300
k_{mc}, kg/(Pa•s)	10.8×10^{-9}	6.8×10^{-9}	2.8×10^{-9}
		Computed values	
f, Hz	29.89	29.44	28.82
X_{da}, m	0.01267	0.01260	0.01250
β_d, deg	49.74	46.68	43.93
$\lvert P_c \rvert$, Pa	1,132,700	1,121,500	1,106,400
β_{Pc}, deg	−12.65	−17.11	−21.73
$\overline{\dot{W}}_{out}$, W	779	1020	1240
η_{it}, %	26.80	35.76	44.68

5. SUMMARY AND CONCLUSIONS

An almost closed-form solution method, the linear harmonic analysis, has been developed for the combined thermodynamic/dynamic problem that is associated with free-piston Stirling engines. The governing equations are differential because most of the parameters describing an FPSE (pressure, temperature, piston position, etc.) are time-dependent. The LHA method is based on three primary assumptions: (1) linearization of the ideal gas law, (2) representation of all time-dependent variables with harmonic functions, and (3) replacement of terms in the governing equations that contain products of harmonic functions with truncated Fourier series. The assumptions reduce the problem to a system of almost linear algebraic equations that are solved using standard matrix algebra, with iterations as required. The motivation for developing this simplified analytical method was not that it saves computer time (although it does do that), but that it reveals causes and effects much more effectively than a column of numerical output.

The present version of the LHA method was developed for the RE-1000 FPSE configuration. The RE-1000 engine contains a single power piston and a displacer sprung to the engine housing. The working space of the engine is divided into only three control volumes, and motion of the engine housing is neglected. However, the LHA method is not limited to such a simple representation, and more control volumes or dynamic equations could be added if they were desired. Cylinder heat transfer, pressure drop, and seal leakage losses are all included in the present version of the LHA. These losses are not calculated separately and then added to the analysis. They are included as a simultaneous part of the thermodynamic/dynamic calculations so that all of the interactions between the losses, thermal performance, and dynamic behavior are accounted for.

The time required for execution of the free-piston dynamic version of the LHA method is about 100 times less than the execution time required for an equivalent numerical integration method. Even with its speed, the LHA method has sufficient mathematical accuracy for most practical Stirling engine applications. The mathematical accuracy of the LHA

assumptions was verified by independently solving the same nonlinear equations using a numerical integration method and comparing the results with the LHA solution. The differences between the LHA and numerical predictions were <5% for all important parameters, which is about equal to or less than the uncertainty associated with typical Stirling engine experimental measurements. This combination of computational speed and mathematical accuracy makes the LHA method ideal for FPSE optimization programs.

In addition to speed, the LHA method has other advantages over time-stepping integration methods. Numerical techniques usually require some artistic guesswork to select step sizes and initial conditions so that the solution is numerically stable, mathematically accurate, and converges quickly to a periodic steady state. The closed-form analytical approach of the LHA method avoids these problems. The LHA method does require iterations, but the assumption of isothermal cylinders provides a good starting point for the calculations, and LHA convergence usually occurs in <20 iterations.

The LHA method also has advantages over other linear closed-form solution methods that have been developed for FPSE dynamic problems. All previously published closed-form solutions are second-order analyses where the losses are treated separately. The LHA method is a third-order analysis where the losses, as well as their interactions, are included intrinsically in the FPSE dynamic solution. Sample LHA calculations have shown that substantial errors in predicting dynamic behavior can occur if an isothermal calculation is used to represent an adiabatic FPSE. LHA predictions have also indicated that unrealistic assumptions about the pressure drop losses can lead to additional errors.

REFERENCES

1. N. C. J. Chen, F. P. Griffin, and C. D. West, *Linear Harmonic Analysis of Stirling Engine Thermodynamics*, ORNL/CON-155, Martin Marietta Energy Systems, Inc., Oak Ridge Natl. Lab., August 1984.

2. N. C. J. Chen, F. P. Griffin, and C. D. West, "Linear Harmonic Analysis for Stirling Machines and Second Law Analysis of Four Important Losses," pp. 1973–81 in *Proceedings of the 19th IECEC*, Paper No. 849141, 1984.

3. E. H. Cooke-Yarborough, *A Proposal for a Heat-Powered Non-Rotating Electrical Alternator*, AERE-M1881, AERE Harwell, Oxfordshire, U.K., 1967.

4. T. J. Marusak and W. S. Chiu, "The Matching of a Free Piston Stirling Engine Coupled with a Free Piston Linear Compressor for a Heat Pump Application," pp. 1820–5 in *Proceedings of the 13th IECEC*, Paper No. 789272, 1978.

5. D. M. Berchowitz and G. F. Wyatt-Mair, "Closed-Form Solutions for a Coupled Ideal Analysis of Free-Piston Stirling Engines," pp. 1114–9 in *Proceedings of the 14th IECEC*, Paper No. 799241, 1979.

6. L. F. Goldberg, "A State Space Analysis of a Symmetrical Compounded Free Piston Stirling Engine," pp. 2251–7 in *Proceedings of the 15th IECEC*, Paper No. 809450, 1980.

7. C. D. West, "Dynamic Analysis of the Fluidyne," pp. 779–84 in *Proceedings of the 18th IECEC*, Paper No. 839126, 1983.

8. I. Urieli and D. M. Berchowitz, *Stirling Cycle Engine Analysis*, Adam Hilger Ltd., Bristol, England, 1984.

9. R. Vincent, W. Rifkin, and G. Benson, "Analysis and Design of Free-Piston Stirling Engines — Thermodynamics and Dynamics," pp. 1686–95 in *Proceedings of the 15th IECEC*, Paper No. 809334, 1980.

10. D. R. Gedeon, "The Optimization of Stirling Cycle Machines," pp. 1784–90 in *Proceedings of the 13th IECEC*, Paper No. 789193, 1978.

11. J. E. Giansante, *A Free Piston Stirling Engine Performance Code*, prepared by Mechanical Technology, Inc. for NASA Lewis Research Center, 81TR17, November 1980.

12. R. C. Tew, "Comparison of Free-Piston Stirling Engine Model Predictions with RE-1000 Engine Test Data," pp. 2073–85 in *Proceedings of the 19th IECEC*, Paper No. 849374, 1984.

13. *Development and Demonstration of a Stirling/Rankine Heat Activated Heat Pump*, prepared by General Electric for Oak Ridge Natl. Lab., GE Document No. 83-AEP-004, Vol. 1, April 1984.

14. W. R. Martini, *Development of Free-Piston Stirling Engine Performance and Optimization Codes Based on Martini Simulation Technique*, prepared for NASA Lewis Research Center, May 1984.

15. J. S. Rauch, "Steady State Analysis of Free-Piston Stirling Engine Dynamics," pp. 961—5 in *Proceedings of the 10th IECEC*, Paper No. 759144, 1975.

16. J. S. Rauch, "Harmonic Analysis of Stirling Engine Thermodynamics," pp. 1696—1700 in *Proceedings of the 15th IECEC*, Paper No. 809335, 1980.

17. J. S. Rauch, "Harmonic Analysis of Stirling-Cycle Performance — A Comparison with Test Data," pp. 2015—20 in *Proceedings of the 19th IECEC*, Paper No. 849174, 1984.

18. J. G. Schreiber, "Initial Results of Sensitivity Tests Performed on the RE-1000 Free-Piston Stirling Engine," pp. 1878—85 in *Proceedings of the 19th IECEC*, Paper No. 849090, 1984.

19. J. Schreiber, *Testing and Performance Characteristics of a 1-kW Free Piston Stirling Engine*, NASA/TM-82999, National Aeronautics and Space Administration, April 1983.

20. K. P. Lee, "A Simplistic Model of Cyclic Heat Transfer Phenomena in Closed Spaces," pp. 720—3 in *Proceedings of the 18th IECEC*, Paper No. 839116, 1983.

21. F. H. Speckhart and W. L. Green, *A Guide to Using CSMP — The Continuous System Modeling Program*, Prentice-Hall Inc., Englewood Cliffs, N.J., 1976.

Appendix A

IMPERFECT HEAT EXCHANGER ANALYSIS

An analysis of imperfect heat exchangers published by Urieli and Berchowitz[1] has been adapted for use with the LHA method. The analysis is based on a simplified approach, where heat transfer in the regenerator and heat exchangers is assumed to occur during two steady flow processes: (1) the hot blow from the expansion to the compression space and (2) the cold blow from the compression back to the expansion space. An effectiveness—number of transfer units (NTU) method is used to perform the heat transfer calculations. The LHA version of the imperfect heat exchanger analysis is described in this appendix. Some sample calculations are also presented.

A.1 Heat Transfer Equations

The nomenclature for the heat transfer analysis is shown in Fig. A.1. The expansion space, heater, cooler, and compression space wall temperatures are all assumed to be uniform and constant with respect to time. The regenerator wall temperature has a linear distribution, but the local temperature is constant with respect to time. The steady state hot blow starts at temperature T_{H1} and ends at T_K. The cold blow starts at T_{K1} and ends at T_H. The heater, regenerator, and cooler effectivenesses are assumed to be identical during the hot and cold blows, and they are defined as

$$\varepsilon_H = \frac{T_{H2} - T_{H1}}{\overline{T}_{wH} - T_{H1}} = \frac{T_H - T_{H3}}{\overline{T}_{wH} - T_{H3}} , \tag{A.1}$$

$$\varepsilon_R = \frac{T_{H2} - T_{K3}}{T_{H2} - T_{K2}} = \frac{T_{H3} - T_{K2}}{T_{H2} - T_{K2}} , \tag{A.2}$$

$$\varepsilon_K = \frac{T_{K3} - T_K}{T_{K3} - \overline{T}_{wK}} = \frac{T_{K1} - T_{K2}}{T_{K1} - \overline{T}_{wK}} . \tag{A.3}$$

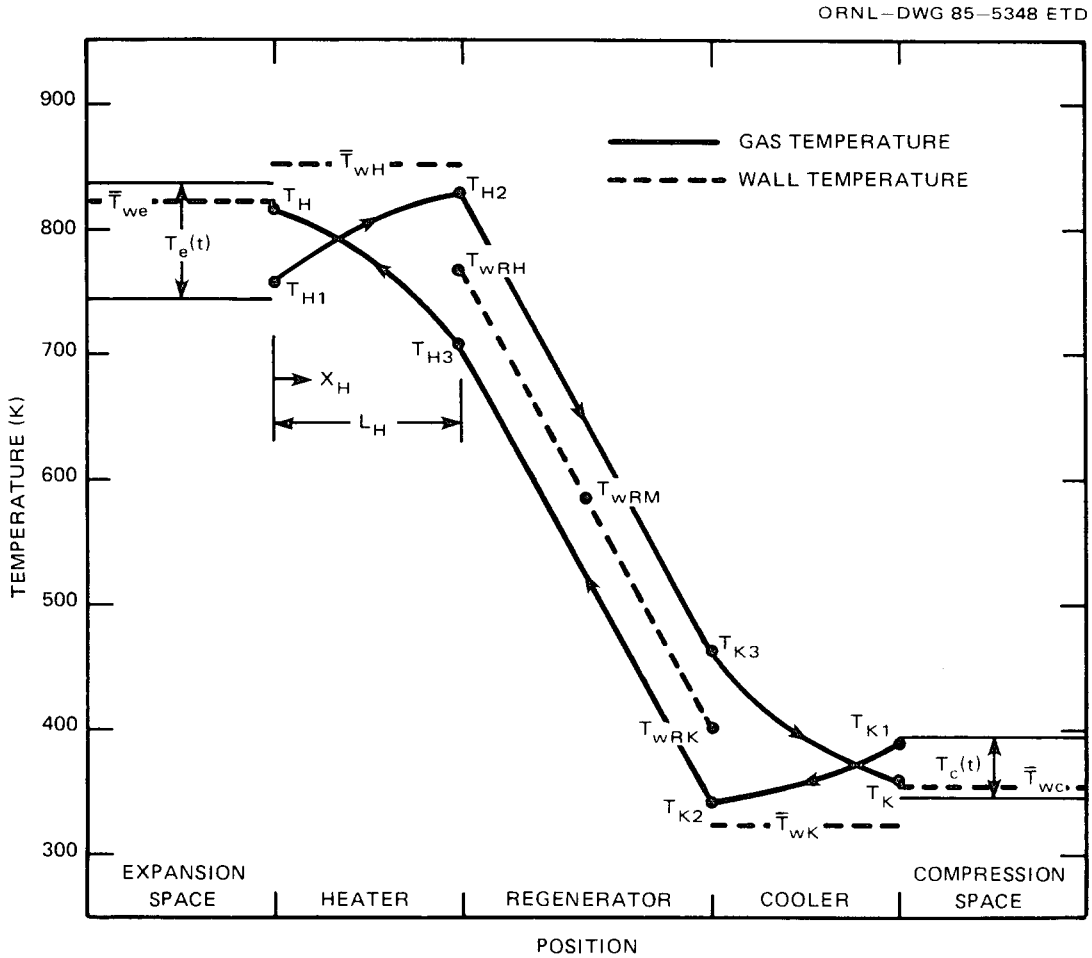

Fig. A.1. Gas and wall temperature nomenclature for imperfect heat exchanger analysis.

In the present version of the LHA, the three effectivenesses must be specified as part of the input data because heat transfer correlations have not yet been added to the analysis. If correlations are added, heat transfer effectiveness can be calculated from the simple NTU equations published by Urieli and Berchowitz.[1]

The imperfect heat exchanger analysis affects the LHA predictions in two ways. First, the gas temperatures leaving the heat exchangers are no longer equal to the heater and cooler wall temperatures, which reduces the effective temperature ratio of the engine such that $(T_H/T_K) < (\bar{T}_{wH}/\bar{T}_{wK})$. Second, there is a regenerator reheat loss that is caused by gas entering the regenerator at a temperature different from that when it leaves.

This regenerator reheat loss from the heater to the cooler $\overline{\dot{H}}_R$ does not change the indicated power of the engine. However, it does increase the heat input and heat output so that the overall energy balance becomes

$$\overline{\dot{Q}}_{in} = \overline{\dot{W}}_e + \overline{\dot{H}}_R \ ,$$

$$\overline{\dot{Q}}_{out} = -\overline{\dot{W}}_c - \overline{\dot{W}}_s + \overline{\dot{H}}_R \ , \tag{A.4}$$

$$\overline{\dot{W}}_{out} = \overline{\dot{W}}_e + \overline{\dot{W}}_c + \overline{\dot{W}}_s \ .$$

The gas temperature at the beginning of hot blow T_{H1} is determined by calculating the average temperature of the gas that flows from the expansion space into the heater. The cyclic average expansion space enthalpy flux was derived in ORNL/CON-155 (Ref. 2) as

$$\overline{\dot{H}^*_e} = \frac{\overline{\dot{H}}_e}{c_v \overline{m}_e \overline{T}_e \omega} = \frac{\gamma}{2\pi}\left(\int_{dm^*_e < 0} T^*_e \frac{dm^*_e}{dt^*}\, dt^* + \int_{dm^*_e > 0} T^*_H \frac{dm^*_e}{dt^*}\, dt^*\right) \ , \tag{A.5}$$

and after evaluation of the integrals,

$$\overline{\dot{H}}_e = Z1(1)(T_H - \overline{T}_e) + Z1(2) \ , \tag{A.6}$$

where Z1(1) and Z1(2) were defined in ORNL/CON-155 (Ref. 2) [Eqs. (3.83) and (3.84)]. T_{H1} is calculated by replacing T^*_e with $(T_{H1}/\overline{T}_e)$ in Eq. (A.5), setting Eq. (A.5) equal to Eq. (A.6), and solving for T_{H1}. After evaluation of the integrals and simplification, the result is

$$Z1(1)(T_H - T_{H1}) = Z1(1)(T_H - \overline{T}_e) + Z1(2) \ , \tag{A.7}$$

or

$$T_{H1} = \overline{T}_e - \frac{Z1(2)}{Z1(1)} \ . \tag{A.8}$$

A similar procedure for the compression space yields

$$T_{K1} = \overline{T}_c - \frac{Z1(4)}{Z1(3)} , \tag{A.9}$$

where Z1(3) and Z1(4) were defined in ORNL/CON-155 (Ref. 2) [Eqs. (3.85) and (3.86)].

After the temperatures at the beginning of the hot and cold blows are known, the other heat exchanger gas temperatures are calculated from the effectiveness definitions in Eqs. (A.1)—(A.3), recalling that the three effectivenesses are treated as specified constants,

$$T_{H2} = \varepsilon_H \overline{T}_{wH} + (1 - \varepsilon_H) T_{H1} , \tag{A.10}$$

$$T_{K2} = \varepsilon_K \overline{T}_{wK} + (1 - \varepsilon_K) T_{K1} , \tag{A.11}$$

$$T_{H3} = \varepsilon_R T_{H2} + (1 - \varepsilon_R) T_{K2} , \tag{A.12}$$

$$T_{K3} = \varepsilon_R T_{K2} + (1 - \varepsilon_R) T_{H2} , \tag{A.13}$$

$$T_H = \varepsilon_H \overline{T}_{wH} + (1 - \varepsilon_H) T_{H3} , \tag{A.14}$$

$$T_K = \varepsilon_K \overline{T}_{wK} + (1 - \varepsilon_K) T_{K3} . \tag{A.15}$$

Two final equations result from the expansion and compression space average energy balances that were presented in Eq. (3.27). The energy balances are used to calculate the expansion and compression space average gas temperatures,

$$\overline{T}_e = \frac{Z1(1)T_H + Z1(2) + h_e \overline{A}_{se} \overline{T}_{we} - \overline{\dot{W}}_e}{Z1(1) + h_e \overline{A}_{se}} , \tag{A.16}$$

$$\overline{T}_c = \frac{Z1(3)T_K + Z1(4) + h_c \overline{A}_{sc} \overline{T}_{wc} - \overline{\dot{W}}_c}{Z1(3) + h_c \overline{A}_{sc}} . \tag{A.17}$$

Equations (A.8)—(A.17) are a system of ten algebraic equations with ten unknown gas temperatures that are solved iteratively. The first eight equations are solved at the beginning of an iteration. Then the matrix calculations are performed to determine y_1, y_2, etc. Equations (A.16) and (A.17) are solved at the end of an iteration, as they were when perfect heat exchangers were assumed. The first iteration is initiated by assuming

$$T_{H1} = T_{K1} = \frac{\overline{T}_{wH} + \overline{T}_{wK}}{2} . \tag{A.18}$$

Other assumptions made during the first iteration, but after T_H and T_K are calculated the first time, are

$$\overline{T}_e = T_H ,$$

$$\overline{T}_c = \overline{T}_s = T_K . \tag{A.19}$$

The gas temperatures in the heater, regenerator, and cooler depend on the heat transfer effectiveness of these components. The effectiveness—NTU equation for the heater will have the form

$$\varepsilon_H = 1 - e^{-NTU_H} , \tag{A.20}$$

or

$$NTU_H = -\ln(1 - \varepsilon_H) . \tag{A.21}$$

The local heater gas temperature during the hot blow T_{Hhot} is a function of axial position in the heater as shown in Fig. A.1. This is expressed analytically as

$$\frac{T_{Hhot} - T_{H1}}{\overline{T}_{wH} - T_{H1}} = \varepsilon_{XH} = 1 - e^{-(X_H/L_H)NTU_H} , \tag{A.22}$$

where the local heater effectiveness ε_{XH} depends on the cumulative heater

surface area, which is proportional to (X_H/L_H). When Eq. (A.21) is substituted into a simplified version of Eq. (A.22), the result is

$$T_{Hhot} = \overline{T}_{wH} - (\overline{T}_{wH} - T_{H1})\, e^{(X_H/L_H)\ln(1-\varepsilon_H)} \quad . \tag{A.23}$$

The average heater gas temperature during the hot blow is found by calculating an average over the length of the heater,

$$\overline{T}_{Hhot} = \int_0^1 T_{Hhot}\, d\left(\frac{X_H}{L_H}\right) \quad . \tag{A.24}$$

The result is

$$\overline{T}_{Hhot} = \overline{T}_{wH} + (\overline{T}_{wH} - T_{H1})\, \frac{\varepsilon_H}{\ln(1 - \varepsilon_H)} \quad . \tag{A.25}$$

The result for the cold blow is similar,

$$\overline{T}_{Hcold} = \overline{T}_{wH} + (\overline{T}_{wH} - T_{H3})\, \frac{\varepsilon_H}{\ln(1 - \varepsilon_H)} \quad . \tag{A.26}$$

The cyclic average heater gas temperature is defined as the average of the hot and cold blows, and the result is

$$\overline{T}_H = \overline{T}_{wH} + \left(\overline{T}_{wH} - \frac{T_{H1} + T_{H3}}{2}\right) \frac{\varepsilon_H}{\ln(1 - \varepsilon_H)} \quad . \tag{A.27}$$

A similar procedure for the cooler yields the cyclic average cooler gas temperature

$$\overline{T}_K = \overline{T}_{wK} + \left(\overline{T}_{wK} - \frac{T_{K1} + T_{K3}}{2}\right) \frac{\varepsilon_K}{\ln(1 - \varepsilon_K)} \quad . \tag{A.28}$$

The regenerator matrix wall temperature is the mean of the hot and cold blow gas temperatures in the regenerator

$$T_{wRH} = \frac{T_{H2} + T_{H3}}{2} ,$$

$$T_{wRK} = \frac{T_{K2} + T_{K3}}{2} , \tag{A.29}$$

as shown in Fig. A.1. The cyclic average regenerator gas temperature is defined in terms of these matrix wall temperatures. A mass weighted average that accounts for different gas densities at the hot and cold ends of the regenerator results in a logarithmic mean,

$$\overline{T}_R = \frac{T_{wRH} - T_{wRK}}{\ln(T_{wRH}/T_{wRK})} . \tag{A.30}$$

The average gas temperatures in the heater, regenerator, and cooler are needed to calculate the average mass of gas in the dead volume,

$$\overline{m}_d = \frac{\overline{P}_w}{R} \left(\frac{\overline{V}_H}{\overline{T}_H} + \frac{\overline{V}_R}{\overline{T}_R} + \frac{\overline{V}_K}{\overline{T}_K} \right) . \tag{A.31}$$

The average mass of gas in the dead volume is used in the matrix calculations to determine y_1, y_2, etc.

The regenerator reheat loss calculation is based on the mass flow rate at the middle of the regenerator. To determine this flow rate, an expression is needed for the mass of gas in the hot end of the working space, m_{wH}, which includes the expansion space, heater, and hot half of the regenerator. m_{wH} is defined in terms of the mass of gas in the expansion space and the hot end of the dead volume

$$m_{wH} = m_e + \frac{\overline{m}_{dH}}{\overline{m}_d} m_d = \overline{m}_e m_e^* + \overline{m}_{dH} m_d^* , \tag{A.32}$$

where

$$\bar{m}_{dH} = \frac{\bar{P}_w}{R}\left(\frac{\bar{V}_H}{\bar{T}_H} + \frac{\bar{V}_R}{2\,\bar{T}_{RH}}\right) \tag{A.33}$$

is the average mass of gas in the hot end of the dead volume,

$$\bar{T}_{RH} = \frac{T_{wRH} - T_{wRM}}{\ln(T_{wRH}/T_{wRM})} \tag{A.34}$$

is the average gas temperature in the hot half of the regenerator, and

$$T_{wRM} = \frac{T_{wRH} + T_{wRK}}{2} \tag{A.35}$$

is the matrix wall temperature at the middle of the regenerator. When Eq. (3.26) for m_e^* and m_d^* are substituted into Eq. (A.32), the result after simplification is

$$m_{wH} = (\bar{m}_e + \bar{m}_{dH}) + (\bar{m}_e y_1 + \bar{m}_{dH} y_3)\sin t^* + (\bar{m}_e y_2 + \bar{m}_{dH} y_4)\cos t^* \,. \tag{A.36}$$

The regenerator reheat loss per cycle is equal to the total enthalpy of the gas passing through the middle of the regenerator during the hot blow minus the total enthalpy of the gas passing through the middle of the regenerator during the cold blow. Therefore, the regenerator reheat loss rate is

$$\bar{\dot{H}}_R = f\ 2|m_{wH}|c_p(T_{H2} - T_{H3}) \,, \tag{A.37}$$

where $2|m_{wH}|$ is the mass of gas flowing through the middle of the regenerator during each half cycle, and

$$|m_{wH}| = \left[(\bar{m}_e y_1 + \bar{m}_{dH} y_3)^2 + (\bar{m}_e y_2 + \bar{m}_{dH} y_4)^2\right]^{1/2} \tag{A.38}$$

is the amplitude of the mass of gas in the hot end of the working space. The regenerator enthalpy flux rate is calculated after the matrix calculations are performed to determine y_1, y_2, etc.

A.2 Sample Results

Some sample LHA imperfect heat exchanger predictions are listed in Table A.1. The first column is the RE-1000 base case predictions from

Table A.1. LHA constrained piston amplitude mode predictions for RE-1000 base case with imperfect heat exchangers

Parameters	Base case	Imperfect regenerator	Imperfect heater, cooler	Imperfect regenerator, heater, cooler
		Specified values		
X_{pa}, m	0.01300	0.01300	0.01300	0.01300
$\overline{T}_{wH}$, K	853.0	853.0	853.0	853.0
$\overline{T}_{wK}$, K	326.0	326.0	326.0	326.0
ε_H, %	100	100	75	75
ε_R, %	100	97	100	97
ε_K, %	100	100	75	75
		Computed values		
f, Hz	29.44	29.45	29.49	29.56
X_{da}, m	0.01260	0.01261	0.01257	0.01253
β_d, deg	46.68	46.67	46.84	47.14
T_H, K	853.0	853.0	848.9	844.9
T_K, K	326.0	326.0	327.7	331.7
$\overline{\dot{H}}_R$, W	0	599	0	573
$\overline{\dot{Q}}_{in}$, W	2852	3456	2851	3421
$\overline{\dot{Q}}_{out}$, W	1832	2434	1846	2443
$\overline{\dot{W}}_{out}$, W	1020	1022	1005	978
η_{it}, %	35.76	29.56	35.24	28.59

Table 4.4. The second column is for an imperfect regenerator. The third column is for an imperfect heater and cooler. The last column is for the combined effects of an imperfect regenerator, heater, and cooler. The imperfect heat exchangers have almost no effect on the dynamic behavior of the engine. The 75% heater and cooler effectivenesses also appear to have only a minor effect on the thermodynamic behavior of the engine, as is seen in the last two columns where the effective temperature ratio of the engine (T_H/T_K) is only slightly less than the actual temperature ratio ($\overline{T}_{wH}/\overline{T}_{wK}$).

The regenerator heat transfer effectiveness has a significant impact on the thermodynamic performance of the engine. A comparison between the first two columns of Table A.1 shows that a 3.0 percentage point drop in regenerator effectiveness results in a 6.2 percentage point drop in indicated thermal efficiency. The selection of a regenerator for a Stirling engine involves a trade-off between the reheat losses and the pressure drop losses. Optimized regenerator designs usually result in large pressure drops to avoid the substantial thermal losses associated with imperfect heat transfer in the regenerator.

References

1. I. Urieli and D. M. Berchowitz, *Stirling Cycle Engine Analysis*, Adam Hilger Ltd., Bristol, England, 1984.

2. N. C. J. Chen, F. P. Griffin, and C. D. West, "*Linear Harmonic Analysis of Stirling Engine Thermodynamics*, ORNL/CON-155, Martin Marietta Energy Systems, Inc., Oak Ridge Natl. Lab., August 1984.

Appendix B

NONLINEAR DASHPOT EQUATIONS

A relationship is derived in this appendix for the power absorbed by a generalized nonlinear dashpot load that is driven sinusoidally. The nonlinear dashpot load force acting on the power piston F_1 is expressed analytically as a function of power piston velocity $\dot{X}_p$ in a form

$$F_1 = -k_1\dot{X}_p(\text{abs } \dot{X}_p)^{n-1} \ , \tag{B.1}$$

where k_1 is the load coefficient, n is the load exponent, and the absolute value is needed to ensure that negative values of velocity will not be raised to fractional powers. The derivation is for sinusoidal power piston motion

$$\begin{aligned} X_p &= X_{pa} \sin(\omega t) \ , \\ \dot{X}_p &= \omega X_{pa} \cos(\omega t) \ . \end{aligned} \tag{B.2}$$

The instantaneous power absorbed by the load $\dot{W}_1$ is equal to the negative of force times velocity,

$$\dot{W}_1 = -F_1\dot{X}_p \ . \tag{B.3}$$

The average power absorbed by the load $\overline{\dot{W}}_1$ is calculated by averaging over a cycle

$$\overline{\dot{W}}_1 = \frac{1}{2\pi} \int_{-\pi/2}^{3\pi/2} (-F_1\dot{X}_p) \ d(\omega t) \ . \tag{B.4}$$

When Eq. (B.1) for a generalized nonlinear dashpot load is substituted into Eq. (B.4), the average load power becomes

$$\overline{\dot{W}}_1 = \frac{k_1}{2\pi} \int_{-\pi/2}^{3\pi/2} \dot{X}_p^2 \ (\text{abs } \dot{X}_p)^{n-1} \ d(\omega t) \ . \tag{B.5}$$

The integral must be split in half so that the absolute value can be eliminated from the equation,

$$\bar{\dot{W}}_1 = \frac{k_1}{2\pi}\left[\int_{-\pi/2}^{\pi/2} \dot{X}_p^2 \,(\text{abs } \dot{X}_p)^{n-1}\, d(\omega t) + \int_{\pi/2}^{3\pi/2} \dot{X}_p^2 \,(\text{abs } \dot{X}_p)^{n-1}\, d(\omega t)\right] . \qquad (B.6)$$

$\dot{X}_p$ is positive between $-\pi/2$ and $\pi/2$. The absolute value can therefore be deleted from the left-hand integral. $\dot{X}_p$ is negative between $\pi/2$ and $3\pi/2$, but $\dot{X}_p^2$ and abs $\dot{X}_p$ in the $\pi/2$ to $3\pi/2$ region are positive and equal to $\dot{X}_p^2$ and $\dot{X}_p$ in the $-\pi/2$ to $\pi/2$ region. The right-hand integral is therefore identical to the left-hand integral. After these simplifications, Eq. (B.6) becomes

$$\bar{\dot{W}}_1 = \frac{k_1}{\pi}\int_{-\pi/2}^{\pi/2} \dot{X}_p^{n+1}\, d(\omega t) . \qquad (B.7)$$

Substitution of Eq. (B.2) into (B.7) yields

$$\bar{\dot{W}}_1 = \frac{k_1\,(\omega X_{pa})^{n+1}}{\pi}\int_{-\pi/2}^{\pi/2} \cos^{n+1}(\omega t)\, d(\omega t) . \qquad (B.8)$$

The integral in Eq. (B.8) can be evaluated directly in terms of the gamma function Γ, and the result is

$$\bar{\dot{W}}_1 = k_1(\omega\, X_{pa})^{n+1}\,\frac{\Gamma\left(\frac{n}{2}+1\right)}{\sqrt{\pi}\,\Gamma\left(\frac{n}{2}+1.5\right)} . \qquad (B.9)$$

The constant term in Eq. (B.9) has been evaluated for some selected values of the dashpot load exponent, and the results are listed in Table B.1.

Table B.1. Numerical values for the constant term in Eq. (B.9) for some selected values of the dashpot load exponent

n	$\dfrac{\Gamma\left(\frac{n}{2} + 1\right)}{\sqrt{\pi}\,\Gamma\left(\frac{n}{2} + 1.5\right)}$
1.0	0.50000
1.5	0.45765
2.0	0.42441
2.5	0.39744
3.0	0.37500

Appendix C

NOMENCLATURE

A_d	Displacer cross-sectional area (m^2)
A_p	Power piston cross-sectional area (m^2)
A_r	Displacer rod cross-sectional area (m^2)
$\overline{A}_{sc}$	Wall heat transfer surface area in compression space (m^2)
$\overline{A}_{se}$	Wall heat transfer surface area in expansion space (m^2)
$\overline{A}_{ss}$	Wall heat transfer surface area in displacer gas spring (m^2)
a_1,a_2,a_3,a_4	Dimensionless volume constants defined in Eq. (3.7) and in ORNL/CON-155 (Ref. 1) [Eq. (3.17)]
a_{11},a_{12},a_{13}	Dimensionless area constants defined in Eq. (3.9)
c_{1d}	Equivalent load damping coefficient [(N•s)/m]
c_{1s}	Equivalent load spring coefficient (N/m)
c_p	Specific heat at constant pressure [J/(kg•K)]
c_v	Specific heat at constant volume [J/(kg•K)]
D(i,j)	i,j = 1, 2, ... 18, Matrix elements defined in Eqs. (3.33) and (3.34)
FF(n)	n = 1, 2, ... 9, Fourier correction factors
F_1	Force on the power piston produced by the load (N)
f	Frequency (Hz)
$\dot{H}_c$	Enthalpy flux rate into the compression space (W)
$\dot{H}_e$	Enthalpy flux rate into the expansion space (W)
$\overline{\dot{H}}_R$	Regenerator reheat loss from heater to cooler (W)
$\dot{H}_s$	Enthalpy flux rate into the displacer gas spring (W)
h_c	Cylinder wall to gas heat transfer coefficient in compression space [W/(m^2•K)]
h_e	Cylinder wall to gas heat transfer coefficient in expansion space [W/(m^2•K)]
h_s	Cylinder wall to gas heat transfer coefficient in displacer gas spring [W/(m^2•K)]
k_1	Nonlinear dashpot load coefficient
k_{mc}	Mass leakage coefficient between compression and buffer spaces [kg/(Pa•s)]
k_{ms}	Mass leakage coefficient between displacer gas spring and buffer spaces [kg/(Pa•s)]

k_{pc}	Pressure drop coefficient between compression and dead spaces [(Pa•s)/kg]
k_{pe}	Pressure drop coefficient between expansion and dead spaces [(Pa•s)/kg]
L_H	Length of heater tubes (m)
m_c	Mass of gas in compression space (kg)
m_d	Mass of gas in dead space (kg)
$\overline{m}_{dH}$	Average mass of gas in hot end of dead space (kg)
m_{dp}	Mass of displacer piston (kg)
m_e	Mass of gas in expansion space (kg)
m_{pp}	Mass of power piston (kg)
m_s	Mass of gas in displacer gas spring (kg)
$\overline{m}_w$	Average total mass of gas in working space, $\overline{m}_w = \overline{m}_e + \overline{m}_d + \overline{m}_c$ (kg)
m_{wH}	Mass of gas in hot end of working space (kg)
NTU_H	Number of transfer units for entire heater
n	Nonlinear dashpot load exponent
P_c	Pressure in compression space (Pa)
P_d	Pressure in dead space (Pa)
P_e	Pressure in expansion space (Pa)
P_s	Pressure in displacer gas spring (Pa)
$\overline{P}_w$	Average pressure in working space (Pa)
$\overline{\dot{Q}}_{in}$	Average total heat input rate (W)
$\overline{\dot{Q}}_{out}$	Average total heat output rate (W)
$\dot{Q}_{wc}$	Heat transfer rate from cylinder wall to gas in compression space (W)
$\dot{Q}_{we}$	Heat transfer rate from cylinder wall to gas in expansion space (W)
$\dot{Q}_{ws}$	Heat transfer rate from cylinder wall to gas in displacer gas spring (W)
R	Gas constant [J/(kg•K)]
T_c	Gas temperature in compression space (K)
$T_{c\ flux}$	Enthalpy flux temperature between compression and dead spaces (K)
$\overline{T}_d$	Average gas temperature in dead space, $\overline{T}_d = \overline{V}_d/[\overline{V}_H/T_H + \overline{V}_R \ln(T_H/T_K)/(T_H - T_K) + \overline{V}_K/T_K]$ (K)
T_e	Gas temperature in expansion space (K)

$T_{e\ flux}$	Enthalpy flux temperature between expansion and dead spaces (K)
T_H	Average temperature of gas flowing from heater to expansion space (K)
$\overline{T}_H$	Average gas temperature in heater (K)
T_{Hcold}	Local gas temperature in heater during cold blow (K)
T_{Hhot}	Local gas temperature in heater during hot blow (K)
T_{H1}	Average temperature of gas flowing from expansion space to heater (K)
T_{H2}	Average temperature of gas flowing from heater to regenerator (K)
T_{H3}	Average temperature of gas flowing from regenerator to heater (K)
T_K	Average temperature of gas flowing from cooler to compression space (K)
$\overline{T}_K$	Average gas temperature in cooler (K)
T_{K1}	Average temperature of gas flowing from compression space to cooler (K)
T_{K2}	Average temperature of gas flowing from cooler to regenerator (K)
T_{K3}	Average temperature of gas flowing from regenerator to cooler (K)
$\overline{T}_R$	Average gas temperature in regenerator (K)
$\overline{T}_{RH}$	Average gas temperature in hot half of regenerator (K)
T_s	Gas temperature in displacer gas spring (K)
$T_{s\ flux}$	Enthalpy flux temperature between displacer gas spring and buffer spaces (K)
$\overline{T}_{wc}$	Average wall temperature in compression space (K)
$\overline{T}_{we}$	Average wall temperature in expansion space (K)
$\overline{T}_{wH}$	Average wall temperature in heater (K)
$\overline{T}_{wK}$	Average wall temperature in cooler (K)
T_{wRH}	Matrix temperature at hot end of regenerator (K)
T_{wRK}	Matrix temperature at cold end of regenerator (K)
T_{wRM}	Matrix temperature at middle of regenerator (K)
$\overline{T}_{ws}$	Average wall temperature in displacer gas spring (K)
t	Time (s)
V_c	Compression space volume (m^3)

$\overline{V}_c$	Average volume in compression space with pistons at midstrokes (m^3)
$\overline{V}_d$	Constant dead space volume, $\overline{V}_d = \overline{V}_K + \overline{V}_H + \overline{V}_R$ (m^3)
V_e	Expansion space volume (m^3)
$\overline{V}_e$	Average volume in expansion space with pistons at midstrokes (m^3)
$\overline{V}_H$	Constant heater volume (m^3)
$\overline{V}_K$	Constant cooler volume (m^3)
$\overline{V}_R$	Constant regenerator volume (m^3)
V_s	Displacer gas spring volume (m^3)
$\overline{V}_s$	Average volume in displacer gas spring with pistons at midstrokes (m^3)
$\dot{W}_c$	PV power by gas in compression space (W)
$\dot{W}_e$	PV power by gas in expansion space (W)
$\dot{W}_l$	Power absorbed by nonlinear dashpot load (W)
$\overline{\dot{W}}_{out}$	Average total power output (W)
$\dot{W}_s$	PV power by gas in displacer gas spring (W)
X_d	Displacer position, zero at midstroke (m)
X_{da}	Displacer amplitude, 1/2 displacer stroke (m)
X_{dm}	Maximum displacer amplitude allowable by mechanical constraints (m)
X_H	Axial position in heater from expansion space end of tubes (m)
X_p	Power piston position, zero at midstroke (m)
X_{pa}	Power piston amplitude, 1/2 power piston stroke (m)
X_{pm}	Maximum power piston amplitude allowable by mechanical constraints (m)
y_n	n = 1, 2, ... 18, Amplitude of harmonic components defined in Eq. (3.26)
Z1(n)	n = 1, 2, ... 6, Defined in Eq. (3.29) and in ORNL/CON-155 (Ref. 1) [Eqs. (3.83)–(3.86)]

Superscripts

$\overline{}$	Average over a cycle
$\cdot$	Derivative with respect to time or d/dt
$\cdot\cdot$	Second derivative with respect to time or d^2/dt^2
*	Dimensionless quantities defined in Eqs. (3.2) to (3.11) and in ORNL/CON-155 (Ref. 1) [Eqs. (3.10)–(3.18)]
$\|\|$	Amplitude of a variable

Greek

β_d	Displacer phase angle relative to power piston (deg)
β_{Pc}	Compression space pressure phase angle relative to power piston (deg)
γ	Ratio of specific heats of gas, $\gamma = c_p/c_v$
ε_H	Heat transfer effectiveness of entire heater
ε_K	Heat transfer effectiveness of entire cooler
ε_R	Heat transfer effectiveness of entire regenerator
ε_{XH}	Heat transfer effectiveness of portion of heater between expansion space end of tubes and position X_H
η_{it}	Indicated thermal efficiency
Θ_s	Defined in Eq. (3.35)
τ_c	Temperature ratio associated with compression space, $\tau_c = (T_K + \overline{T}_c)/2\overline{T}_c$
τ_e	Temperature ratio associated with expansion space, $\tau_e = (T_H + \overline{T}_e)/2\overline{T}_e$
τ_s	Temperature ratio associated with displacer gas spring, $\tau_s = (T_K + \overline{T}_s)/2\overline{T}_s$
ω	Angular frequency (rad/s)
ω_{high}	Upper boundary for frequency root-finding routine (rad/s)
ω_{low}	Lower boundary of frequency root-finding routine (rad/s)

Reference

1. N. C. J. Chen, F. P. Griffin, and C. D. West, *Linear Harmonic Analysis of Stirling Engine Thermodynamics*, ORNL/CON-155, Martin Marietta Energy Systems, Inc., Oak Ridge Natl. Lab., August 1984.

Appendix D

COMPUTER PROGRAM: LHA VERSION 1

A computer program, called LHA Version 1 (LHA1), was written in FORTRAN to perform the sample LHA calculations for the RE-1000 FPSE configuration. The computer code was developed mainly to prove the principle of the LHA solution method. Since the development of user-friendly software was not one of the LHA project objectives, the FORTRAN code contains few comment cards. The thermodynamic calculations contained in the LHA1 program were discussed previously in ORNL/CON-155 (Ref. 1), and the dynamic and imperfect heat exchanger calculations are discussed in this report. The FORTRAN variable names used in LHA1 are similar to the nomenclature used in the two reports. This appendix contains a short description of the LHA1 program, the program listing, and the input data and FORTRAN output for the RE-1000 base case.

Two FORTRAN subroutines called DECOMP and SOLVE are used to perform the matrix calculations. The compiler must supply these subroutines from a standard FORTRAN library. All real variables in the LHA1 program are declared REAL*8 because the DECOMP and SOLVE subroutines are written in double precision. LHA1 is written entirely in SI units (kg, m, s), which avoids the need for unit conversions in the program.

The LHA1 program is set up for batch execution. All FORTRAN variables that must be specified in the input data are contained in a single NAMELIST called INPUT, so that a NAMELIST convention for READ statements can be used. Comment cards at the beginning of the program define all of the variables in INPUT. There are two READ statements in the LHA1 program. The first READ is executed only once, and it is used to initialize all of the variables in INPUT. A value should be assigned to the integer variable ILOOP when the first READ is executed because ILOOP defines the number of times that a large loop (DO 5) is executed. The loop DO 5 contains the second READ and the entire program including output statements, and it enables multiple cases to be executed from a single job.

The LHA1 program is designed to handle either kinematic or free-piston calculations. The appropriate option is selected by changing the integer variable IMODE in the input data. In kinematic mode (IMODE = 1),

the piston motions are defined by specifying the variables FH, XPAXPM, BDD, and XDAXPA. The variables FHLOW, FHHIGH, FHTOL, MPP, MDP, and BLD should be specified nonzero, but they are not used in kinematic mode. In free-piston mode (IMODE = 3), the power piston amplitude and the load force phase angle are defined by specifying XPAXPM and BLD, and the frequency root-finding routine is initialized by specifying FH, FHLOW, FHHIGH, and FHTOL. The variables BDD and XDAXPA should be specified nonzero, but BDD, XDAXPA, and FH are calculated from the dynamic equations in free-piston mode.

D.1 LHA1 Program Listing

```
      IMPLICIT REAL*8(A-H,K-Z)
      DIMENSION IPVT(18),D(18,18),Y(18),Z1(18),FF(9)
C  DEFINITIONS OF VARIABLES IN NAMELIST/INPUT/
C  ----------------------------------------------------------------
C    NAME  UNITS        DEFINITION
C  ----------------------------------------------------------------
C       R  J/(KG*K)     GAS CONSTANT
C      CP  J/(KG*K)     CONSTANT PRESSURE SPECIFIC HEAT OF GAS
C   XPMAX  M            MAXIMUM AMPLITUDE OF POWER PISTON
C   XDMAX  M            MAXIMUM AMPLITUDE OF DISPLACER
C      AP  M**2         CROSS-SECTIONAL AREA OF POWER PISTON
C      AR  M**2         CROSS-SECTIONAL AREA OF DISPLACER ROD
C      AD  M**2         CROSS-SECTIONAL AREA OF DISPLACER
C   VEAVG  M**3         AVERAGE VOLUME IN EXPANSION SPACE
C   VHAVG  M**3         CONSTANT VOLUME IN HEATER
C   VRAVG  M**3         CONSTANT VOLUME IN REGENERATOR
C   VKAVG  M**3         CONSTANT VOLUME IN COOLER
C   VCAVG  M**3         AVERAGE VOLUME IN COMPRESSION SPACE
C   VSAVG  M**3         AVERAGE VOLUME IN GAS SPRING
C  ASEAVG  M**2         HEAT TRANS SURFACE AREA IN EXPANSION SPACE
C  ASCAVG  M**2         HEAT TRANS SURFACE AREA IN COMPRESSION SPACE
C  ASSAVG  M**2         HEAT TRANS SURFACE AREA IN GAS SPRING
C     MPP  KG           MASS OF POWER PISTON
C     MDP  KG           MASS OF DISPLACER
C      FH  HZ           FREQUENCY
C   FHLOW  HZ           FREQUENCY ROOT-FINDING LOWER BOUNDARY
C  FHHIGH  HZ           FREQUENCY ROOT-FINDING UPPER BOUNDARY
C   FHTOL  HZ           FREQUENCY ROOT-FINDING TOLERANCE
C  XPAXPM  -            POWER PISTON AMPLITUDE DIVIDED BY XPMAX
C     BDD  DEG          DISPLACER PHASE RELATIVE TO POWER PISTON
C  XDAXPA  -            DISPLACER AMPL DIVIDED BY POWER PISTON AMPL
C   PWAVG  PA           AVERAGE PRESSURE IN WORKING SPACE
C  TWHAVG  K            AVERAGE WALL TEMPERATURE IN HEATER
C  TWEAVG  K            AVERAGE WALL TEMPERATURE IN EXPANSION SPACE
C  TWKAVG  K            AVERAGE WALL TEMPERATURE IN COOLER
C  TWCAVG  K            AVERAGE WALL TEMPERATURE IN COMPRESSION SPACE
C  TWSAVG  K            AVERAGE WALL TEMPERATURE IN GAS SPRING
C     KMC  KG/(PA*S)    MASS LEAK COEF BETWEEN COMP AND BUFFER SPACES
C     KPE  (PA*S)/KG    PRES DROP COEF BETWEEN EXP AND DEAD SPACES
C     KPC  (PA*S)/KG    PRES DROP COEF BETWEEN COMP AND DEAD SPACES
C      HE  W/(M**2*K)   HEAT TRANS COEFICIENT IN EXPANSION SPACE
C      HC  W/(M**2*K)   HEAT TRANS COEFICIENT IN COMPRESSION SPACE
C     KMS  KG/(PA*S)    MASS LEAK COEF BETWEEN GS AND BUFFER SPACES
C      HS  W/(M**2*K)   HEAT TRANS COEFICIENT IN GAS SPRING
C   IMODE  -            CONTROL INTEGER: KINEMATIC=1, FREE-PISTON=3
C   IITER  -            MAXIMUM NUMBER OF ITERATIONS PER CASE
C    EPSH  -            HEAT TRANS EFFECTIVENESS OF ENTIRE HEATER
C    EPSR  -            HEAT TRANS EFFECTIVENESS OF ENTIRE REGEN
C    EPSK  -            HEAT TRANS EFFECTIVENESS OF ENTIRE COOLER
```

```
C     BLD  DEG          LOAD FORCE PHASE RELATIVE TO POWER PISTON:
C                       PURE DISSIPATION =-90.
C   ILOOP  -            NUMBER OF CASES PER JOB
C  ------------------------------------------------------------------
      NAMELIST/INPUT/R,CP,XPMAX,XDMAX,AP,AR,AD,VEAVG,VHAVG,VRAVG
     C,VKAVG,VCAVG,VSAVG,ASEAVG,ASCAVG,ASSAVG,MPP,MDP,FH,FHLOW
     C,FHHIGH,FHTOL,XPAXPM,BDD,XDAXPA,PWAVG,TWHAVG,TWEAVG,TWKAVG
     C,TWCAVG,TWSAVG,KMC,KPE,KPC,HE,HC,KMS,HS,IMODE,IITER,EPSH,EPSR
     C,EPSK,BLD,ILOOP
C  SPECIFIED PARAMETERS
      IDIM=18
      ILOOP=1
      READ(5,INPUT)
      DO 5 IL=1,ILOOP
      READ(5,INPUT)
C  CALCULATED PARAMETERS
      CV=CP-R
      G=CP/CV
      GM1=G-1.
      VWAVG=VEAVG+VHAVG+VRAVG+VKAVG+VCAVG
      A1=AD*XPMAX/VEAVG
      A2=(AD-AR)*XPMAX/VCAVG
      A3=AP*XPMAX/VCAVG
      A4=AR*XPMAX/VSAVG
      A11=AD/AP
      A12=AR/AP
      A13=(AD-AR)/AP
      PI=3.141592654
      FR=FH*2.*PI
      FRLOW=FHLOW*2.*PI
      FRHIGH=FHHIGH*2.*PI
      FRTOL=FHTOL*2.*PI
      BLR=BLD/180.*PI
      Z2H=0.
      IF(EPSH.LT.0.000001) Z2H=-1.
      IF(EPSH.GE.0.000001.AND.EPSH.LE.0.999999)
     C  Z2H=EPSH/DLOG(1.-EPSH)
      Z2K=0.
      IF(EPSK.LT.0.000001) Z2K=-1.
      IF(EPSK.GE.0.000001.AND.EPSK.LE.0.999999)
     C  Z2K=EPSK/DLOG(1.-EPSK)
C  ITERATIVE LOOP FOR CALCULATION OF FOURIER CORRECTION FACTORS,
C  TEAVG, TCAVG, AND TSAVG
      DO 12 I=1,9
      FF(I)=0.
12    CONTINUE
      TH1=(TWHAVG+TWKAVG)/2.
      TK1=(TWHAVG+TWKAVG)/2.
      CLSS=0.
      DO 99 ITER=1,IITER
C  IMPERFECT HEAT EXCHANGER ANALYSIS
      IF(ITER.EQ.1) GO TO 35
```

```
      TH1=TEAVG-Z1(2)/Z1(1)
      TK1=TCAVG-Z1(4)/Z1(3)
35    CONTINUE
      TH2=EPSH*TWHAVG+(1.-EPSH)*TH1
      TK2=EPSK*TWKAVG+(1.-EPSK)*TK1
      TH3=EPSR*TH2+(1.-EPSR)*TK2
      TK3=EPSR*TK2+(1.-EPSR)*TH2
      THEAT=EPSH*TWHAVG+(1.-EPSH)*TH3
      TCOOL=EPSK*TWKAVG+(1.-EPSK)*TK3
C  HEAT EXCHANGER AVERAGE GAS TEMPERATURES
      THAVG=TWHAVG+(TWHAVG-(TH1+TH3)/2.)*Z2H
      TWRH=(TH2+TH3)/2.
      TWRK=(TK2+TK3)/2.
      TWRM=(TWRH+TWRK)/2.
      TRAVG=(TWRH+TWRK)/2.
      IF(DABS(TWRH/TWRK-1.).GE.0.000001)
     C  TRAVG=(TWRH-TWRK)/DLOG(TWRH/TWRK)
      TRHAVG=(TWRH+TWRM)/2.
      IF(DABS(TWRH/TWRM-1.).GE.0.000001)
     C  TRHAVG=(TWRH-TWRM)/DLOG(TWRH/TWRM)
      TKAVG=TWKAVG+(TWKAVG-(TK1+TK3)/2.)*Z2K
C  TEMPERATURE DEPENDENT PARAMETERS
      IF(ITER.GE.2) GO TO 40
      TEAVG=THEAT
      TCAVG=TCOOL
      TSAVG=TCOOL
40    CONTINUE
      MDAVG=PWAVG/R*(VHAVG/THAVG+VRAVG/TRAVG+VKAVG/TKAVG)
      MDHAVG=PWAVG/R*(VHAVG/THAVG+VRAVG/2./TRHAVG)
      MEAVG=PWAVG*VEAVG/R/TEAVG
      MCAVG=PWAVG*VCAVG/R/TCAVG
      MWAVG=MEAVG+MDAVG+MCAVG
      MSAVG=PWAVG*VSAVG/R/TSAVG
      IF(IMODE.EQ.1.OR.IMODE.EQ.2) GO TO 200
C  FREE-PISTON MODE : SECANT-BISECTION METHOD FOR CALCULATING
C  FREQUENCY.  FR1 AND FR5 ARE THE LOWER AND UPPER BOUNDARIES FOR
C  ANGULAR FREQUENCY DEFINED BY THE BISECTION METHOD.  FR2 AND FR4
C  ARE THE LOWER AND UPPER ANGULAR FREQUENCIES USED TO CALCULATE
C  SLOPE FOR THE SECANT METHOD.  FR3 IS THE CURRENT ESTIMATE FOR
C  ANGULAR FREQUENCY.
      FR3=FR
      FR=FRLOW
      IMODE=3
      GO TO 200
230   CONTINUE
      FR1=FR
      DET1=DET
      FR=FRHIGH
      IMODE=4
      GO TO 200
240   CONTINUE
      FR5=FR
      DET5=DET
```

```
      IF(((DET1.LT.0.0.AND.DET5.GT.0.0).OR.(DET1.GT.0.0.AND.
     C    DET5.LT.0.0)).AND.FR1.LT.FR5) GO TO 215
      WRITE(6,298) FR1,DET1,FR5,DET5
298   FORMAT(' ','FREQUENCY SEARCH INTERVAL SPECIFIED IMPROPERLY'
     1/' ','FR1 = ',F8.3,8X,'DET1 = ',G13.6
     2/' ','FR5 = ',F8.3,8X,'DET5 = ',G13.6/)
      GO TO 295
215   CONTINUE
      FR=FR3-.5*FRTOL
      IMODE=5
      GO TO 200
250   CONTINUE
      FR2=FR
      DET2=DET
      IF((DET1.LE.0.0.AND.DET2.GE.0.0).OR.(DET1.GE.0.0.AND.
     C    DET2.LE.0.0)) GO TO 225
      FR1=FR2
      DET1=DET2
225   CONTINUE
      FR=FR3+.5*FRTOL
      IMODE=6
      GO TO 200
260   CONTINUE
      FR4=FR
      DET4=DET
      IF((DET4.LE.0.0.AND.DET5.GE.0.0).OR.(DET4.GE.0.0.AND.
     C    DET5.LE.0.0)) GO TO 235
      FR5=FR4
      DET5=DET4
235   CONTINUE
      FR3=FR2+FRTOL*DET2/(DET2-DET4)
      IF(FR3.GE.FR2.AND.FR3.LE.FR4) GO TO 245
      IF(FR3.GE.FR1.AND.FR3.LE.FR5) GO TO 215
      FR3=.5*(FR1+FR5)
      GO TO 215
245   CONTINUE
      FR=FR3
      IMODE=7
      GO TO 200
C  * * * * * * * * * * * * * * * * * * * * * * * * * * * * * * * * * *
C  SUBSECTION FOR COMPUTING MATRIX ELEMENTS
200   CONTINUE
C  FREQUECY DEPENDENT PARAMETERS
      MPPS=MPP*FR**2*XPMAX/PWAVG/AP
      MDPS=MDP*FR**2*XPMAX/PWAVG/AP
      KMCS=KMC*PWAVG/MWAVG/FR
      KPES=KPE*MWAVG*FR/PWAVG
      KPCS=KPC*MWAVG*FR/PWAVG
      HES=HE*ASEAVG/FR/MEAVG/CV
      HCS=HC*ASCAVG/FR/MCAVG/CV
      KMSS=KMS*PWAVG/MSAVG/FR
      HSS=HS*ASSAVG/FR/MSAVG/CV
```

```
C  HOMOGENEOUS ALGEBRAIC EQUATIONS
      IHOMOG=18
      DO 10 I=1,IHOMOG
      DO 15 J=1,IHOMOG
      D(I,J)=0.
15    CONTINUE
10    CONTINUE
      D(1,1)=1.
      D(1,2)=-KPES*MEAVG/MWAVG
      D(1,3)=-1.
      D(1,7)=1.
      D(1,11)=A1
      D(2,1)=KPES*MEAVG/MWAVG
      D(2,2)=1.
      D(2,4)=-1.
      D(2,8)=1.
      D(2,12)=A1
      D(3,2)=-KPCS*MEAVG/MWAVG
      D(3,3)=1.
      D(3,4)=-KPCS*MDAVG/MWAVG
      D(3,5)=-1.
      D(3,9)=-1.
      D(3,11)=A2
      D(3,14)=-A3
      D(4,1)=KPCS*MEAVG/MWAVG
      D(4,3)=KPCS*MDAVG/MWAVG
      D(4,4)=1.
      D(4,6)=-1.
      D(4,10)=-1.
      D(4,12)=A2
      D(5,2)=-MEAVG/MWAVG
      D(5,4)=-MDAVG/MWAVG
      D(5,5)=KMCS
      D(5,6)=-MCAVG/MWAVG
      D(5,9)=KMCS
      D(5,11)=-A2*KMCS
      D(5,14)=A3*KMCS
      D(6,1)=MEAVG/MWAVG
      D(6,3)=MDAVG/MWAVG
      D(6,5)=MCAVG/MWAVG
      D(6,6)=KMCS
      D(6,10)=KMCS
      D(6,12)=-A2*KMCS
      D(7,1)=FF(1)
      D(7,2)=-1.+G*(THEAT+TEAVG)/2./TEAVG+FF(2)
      D(7,7)=HES
      D(7,8)=-1.
      D(7,12)=GM1*A1
      D(8,1)=1.-G*(THEAT+TEAVG)/2./TEAVG+FF(3)
      D(8,2)=-FF(1)
      D(8,7)=1.
      D(8,8)=HES
      D(8,11)=-GM1*A1
```

```
D(9,5)=FF(4)
D(9,6)=-1.+G*(TCOOL+TCAVG)/2./TCAVG+FF(5)
D(9,9)=HCS
D(9,10)=-1.
D(9,12)=-GM1*A2
D(10,5)=1.-G*(TCOOL+TCAVG)/2./TCAVG+FF(6)
D(10,6)=-FF(4)
D(10,9)=1.
D(10,10)=HCS
D(10,11)=GM1*A2
D(10,14)=-GM1*A3
D(11,1)=A11
D(11,5)=-A13
D(11,7)=A11
D(11,9)=-A13
D(11,11)=A1*A11+A4*A12+A2*A13-MDPS
D(11,14)=-A3*A13
D(11,15)=-A12
D(11,17)=-A12
D(12,2)=A11
D(12,6)=-A13
D(12,8)=A11
D(12,10)=-A13
D(12,12)=A1*A11+A4*A12+A2*A13-MDPS
D(12,16)=-A12
D(12,18)=-A12
D(13,5)=1.
D(13,9)=1.
D(13,11)=-A2
D(13,14)=A3-MPPS+CLSS
D(14,6)=1.
D(14,10)=1.
D(14,12)=-A2
D(14,13)=FR/60./PI
D(15,11)=-A4*KMSS
D(15,15)=KMSS
D(15,16)=-1.
D(15,17)=KMSS
D(16,12)=-A4*KMSS
D(16,15)=1.
D(16,16)=KMSS
D(16,18)=KMSS
D(17,12)=-GM1*A4
D(17,15)=FF(7)
D(17,16)=-1.+G*(TCOOL+TSAVG)/2./TSAVG+FF(8)
D(17,17)=HSS
D(17,18)=-1.
D(18,11)=GM1*A4
D(18,15)=1.-G*(TCOOL+TSAVG)/2./TSAVG+FF(9)
D(18,16)=-FF(7)
D(18,17)=1.
D(18,18)=HSS
```

```
      IF(IMODE.EQ.1) GO TO 210
      IF(IMODE.EQ.8) GO TO 280
      CALL DECOMP(IDIM,IHOMOG,D,COND,IPVT,Z1)
      DET=IPVT(IHOMOG)
      DO 55 I=1,IHOMOG
      DET=DET*D(I,I)
55    CONTINUE
      IF(IMODE.NE.2) GO TO 220
C  SPECIAL FREE-PISTON MODE
      WRITE(6,299) FH,DET
299   FORMAT(' ','FH = ',F7.3,8X,'DET = ',G13.6/)
      GO TO 295
220   CONTINUE
      IF(IMODE.EQ.3) GO TO 230
      IF(IMODE.EQ.4) GO TO 240
      IF(IMODE.EQ.5) GO TO 250
      IF(IMODE.EQ.6) GO TO 260
      IF(IMODE.EQ.7) GO TO 270
C  END OF SUBSECTION FOR COMPUTING MATRIX ELEMENTS
C  * * * * * * * * * * * * * * * * * * * * * * * * * * * * * * * * * *
270   CONTINUE
C  FREE-PISTON MODE : NONHOMOGENEOUS ALGEBRAIC EQUATIONS
      IMODE=8
      GO TO 200
280   CONTINUE
      Y14=XPAXPM
      ISIZE=IHOMOG-1
      DO 305 J=1,IHOMOG
      D(13,J)=D(13,J)+D(14,J)
305   CONTINUE
      DO 310 I=14,ISIZE
      DO 315 J=1,IHOMOG
      D(I,J)=D(I+1,J)
315   CONTINUE
310   CONTINUE
      DO 320 I=1,ISIZE
      Y(I)=-Y14*D(I,14)
320   CONTINUE
      DO 325 J=14,ISIZE
      DO 330 I=1,ISIZE
      D(I,J)=D(I,J+1)
330   CONTINUE
325   CONTINUE
      CALL DECOMP(IDIM,ISIZE,D,COND,IPVT,Z1)
      IF(COND.GE.1000000.) WRITE(6,102) COND
102   FORMAT(' ','****NOTICE**** CONDITION OF MATRIX = ',G13.6/)
      CALL SOLVE(IDIM,ISIZE,D,Y,IPVT)
      IE=(IHOMOG+1)-14-1
      DO 335 I=1,IE
      Y((IHOMOG+1)-I)=Y((IHOMOG+1)-I-1)
335   CONTINUE
      Y(14)=Y14
      GO TO 395
```

```
C  KINEMATIC MODE
210    CONTINUE
       BDR=BDD/180.*PI
       Y11=XPAXPM*XDAXPA*DCOS(BDR)
       Y12=XPAXPM*XDAXPA*DSIN(BDR)
       Y13=0.
       Y14=XPAXPM
       ISIZE=IHOMOG-4
       DO 350 I=11,ISIZE
       DO 355 J=1,IHOMOG
       D(I,J)=D(I+4,J)
355    CONTINUE
350    CONTINUE
       DO 360 I=1,ISIZE
       Y(I)=-Y11*D(I,11)-Y12*D(I,12)-Y13*D(I,13)-Y14*D(I,14)
360    CONTINUE
       DO 365 J=11,ISIZE
       DO 370 I=1,ISIZE
       D(I,J)=D(I,J+4)
370    CONTINUE
365    CONTINUE
       CALL DECOMP(IDIM,ISIZE,D,COND,IPVT,Z1)
       IF(COND.GE.1000000.) WRITE(6,102) COND
       CALL SOLVE(IDIM,ISIZE,D,Y,IPVT)
       IE=(IHOMOG+1)-11-4
       DO 375 I=1,IE
       Y((IHOMOG+1)-I)=Y((IHOMOG+1)-I-4)
375    CONTINUE
       Y(11)=Y11
       Y(12)=Y12
       Y(13)=Y13
       Y(14)=Y14
395    CONTINUE
C  COMPUTE INTEGRALS IN INTEGRATED ENERGY EQUATIONS
       WDEA=PWAVG*VEAVG*FR/2.*((Y(1)+Y(7))*(A1*Y(12))
      C+(Y(2)+Y(8))*(-A1*Y(11)))
       Z1(1)=CP*FR*MEAVG/PI*(Y(1)**2+Y(2)**2)**.5
       Z1(2)=G*FR*PWAVG*VEAVG/4./GM1*(Y(1)*Y(8)-Y(2)*Y(7))
       HDEA=Z1(1)*(THEAT-TEAVG)+Z1(2)
       QDWEA=HE*ASEAVG*(TWEAVG-TEAVG)
       WDCA=PWAVG*VCAVG*FR/2.*((Y(5)+Y(9))*(-A2*Y(12))
      C+(Y(6)+Y(10))*(A2*Y(11)-A3*Y(14)))
       Z1(3)=CP*FR*MCAVG/PI*(Y(5)**2+Y(6)**2)**.5
       Z1(4)=G*FR*PWAVG*VCAVG/4./GM1*(Y(5)*Y(10)-Y(6)*Y(9))
       HDCA=Z1(3)*(TCOOL-TCAVG)+Z1(4)
       QDWCA=HC*ASCAVG*(TWCAVG-TCAVG)
       WDSA=PWAVG*VSAVG*FR/2.*((Y(15)+Y(17))*(-A4*Y(12))
      C+(Y(16)+Y(18))*(A4*Y(11)))
       Z1(5)=CP*FR*MSAVG/PI*(Y(15)**2+Y(16)**2)**.5
       Z1(6)=G*FR*PWAVG*VSAVG/4./GM1*(Y(15)*Y(18)-Y(16)*Y(17))
       HDSA=Z1(5)*(TCOOL-TSAVG)+Z1(6)
       QDWSA=HS*ASSAVG*(TWSAVG-TSAVG)
```

```
      IF(DABS((HDEA+QDWEA-WDEA)/WDEA).LT.0.00001.AND.
     C   DABS((HDCA+QDWCA-WDCA)/WDCA).LT.0.00001) GO TO 30
C  NEW ESTIMATES FOR ITERATIVE PARAMETERS
      TEAVG= (Z1(1)*THEAT+Z1(2)+HE*ASEAVG*TWEAVG-WDEA)
     C/ (Z1(1)+HE*ASEAVG)
      Z1(7)=Y(1)/(Y(1)**2+Y(2)**2)**.5
      Z1(8)=Y(2)/(Y(1)**2+Y(2)**2)**.5
      FF(1)=-2.*G/3./PI*(Y(8)*Z1(8)**3-Y(7)*Z1(7)**3)
      FF(2)=-2.*G/3./PI*(Y(8)*Z1(7)**3-Y(7)*Z1(8)*(Z1(7)**2+2.))
      FF(3)=-2.*G/3./PI*(Y(7)*Z1(8)**3-Y(8)*Z1(7)*(Z1(8)**2+2.))
      TCAVG= (Z1(3)*TCOOL+Z1(4)+HC*ASCAVG*TWCAVG-WDCA)
     C/ (Z1(3)+HC*ASCAVG)
      Z1(9)=Y(5)/(Y(5)**2+Y(6)**2)**.5
      Z1(10)=Y(6)/(Y(5)**2+Y(6)**2)**.5
      FF(4)=-2.*G/3./PI*(Y(10)*Z1(10)**3-Y(9)*Z1(9)**3)
      FF(5)=-2.*G/3./PI*(Y(10)*Z1(9)**3-Y(9)*Z1(10)*(Z1(9)**2+2.))
      FF(6)=-2.*G/3./PI*(Y(9)*Z1(10)**3-Y(10)*Z1(9)*(Z1(10)**2+2.))
      TSAVG=TWSAVG/(1.-.5*(GM1*A4)**2*(Y(11)**2+Y(12)**2))
      IF(HSS.LT.0.0001.AND.KMSS.LT.0.0001) GO TO 45
      TSAVG= (Z1(5)*TCOOL+Z1(6)+HS*ASSAVG*TWSAVG-WDSA)
     C/ (Z1(5)+HS*ASSAVG)
45    CONTINUE
      FF(7)=0.
      FF(8)=1.-G*(TCOOL+TSAVG)/2./TSAVG
      FF(9)=G*(TCOOL+TSAVG)/2./TSAVG-1.
      IF(KMSS.LT.0.0001) GO TO 50
      Z1(11)=Y(15)/(Y(15)**2+Y(16)**2)**.5
      Z1(12)=Y(16)/(Y(15)**2+Y(16)**2)**.5
      FF(7)=-2.*G/3./PI*(Y(18)*Z1(12)**3-Y(17)*Z1(11)**3)
      FF(8)=-2.*G/3./PI*(Y(18)*Z1(11)**3-Y(17)*Z1(12)*(Z1(11)**2+2.))
      FF(9)=-2.*G/3./PI*(Y(17)*Z1(12)**3-Y(18)*Z1(11)*(Z1(12)**2+2.))
50    CONTINUE
      CLDS=Y(13)/Y(14)
      CLD=CLDS*PWAVG*AP/60./PI/XPMAX
      CLS=-FR*CLD*DTAN(BLR+PI/2.)
      CLSS=CLS*XPMAX/PWAVG/AP
99    CONTINUE
      WRITE(6,103)
103   FORMAT(' ','*****NOTICE*****  ENERGY BAL DID NOT CONVERGE'/)
C  END OF ITERATIVE LOOP FOR CALCULATION OF FOURIER CORRECTION
C  FACTORS, TEAVG, TCAVG, AND TSAVG
30    CONTINUE
C  COMPUTE DYNAMIC PARAMETERS
      XPAMP=XPMAX*Y(14)
      XDAMP=XPMAX*(Y(11)**2+Y(12)**2)**.5
      CLDS=Y(13)/Y(14)
      CLD=CLDS*PWAVG*AP/60./PI/XPMAX
      IF(IMODE.EQ.1) GO TO 60
      FH=FR/2./PI
      XDAXPA=XDAMP/XPAMP
      IF(XDAMP.GE.XDMAX) WRITE(6,104)
104   FORMAT(' ','*****NOTICE*****  DISP AMPLITUDE IS TOO LARGE'/)
```

```
      BDR=DARCOS(Y(11)/(Y(11)**2+Y(12)**2)**.5)
      IF(Y(12).LT.0.0) BDR=-BDR
      BDD=BDR/PI*180.
60    CONTINUE
C  COMPUTE OVERALL ENERGY BALANCE
      HDRA=FR/PI*CP*(TH2-TH3)*((MEAVG*Y(1)+MDHAVG*Y(3))**2
     C+(MEAVG*Y(2)+MDHAVG*Y(4))**2)**.5
      QDIA=WDEA+HDRA
      QDOA=-WDCA-WDSA+HDRA
      WDOA=WDEA+WDCA+WDSA
      ETAQ=WDOA/QDIA*100.
      WDPA=PWAVG*VCAVG*FR/2.*A3*Y(14)*(A2*Y(12)-Y(6)-Y(10))
      WDDA=WDOA-WDPA
C  OUTPUT STATEMENTS
      WRITE(6,115) KMC,KMCS,KPE,KPES,KPC,KPCS,HE,HES,HC,HCS,KMS,KMSS
     C,HS,HSS,CLD,CLDS,CLS,CLSS
115   FORMAT(' ',44X,'COEFFICIENT      NONDIM'
     1/' ','  WORKING SPACE SEAL LEAKAGE (KG/SEC-PA)',D15.5,F15.6
     2/' ','        HEATER PRESSURE DROP (PA-SEC/KG)',D15.5,F15.6
     3/' ','        COOLER PRESSURE DROP (PA-SEC/KG)',D15.5,F15.6
     4/' ','  EXPANSION SPACE HEAT TRANSFER (W/M2-K)',D15.5,F15.6
     5/' ','COMPRESSION SPACE HEAT TRANSFER (W/M2-K)',D15.5,F15.6
     6/' ','     GAS SPRING SEAL LEAKAGE (KG/SEC-PA)',D15.5,F15.6
     7/' ','       GAS SPRING HEAT TRANSFER (W/M2-K)',D15.5,F15.6
     8/' ','     LOAD DAMPING COEFFICIENT (NT-SEC/M)',D15.5,F15.6
     9/' ','          LOAD SPRING COEFFICIENT (NT/M)',D15.5,F15.6/)
      WRITE(6,118) VWAVG,PWAVG,MWAVG,TEAVG,TWEAVG,FH,THAVG,TWHAVG
     C,XPAMP,TRAVG,XDAXPA,TKAVG,TWKAVG,BDD,TCAVG,TWCAVG,ITER,TSAVG
     C,TWSAVG
118   FORMAT(' ','  AVERAGE VOLUME (M3)',D15.6,23X,'TEMPERATURE (K)'
     1/' ','AVERAGE PRESSURE (PA)',D15.6,22X,'AVG GAS    WALL'
     2/' ','    AVERAGE MASS (KG)',D15.6,10X,'EXPANSION',2F10.3
     3/' ','       FREQUENCY (HZ)',F10.4,18X,'HEATER',2F10.3
     4/' ',' PISTON AMPLITUDE (M)',D15.6,8X,'REGENERATOR',F10.3
     5/' ','DISP/PISTON AMP RATIO',F11.6,17X,'COOLER',2F10.3
     6/' ','DISPLACER PHASE (DEG)',F10.4,13X,'COMPRESSION',2F10.3
     7/' ',11X,'ITERATIONS',I6,22X,'SPRING',2F10.3/)
      WRITE(6,128) EPSH,EPSR,EPSK,TH1,TH2,TK3,TCOOL
     C,THEAT,TH3,TK2,TK1
128   FORMAT(' ',32X,'HEATER  REGENERATOR  COOLER'
     1/' ',11X,'EFFECTIVENESS     ',3F10.5
     2/' ','EXP TO COMP GAS TEMP (K)',4F10.3
     3/' ','COMP TO EXP GAS TEMP (K)',4F10.3/)
      WRITE(6,130) QDIA,HDRA,QDOA,WDOA,WDPA,ETAQ,WDDA
130   FORMAT(' ','   HEAT INPUT TO WORKING GAS (W)  ',G13.6
     C,'   REG FLUX (W)',G13.6
     1/' ',      'HEAT OUTPUT FROM WORKING GAS (W)  ',G13.6
     2/' ',      '      INDICATED POWER OUTPUT (W)  ',G13.6
     C,'     PISTON (W)  ',G13.6
     3/' ',      '    THERMODYNAMIC EFFICIENCY (%)  ',F7.3
     C,13X,'DISP (W)  ',G13.6/)
```

```
      WRITE(6,135) WDEA,QDWEA,HDEA,WDCA,QDWCA,HDCA,WDSA,QDWSA,HDSA
135   FORMAT(' ',14X,'SUM P*DV (W)      Q WALL (W)       H FLUX (W)'
     1/' ','   EXPANSION',3G16.6
     2/' ',' COMPRESSION',3G16.6
     3/' ','       SPRING',3G16.6/)
C  OUTPUT FOR VOLUME, PRESSURE, MASS, AND TEMPERATURE HARMONIC
C  FUNCTIONS.  COEFFICIENTS FOR CONSTANT, SIN, AND COS TERMS ARE
C  STORED TEMPORARILY IN D(I,J) ARRAY.
      D(1,1)=VEAVG/VWAVG
      D(1,2)=-VEAVG/VWAVG*A1*Y(11)
      D(1,3)=-VEAVG/VWAVG*A1*Y(12)
      D(2,1)=(VHAVG+VRAVG+VKAVG)/VWAVG
      D(2,2)=0.
      D(2,3)=0.
      D(3,1)=VCAVG/VWAVG
      D(3,2)=VCAVG/VWAVG*(A2*Y(11)-A3*Y(14))
      D(3,3)=VCAVG/VWAVG*A2*Y(12)
      D(7,1)=VSAVG/VWAVG
      D(7,2)=VSAVG/VWAVG*A4*Y(11)
      D(7,3)=VSAVG/VWAVG*A4*Y(12)
      D(1,4)=1.
      D(1,5)=Y(1)+Y(7)+A1*Y(11)
      D(1,6)=Y(2)+Y(8)+A1*Y(12)
      D(2,4)=1.
      D(2,5)=Y(3)
      D(2,6)=Y(4)
      D(3,4)=1.
      D(3,5)=Y(5)+Y(9)-A2*Y(11)+A3*Y(14)
      D(3,6)=Y(6)+Y(10)-A2*Y(12)
      D(7,4)=1.
      D(7,5)=Y(15)+Y(17)-A4*Y(11)
      D(7,6)=Y(16)+Y(18)-A4*Y(12)
      D(4,1)=MEAVG/MWAVG
      D(4,2)=MEAVG/MWAVG*Y(1)
      D(4,3)=MEAVG/MWAVG*Y(2)
      D(5,1)=MDAVG/MWAVG
      D(5,2)=MDAVG/MWAVG*Y(3)
      D(5,3)=MDAVG/MWAVG*Y(4)
      D(6,1)=MCAVG/MWAVG
      D(6,2)=MCAVG/MWAVG*Y(5)
      D(6,3)=MCAVG/MWAVG*Y(6)
      D(8,1)=MSAVG/MWAVG
      D(8,2)=MSAVG/MWAVG*Y(15)
      D(8,3)=MSAVG/MWAVG*Y(16)
      D(4,4)=TEAVG/TWHAVG
      D(4,5)=TEAVG/TWHAVG*Y(7)
      D(4,6)=TEAVG/TWHAVG*Y(8)
      D(5,4)=PWAVG*(VHAVG+VRAVG+VKAVG)/MDAVG/R/TWHAVG
      D(5,5)=0.
      D(5,6)=0.
      D(6,4)=TCAVG/TWHAVG
      D(6,5)=TCAVG/TWHAVG*Y(9)
      D(6,6)=TCAVG/TWHAVG*Y(10)
```

```
      D(8,4)=TSAVG/TWHAVG
      D(8,5)=TSAVG/TWHAVG*Y(17)
      D(8,6)=TSAVG/TWHAVG*Y(18)
      WRITE(6,120) (D(1,I),I=1,6),(D(2,I),I=1,6),(D(3,I),I=1,6)
     C,(D(7,I),I=1,6)
120   FORMAT(' ',25X,'V/VWAVG',26X,'P/PWAVG'
     1/' ',8X,2('       CONST       SIN        COS')
     2/' ','  EXPANSION',6F11.6
     3/' ','       DEAD',6F11.6
     4/' ','COMPRESSION',6F11.6
     5/' ',' GAS SPRING',6F11.6/)
      WRITE(6,125) (D(4,I),I=1,6),(D(5,I),I=1,6),(D(6,I),I=1,6)
     C,(D(8,I),I=1,6)
125   FORMAT(' ',25X,'M/MWAVG',26X,'T/TWHAVG'
     1/' ',8X,2('       CONST       SIN        COS')
     2/' ','  EXPANSION',6F11.6
     3/' ','       DEAD',6F11.6
     4/' ','COMPRESSION',6F11.6
     5/' ',' GAS SPRING',6F11.6//////)
295   CONTINUE
5     CONTINUE
      RETURN
      END
```

D.2 LHA1 Input Data for RE-1000 Base Case

```
&INPUT          R=2080.,        CP=5200.,       XPMAX=.0210,
XDMAX=.0202,    AP=.002572,     AR=.000218,     AD=.002572,
VEAVG=.0000636, VHAVG=.0000396, VRAVG=.0000594, VKAVG=.0000285,
VCAVG=.0001036, VSAVG=.0000318, ASEAVG=.01392,  ASCAVG=.02292,
ASSAVG=.00979,  MPP=6.2,        MDP=.426,       FH=30.6,
FHLOW=25.,      FHHIGH=35.,     FHTOL=.01,      XPAXPM=.619,
BDD=55.5,       XDAXPA=.958,    PWAVG=7085000., TWHAVG=853.,
TWEAVG=853.,    TWKAVG=326.,    TWCAVG=326.,    TWSAVG=326.,
KMC=.68D-8,     KPE=.15D7,      KPC=.15D7,      HE=1000.,
HC=1000.,       KMS=.20D-8,     HS=1000.,       IMODE=3,
IITER=50,       EPSH=1.,        EPSR=1.,        EPSK=1.,
BLD=-90.,       ILOOP=1,        &END
&INPUT          &END
```

D.3 LHA1 Output for RE-1000 Base Case

	COEFFICIENT	NONDIM
WORKING SPACE SEAL LEAKAGE (KG/SEC-PA)	0.68000D-08	0.121945
HEATER PRESSURE DROP (PA-SEC/KG)	0.15000D 07	0.083644
COOLER PRESSURE DROP (PA-SEC/KG)	0.15000D 07	0.083644
EXPANSION SPACE HEAT TRANSFER (W/M2-K)	0.10000D 04	0.091840
COMPRESSION SPACE HEAT TRANSFER (W/M2-K)	0.10000D 04	0.037891
GAS SPRING SEAL LEAKAGE (KG/SEC-PA)	0.20000D-08	0.233265
GAS SPRING HEAT TRANSFER (W/M2-K)	0.10000D 04	0.051654
LOAD DAMPING COEFFICIENT (NT-SEC/M)	0.35296D 03	0.076671
LOAD SPRING COEFFICIENT (NT/M)	0.0	0.0

AVERAGE VOLUME (M3)	0.294700D-03
AVERAGE PRESSURE (PA)	0.708500D 07
AVERAGE MASS (KG)	0.213613D-02
FREQUENCY (HZ)	29.4359
PISTON AMPLITUDE (M)	0.129990D-01
DISP/PISTON AMP RATIO	0.969505
DISPLACER PHASE (DEG)	46.6818
ITERATIONS	6

	TEMPERATURE (K)	
	AVG GAS	WALL
EXPANSION	824.779	853.000
HEATER	853.000	853.000
REGENERATOR	547.896	
COOLER	326.000	326.000
COMPRESSION	336.640	326.000
SPRING	329.792	326.000

	HEATER	REGENERATOR	COOLER	
EFFECTIVENESS	1.00000	1.00000	1.00000	
EXP TO COMP GAS TEMP (K)	789.815	853.000	326.000	326.000
COMP TO EXP GAS TEMP (K)	853.000	853.000	326.000	351.762

HEAT INPUT TO WORKING GAS (W)	2852.16	REG FLUX (W)	0.0
HEAT OUTPUT FROM WORKING GAS (W)	1832.10		
INDICATED POWER OUTPUT (W)	1020.06	PISTON (W)	1020.06
THERMODYNAMIC EFFICIENCY (%)	35.764	DISP (W)	-0.125056D-11

	SUM P*DV (W)	Q WALL (W)	H FLUX (W)
EXPANSION	2852.16	392.837	2459.31
COMPRESSION	-1740.36	-243.867	-1496.49
SPRING	-91.7454	-37.1199	-54.6258

	V/VWAVG			P/PWAVG		
	CONST	SIN	COS	CONST	SIN	COS
EXPANSION	0.215813	-0.075458	-0.080023	1.000000	0.141389	-0.045816
DEAD	0.432643	0.0	0.0	1.000000	0.145554	-0.048543
COMPRESSION	0.351544	-0.044387	0.073241	1.000000	0.151288	-0.046567
GAS SPRING	0.107906	0.006396	0.006783	1.000000	-0.047074	-0.124214

	M/MWAVG			T/TWHAVG		
	CONST	SIN	COS	CONST	SIN	COS
EXPANSION	0.122961	-0.032603	-0.049797	0.966916	0.055012	-0.011252
DEAD	0.386309	0.056229	-0.018753	0.616985	0.0	0.0
COMPRESSION	0.490730	-0.017947	0.086998	0.394654	0.024310	-0.006121
GAS SPRING	0.153757	0.004455	-0.001688	0.386626	-0.006487	-0.019477

Reference

1. N. C. J. Chen, F. P. Griffin, and C. D. West, *Linear Harmonic Analysis of Stirling Engine Thermodynamics*, ORNL/CON-155, Martin Marietta Energy Systems, Inc., Oak Ridge Natl. Lab., August 1984.

INTERNAL DISTRIBUTION

1. D. W. Burton
2. J. G. Carbonell, Consultant
3-12. F. C. Chen
13-22. N. C. J. Chen
23. F. A. Creswick
24. N. Domingo
25. S. K. Fischer
26. W. Fulkerson
27. J. A. Getsi
28. S. M. Gillis, Consultant
29-38. F. P. Griffin
39. F. R. Kalhammer, Consultant
40. R. E. Kasperson, Consultant
41. M. A. Kuliasha
42. M. Lessen, Consultant
43. F. C. Maienschein, Consultant
44. R. W. Murphy
45. G. T. Privon
46. H. E. Trammell
47. C. D. West
48. ORNL Patent Office
49. Central Research Library
50. Document Reference Section
51-52. Laboratory Records Department
53. Laboratory Records (RC)

EXTERNAL DISTRIBUTION

54. R. A. Ackermann, Mechanical Technology, Inc., 968 Albany-Shaker Rd., Latham, NY 12110
55. William Beale, Sunpower, Inc., 6 Byard Street, Athens, OH 45701
56. D. M. Berchowitz, Sunpower, Inc., 6 Byard Street, Athens, OH 45701
57. Don Beremand, NASA-Lewis Research Center, 21000 Brookpark Rd., Cleveland, OH 44135
58. Dick Bloomquist, Code 2752, David W. Taylor Naval Ship Research and Development Center, Annapolis, MD 21402
59. Dick Cawley, Lennox Industries, Inc., 1600 Metrocrest Dr., Carrollton, TX 75006
60. M. Clinch, Gas Research Institute, 8600 W. Bryn Mawr Avenue, Chicaco, IL 60631
61 E. H. Cooke-Yarborough, Lincoln Lodge, Longworth Nr Abingdon, Oxfordshire, OX13, 5DU, England
62. J. G. Daley, Argonne National Laboratory, 9700 South Cass Avenue, Argonne, IL 60439
63. D. K. Darooka, Advanced Energy Programs Department, General Electric Co., P.O. Box 527, King of Prussia, PA 19406
64. G. R. Dochat, Mechanical Technology, Inc., 968 Albany-Shaker Rd., Latham, NY 12110
65. J. E. Dudenhoefer, NASA-Lewis Research Center, 21000 Brookpark Rd., Cleveland, OH 44135
66. T. Finkelstein, Stirling Associates International, P.O. Box 643, Beverly Hills, CA 90213
67. R. J. Fiskum, Energy Conversion Equipment Branch, CE-132, GF-217/FORS, Department of Energy, 1000 Independence Avenue S.W., Washington, DC 20585

68. A. A. Frank, Department of Mechanical Engineering, University of California at Davis, Davis, CA 95616
69. S. Freedman, Gas Research Institute, 8600 W. Bryn Mawr Ave., Chicago, IL 60631
70. D. R. Gedeon, Gedeon Associates, Box 141 A, South Canaan Rd., Athens, OH 45701
71. L. Goldberg, University of Minnesota, Dept. of Civil and Mineral Engineering, 500 Pillsbury Drive SE, Minneapolis, MN 55455
72. M. Gunn, Energy Conservation and Utilization Technology Division, CE-142, SE-091/FORS, Department of Energy, 1000 Independence Avenue S.W., Washington, DC 20585
73. Bob Holtz, Argonne National Laboratory, 9700 South Cass Avenue, Argonne, IL 60439
74. C. Hylin, Rocketdyne Division, Mail Code LB24, Rockwell International, 6633 Canoga Avenue, Canoga Park, CA 91303
75. L. N. Johansson, Stirling Power Systems, 7101 Jackson Rd., Ann Arbor, MI 48103
76. R. H. Kim, Mechanical Engineering and Engineering Science Department, University of North Carolina at Charlotte, Charlotte, NC 28223
77. K. P. Lee, Aspen Systems, Inc., 275 Boston Post Road, Marlborough, MA 01752
78. G. A. McLennan, Argonne National Laboratory, 9700 South Cass Avenue, Argonne, IL 60439
79. R. J. Meijer, Stirling Thermal Motors, Inc., 2841 Boardwalk, Ann Arbor, MI 48104
80. V. Naso, Dipartimento di Meccanica e Aeronautica, Universita "La Sapienza", via Eudossiana 18-00184, Rome, Italy
81. N. P. Nightingale, Mechanical Technology, Inc., 968 Albany-Shaker Rd., Latham, NY 12110
82. L. B. Penswick, Sunpower Inc., 6 Byard Street, Athens, OH 45701
83. J. S. Rauch, Mechanical Technology Inc., 968 Albany-Shaker Road, Latham, NY 12110
84. G. T. Reader, Royal Naval Engineering College, Manadon, Plymouth, Devon PL5 3AQ, England
85. P. Riggle, Joint Center for Graduate Study, University of Washington, 100 Sprout Rd., Richland, WA 99352
86. J. D. Ryan, Energy Conversion Equipment Branch, CE-132, GF-217/FORS, Department of Energy, 1000 Independence Avenue S.W., Washington, DC 20585
87. J. R. Senft, Department of Mathematics/Computer Science, University of Wisconsin, River Falls, WI 54022
88. J. G. Slaby, NASA-Lewis Research Center, 21000 Brookpark Rd., Cleveland, OH 44135
89. J. L. Smith, Jr., Mechanical Engineering Department, Massachusetts Institute of Technology, Cambridge, MA 02139
90. W. P. Teagan, Arthur D. Little, Inc., 20 Acorn Park, Cambridge, MA 02140
91. R. C. Tew, NASA-Lewis Research Center, 21000 Brookpark Rd., Cleveland, OH 44135

92. I. Urieli, Department of Mechanical Engineering, Stocker Center, College of Engineering and Technology, Ohio University, Athens, OH 45701
93. V. J. Van Griethuysen, Air Force Wright Aeronautical Laboratories, Wright-Paterson Air Force Base, OH 45433
94. D. A. Vaughn, Belvoir Research and Development Center, Ft. Belvoir, VA 22060 ATTN: STRBE-EMP
95. R. Vincent, Mechanical Technology Inc., 968 Albany-Shaker Road, Latham, NY 12110
96. G. Walker, University of Calgary, Dept. of Mechanical Engineering, 2500 University Drive NW, Calgary, Canada T2N1N4
97. M. A. White, University of Washington, Joint Center for Graduate Study, 100 Sprout Road, Richland, WA 99352
98. G. Wood, Sunpower Inc., 6 Byard Street, Athens, OH 45701
99. Office of the Assistant Manager for Energy Research and Development, U.S. Department of Energy, Oak Ridge Operations, Oak Ridge, TN 37831

100-126. Technical Information Center, Department of Energy, P.O. Box 62, Oak Ridge, TN 37831